# INFLUENCE OF INTERNAL DETERIORATION MECHANISMS ON THE SYSTEM-LEVEL BEHAVIOR OF COMPOSITE PRESTRESSED CONCRETE GIRDER BRIDGES

---

A Thesis

Presented to

the faculty of the School of Engineering and Applied Science

University of Virginia

---

in partial fulfillment

of the requirements for the degree

Master of Science

By

Mark Saliba

May

2015

APPROVAL SHEET

The thesis

Is submitted in partial fulfillment of the requirements

for the degree of

MASTER OF SCIENCE

Mark Saliba

AUTHOR

This Thesis has been read and approved by the following committee:

**_____Devin Harris_____**

Dr. Devin Harris, Advisor

**_____Michael Brown_____**

Dr. Michael Brown

**_____Osman Ozbulut_____**

Dr. Osman Ozbulut

Accepted for the School of Engineering and Applied Science:

Dean, School of Engineering and Applied Science

May

2015

# ACKNOWLEDGEMENTS

The author would like to sincerely thank the following for their support and contributions to this work:

- **Dr. Devin Harris**, for providing me with the opportunity to join the graduate research team, and trusting me with taking on this project. Your continuous praise and support were always reassuring, especially in the early, and sometimes frustrating, beginning. Your experience and technical knowledge guided my development as an engineer, and I will always be grateful for your help along the way.
- **Dr. Michael Brown**, for serving on my committee, as well as helping me dig up all the old codes and documents I needed to recover some of the unreported information from the referenced studies.
- **Dr. Osman Ozbulut**, for serving on my committee, as well as being readily available to answer any concerns I had on the structural aspects of my research or otherwise.
- **Dr. Amir Gheitasi**, for all the time and effort you invested in helping me learn my way through finite element modeling. Even when you were incredibly busy, you always found the time to look over my work and give feedback. I will always remember your patience and genuine desire to help.
- **Muhammad Sherif**, for your devotedness to help me take my first steps using ANSYS. Constantly discussing ideas with you in the office, or studying some of your previously designed FE scripts, accelerated my work and helped me troubleshoot various used modeling approaches.

- To the rest of my graduate friends and colleagues including **Sherif Daghash**, **Mohamad Amine, Johnathan Tanks, Lauren Bolton, Evelina Khakimova, John Civitillo, Layth Hussein, Mohamad Alipour, Salman Usmani,** and **Mathew Reardon**. I appreciate all your help and company over the past two years. Your good vibes in the office and out kept me positive as the project progressed.
- To my parents, **Wadih and Gladess Saliba**, I owe everything I accomplished so far to you. If it weren't for your generous love, trust and support, I would never have had the chance to complete this work and reach this point in my life.
- To my sisters, **Carla and Perla Saliba**, ever since I left home, you two have been nothing but reassuring, loving, and encouraging. I appreciate all your support over the years and I wish you nothing but the best.

INFLUENCE OF INTERNAL DETERIORATION MECHANISMS ON THE SYSTEM-LEVEL BEHAVIOR OF COMPOSITE PRESTRESSED CONCRETE GIRDER BRIDGES

MARK SALIBA

# Abstract

The ASCE's 2013 Report Card for America's Infrastructure assigned in-service bridges a score of C+. This rating reflects the extent of the deteriorating conditions and deficiency of the national aging infrastructure network. Currently, transportation agencies depend heavily on experiential-based practices to make decisions regarding maintenance and preservation. While practitioners and decision-makers already invest ample efforts towards this cause, the lack of a rational understanding of system-level behavior of in-service structures makes resolving the problem even more complicated. This constraint, coupled with limited resources and the vast network of existing structures in service, highlights the need to develop strategies to better understand the operational safety and remaining life of these structures.

In pursuit of this objective, this study focuses on understanding the performance of deteriorated prestressed concrete bridges. A performance-based assessment framework was developed, which allows for the integration of the various sources of damage within the primary load carrying members. This framework is then used to quantify the implications of these mechanisms on the serviceability, capacity, and remaining service life of the structure. The investigation, conducted using a numerical analysis platform, is expected to help support the maintenance decision through rational and risk-based techniques, which will ultimately integrate condition-based system behavior.

**Keywords**: Nonlinear Finite-Element Analysis; Ultimate Capacity; Full Scale Destructive Test; Performance Evaluation; Case Study; ANSYS

# Table of Contents

# List of Figures

# List of Tables

# 1.0 INTRODUCTION

The American Society of Civil Engineers' Report Card for America's Infrastructure has been a source well-trusted by the general public to describe the condition of United States' infrastructure network. Today's aging roads and bridges are plagued with a variety of structural deficiencies ranging from corrosion and cracking to section loss and other common modes of deterioration, earning a grade C+ for in-service bridges on a national level (FHWA 2012). The Federal Highway Administration (FHWA) estimates that 30% of the national bridge inventory have exceeded their 50-year design life and the average age of all bridges is about 42 years. To overcome this deficiency backlog by 2028, $20.5 billion USD must be annually invested towards rehabilitation instead of the $12.8 billion USD being invested currently (ASCE 2013). As bridges near the end of their design lives, rehabilitation or replacement will become inevitable. While current maintenance practices perform satisfactorily, some of their aspects must be improved for the impending transportation infrastructure repair bottleneck to be traversed as safely and as efficiently as possible.

Following catastrophic bridge collapses like that of the I-5 Skagit River Bridge (NTSB 2014) and the I-35 Mississippi River Bridge (NTSB 2008), inspectors and engineers in Departments of Transportation (DOTs) around the nation have been under scrutiny concerning their inspection and maintenance practices. However, the public might not realize the gravity of the maintenance backlog that inspectors have to deal with and plan to overcome. Today's engineers have inherited the result of a surge in bridge building shortly after World War II. This spike in road and bridge construction endured until the mid-1960s (NBI 2013). Naturally, since there was a sharp rise in bridge building, a large percentage of those bridges would reach the end of their design lives at around the same time.

The essence of the problem lies in the insufficiency of funds and manpower required to rehabilitate all structurally deficient bridges immediately. It is then the responsibility of engineers working for the public to allocate the appropriate amount of funding for structures in need of maintenance. Engineers prioritize bridge repairs by degree of structure importance, damage severity, and repair urgency. Currently, comprehensive structural inspection data and extensive repair experience guide optimization efforts for the prioritization process of deficient bridges. However, due to the variety of possible damage conditions and available maintenance options, engineers can experience difficulties pairing appropriate solutions to damages and determining the best courses of action (FHWA 2012).

In general, DOTs and practitioners attempt to maintain constant awareness of the integrity of all structures in their area of operations through biennial routine visual inspections on bridge superstructures and substructures (FHWA 2012). Nondestructive evaluation (NDE) techniques such as impact-echo, ground penetration radar and ultrasonic testing can provide field engineers with a significant amount of information on the degradation that the structure accumulates over time (SHRP 2). Nevertheless, as detailed and extensive as these inspection practices can be, they deliver information on the status of localized features in the structure, and they do not accurately relate the implications of those features to the overall system behavior of the bridge.

NDE techniques perform remarkably well in capturing the current status of geometric and material characteristics of structural components in bridges; however, they do not have the capability of determining the effects of those characteristics on the overall capacity and performance of the structure. Furthermore, decisions based on collected inspection data are seldom objective as different engineers can develop different verdicts on bridge maintenance procedures while referring to the same inspection results. Due to the locality and subjectivity of today's

maintenance practices, it is difficult to predict the exact effects that common types of damage impose on the performance and serviceability of an entire bridge system. With the lack of accurate, objective information on overall system performance, engineers are left to make subjective judgments on the most appropriate maintenance practices. For those practices to be efficient and successful, sufficient knowledge of the condition of the bridge system is crucial.

Bridges are required to be inspected on a biennial basis, and whenever there has been a change in the configuration of the bridge. These routine inspections must provide the necessary information required to satisfy the National Bridge Inspection Standards. Load rating is another process which aims to determine the structure's safe load carrying capacity. When inspectors find that a more rigorous investigation is necessary, a thorough re-examination is scheduled where more exhaustive nondestructive evaluation techniques can be used to help determine the most suitable course of maintenance action (AASHTO 2011). Because of the non-comprehensiveness of extracted performance data, additional reserve capacity and inherent system redundancy are assumed to be limited to decrease the likelihood of system failure. Load postings may be used to prohibit heavy axle load presence on bridges pending repair or replacement. These constrictions greatly affect individuals and industries who depend on well-organized and wide-spreading transportation networks, so unnecessary restrictions should be avoided at all costs. Moreover, decisions that deem structures to be significantly more deficient than they really are would require more radical and expensive repair approaches. Conservative decisions translate to inefficient solutions and DOTs that invest funds inappropriately are unlikely to overcome the backlog in bridge rehabilitation by 2028 or even worse (AASHTO 2011, ASCE 2013).

Furthermore, each type of bridge superstructure is afflicted with its unique set of maintenance problems, which in turn requires a unique set of evaluation techniques, and engineers

usually employ a generic solution for certain ranges of each specific type of damage. Even with a wide collection of inspection data, these solutions are very often conservative in nature. When engineers lack the full understanding of the damaged bridge's residual capacity, structural integrity, and remaining service life, system efficiency is usually critically undermined and decisions on maintenance are overly conservative. Since there is no quick and efficient method capable of measuring the overall structural performance of a bridge, a rationally driven framework was devised to help support the decision-making process by evaluating the current status of the bridge system to estimate reserve capacity, redundancy, and ductility.

This thesis describes a study that supports the development of a behavior-driven approach to the decision-making process for maintenance of a specific family of bridge superstructures (i.e. prestress concrete girder bridges). The end objective of this approach is to ensure that the bridges' expected life and serviceability are extended with minimal restrictions and cost. The proposed approach relies more heavily on physical behavior derived from mechanics, and objective practices in lieu of experience-based, subjective methods. These practices are embodied in a framework brought about by numerical investigation.

The main use of this framework is to guide rational and risk-based maintenance and preservation decisions based on the condition-based system behavior by evaluating the effects of damage on serviceability and remaining service life of deteriorated superstructures. This quantitative framework employs numerical modeling techniques to capture the system-level full-scale behavior of prestressed concrete girder bridges, while focusing mostly on the different stages of failure. Another important objective of this work is to simulate and understand how this family of bridges behaves in the presence of common forms of damage in order to streamline the decision-making process and improve current maintenance efforts.

This work shall be divided into multiple chapters that explain and illustrate the development of the investigative approach to reach the sought objective. The following chapter presents a summary of the literature relevant to this study. The review discusses the history of prestressed concrete and its contributions to the bridge industry, in addition to background information on structural analysis methods. The evolution of the structural analysis of prestressed concrete is also illustrated in this chapter, and the lessons learned from past researchers along the development of this work are highlighted and discussed as well. Chapter 3 describes the investigation approach in detail, and it presents the three phases of the proposed framework. The case studies referenced in each of the framework's phases and their respective finite element models were also thoroughly described. Chapter 4 introduces the results from each phase, and it describes how these results fit within the larger-scale proposed framework. Later in that chapter, the models' ability to predict structural performance and the effects of damage on that performance are discussed as well. Chapter 5 follows with concluding remarks on the work done and the goals achieved. Chapter 6 serves to propose directions for future research on the improvement of this work or widening its applications.

# 2.0 BACKGROUND AND RESEARCH SIGNIFICANCE

This chapter discusses the history of prestressed concrete and its rise in popularity within the fields of civil engineering. The structural analysis of prestressed concrete is discussed as well through the various contributions of engineers and researchers in those fields.

## 2.1 Prestressed Concrete

Prestressed concrete as a theory dates back to the late 19th century with its introduction by Jackson and Doehring (Nawy, 2009). These engineers introduced the concept, but they could not overcome some structural challenges that made the method unpractical. It was not until the early to mid-1900s, with contributions from Freyssinet, Guyon and Magnel, that prestressing became an attractive option for structural engineers (Nawy, 2009). Prestressed concrete's introduction to the construction and transportation industries sparked an overhaul in its research and development. Its significant advantages over its counterpart, passively reinforced concrete, and the low costs associated with those advantages attracted much interest from the industry. As shown in Figure 1, prestressed concrete allows for the prevention or minimization of crack formation, which in turn promotes longevity and ease of maintenance. It also allows for smaller cross-sections and much longer spans, which usually translate to lower costs.

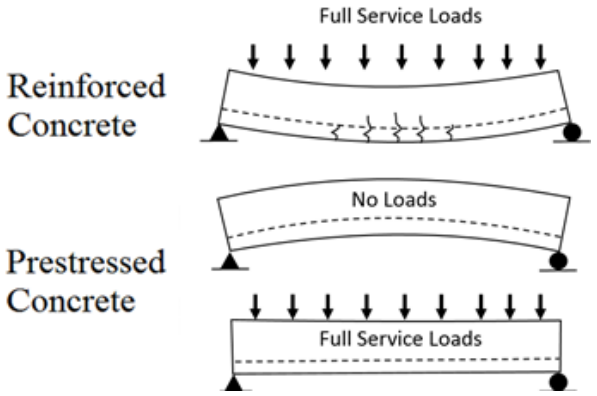


*Figure 1 - Comparison between Reinforced and Prestressed Concrete*

Over time, engineers and researchers have increased the efficiency, practicality, safety, consistency, and reliability of this type of construction. The efforts and innovations of numerous scientists over the years have transformed prestressed concrete from a mere theoretical concept that had minimal practical purposes to one of the indispensable building blocks of the transportation and construction industry (Nawy, 2009; Mamlouk, 2011).

Gaining all these benefits while maintaining economic competitiveness cemented prestressed concrete in the industries of bridge and building construction. Interest for this type of construction dramatically grew in the mid-1950s. According to the National Bridge Inventory, the number of prestressed bridges constructed per year in the U.S. increased from 234 to 1573 from 1955 to 1960 (NBI 2013). Today, after decades of experience with the various features of prestressed concrete, engineers learned to make the most out of the structural system without compromising public safety. To assess the structural integrity and full capacity of the designed structures, engineers frequently employed destructive methods such as proof testing and full-capacity loading (Lau and Tung, 1988; Oh, 2002; McDonald, 2003, Aguilar et. al, 2015). In addition to requiring a vast amount of manpower and resources, irreversible damage was applied to the structures for significant performance data to be extracted.

## 2.2 Finite Element Analysis – Prestressed Concrete

Theoretical structural analysis methods vary widely and improved vastly in the last several decades. Due to the convenience and relative accuracy of non-destructive structural evaluation techniques, such as sonic, ultrasonic, and magnetic evaluation, researchers invested much effort into various numerical and computational simulations, which can recreate similar results to those provided through destructive field-testing (McClure and West, 1984; Araujo, 2009). Complex numerical theories were integrated into computer software packages that made these operations

more efficient and more accessible to engineers and analysts. These refined methods include grillage, strut-and-tie method, and finite-element method. The grillage method is a common form of analysis method mainly applied on composite bridge decks and beams. The strut-and-tie method is another powerful and versatile method that involves the transformation of members into equivalent trusses that carry loads across members or regions of members.

Finite Element Analysis (FEA) is a popular alternative to the methods stated above. FEA is one of several discrete analyses that function by reducing differential equations to linear algebraic ones which can be solved numerically. The formulation of the finite element method requires boundary-value problems that are solved through the derivation of the potential energy in the system either through the direct variational method or through the method of weighted residuals (Stolarski et. al, 2006). FEA software creates a numerical platform through which various types of structures could be modeled by inputting geometries and applying forces, and boundary conditions on the system. However, there are some challenges and drawbacks associated with the use of this method. Setting up the model (pre-processing) can take a significantly long time to plan and solve; result extraction (post-processing) requires a long time as well. The analysis method has a steep learning curve and it requires much practice for the user to model with confidence and to reduce chances of error and subsequent debugging. Finite element (FE) models are also very sensitive to assumptions, and a very comprehensive set of information is required for accurate modeling (Gheitasi 2014).

One of the advantages behind the use of FEA is its ability to capture plasticity and failure modes in materials like mild steel, prestressing strands, and concrete. Another strength of this technique is its ability to recreate the various failure stages experienced by the structure as the applied load approaches the materials' ultimate capacity. Since one of this study's objectives

entails nonlinear modeling and the capture of structural failure stages, those FEA features were essential. Finite element modeling has been commonly used for structural engineering purposes and with major improvements in graphical interfaces, analytical tools, accuracy of results, and computing power, it was deemed to be the most appropriate choice for the current study.

An indispensable stage in the formulation of FEA is proper technique usage for the accurate modeling of different features in the actual structure. Initial stress conditions, composite action, load transfer between the strands and surrounding concrete, and steel bond-slip behavior are some of the more crucial mechanisms of the prestressed structural system that require special attention to be properly modeled. Successful capturing these features has been attempted by a number of researchers who have explored the applicability of this method through different means and modeling approaches. Early contributions include those of Phillips and Zienkiewicz (1976) who helped overcome the problem of mesh dependency in prestressed concrete FE (finite element) modeling. Van Greunen and Scordelis (1983) utilized an early form of FE modeling compiled through a written code instead of software packages to model nonlinear behavior of prestressed concrete slabs. McClure and West (1984) loaded a specially constructed prestressed concrete segmental bridge to failure, studied its response, and compared it to a finite element model and standard beam theory. These investigators used early forms of FE software to model the nonlinear behavior of various components in prestressed concrete structures, and predict the response of the systems under different load and boundary conditions. Their works suggested modeling techniques and approaches for several specific major components in different types of structures.

Other early examples of research on modeling improvements include the work of Chang et al. (1987) who presented a novel approach for incorporation of reinforcement into FE models. Their work discussed the modeling approach of many major components in the structure and

predicted the response of prestressed slabs under different load conditions. Hucklebridge Jr. et al. (1995) used FE models to determine the capacity of shear keys in multi-beam box girder bridges. Aalami (2000) suggested multiple strategies for modeling tendons and their loads in prestressed beams through various forms of internal load balancing, and Tavarez (2001) suggested a variety of routes to numerically model the behavior of reinforcement and accurately incorporate it with the concrete elements. Chung and Sotelino (2005) investigated different finite element techniques to model the overall behavior of girder bridges, while Thomas and Ramaswamy (2006) used FE to specifically model prestressed concrete beams under shear loading. These studies provided several suggestions on modeling approaches of different components.

Various studies have demonstrated the power of this analysis technique by including supportive refined analyses to numerically recreate experimental results or to test specimens under different loading conditions to produce other failure scenarios. Lau and Tung (1988) tested to failure precast prestressed U-beams extracted from 30-meter (98.4-feet) bridge spans and Seraj et al. (1992) evaluated four case studies on prestressed I-beams and T-beams using the finite element method. Both studies successfully replicated the experimental results achieved by the investigators and proposed modeling approaches specific to this type of construction. Similarly, Nikolic and Mihanovic (1996) performed a series of non-linear numerical analyses on post-tensioned concrete structures. Their approaches were valid and accurate for their case studies and some of their methods were applicable for scenarios considered in this study.

After decades of research, finite element modeling has become one of the most popular and practical structural analysis methods for prestressed concrete beams. The applications for this modeling ranged from simple analysis of structural components to ultimate capacity prediction for entire structures. Oh et al. (2002) conducted an in-place failure test on a 30-year old prestressed

concrete I-girder bridge span and Feng et al. (2009) tested a continuous three-span concrete box-girder bridge to failure. Both sets of investigators created FE models to accompany and recreate test results from an experimental program. Laskar et al. (2010) discuss the development of their model which has been efficiently used to predict the behavior of prestressed concrete beams under critical shear loads. The model was compared to experimental testing on five full-scale prestressed girders and the studied phenomena consisted of web-shear and flexural shear behavior.

The work of Ayoub et al. (2011) provided significant contribution to this sector of structural analysis, in which their study compared the performance of regular prestressed concrete beams with ones reinforced with fiber-reinforced polymers through finite element analysis. Their models for both specimens, especially the controls, helped define the appropriate methodology for the current study's model construction. Ayoub (2011) also presented a novel approach to model prestressed concrete beams by taking into account important factors like bond-slip behavior, as well as short-term and long-term losses. Plos and Gylltoft (2006) explored the capabilities of the FE method even further through the modeling of a 45-year-old prestressed concrete box-girder bridge. The purpose behind the creation of the model was comparison between it and the free cantilever method, an alternative way of calculating the shear and torsional capacity of the structure. The listed authors successfully incorporated FEA into their studies to support their experiments; however, these analyses can be taken some steps further by expanding to the non-linear section of the structures' response. In addition to recreating the response from the unloaded state to the ultimate capacity, the evolution of different behavioral phenomena can be captured at different stages of loading.

## 2.3 Non-linear Finite Element Analysis

As shown, due to its efficiency and accuracy, this platform is regularly exploited by engineers and scientists to analyze the full response of prestressed and reinforced concrete structures. In addition to the works listed above, other contributions include those of Fanning (2001), who employed the finite element method to model the performance and behavior of reinforced and post-tensioned concrete girders. Through those models and comparisons to beam responses, recommendations were made on modeling strategies and approaches. Zaeem (2013) employed non-linear finite element analysis to effectively and efficiently simulate and analyze reinforced concrete bridges. Similarly, Hossain et al. (2014) employed finite element theory to model a three-span continuous prestressed concrete girder bridge and applied live loads on the structure to further understand its behavior.

The aforementioned contributions to the field of non-destructive evaluation and FEA have been crucial to the proper development and current status of prestressed concrete FE modeling. While intact structural models have been prevalent in these studies, a substantial degree of complexity is introduced into bridge models when any damage scenario is considered. Regardless of the type, extent, or cause of damage, the degradation location usually serves as an initiation platform for further damage propagation and contributes to a reduction in capacity of the entire bridge system. Consequently, several other studies targeting the appropriate modeling of damage were conducted to further understand the effects of different damage inputs on numerical models (Dagher and Kulendran 1992, Coronelli 2002, Zhou 2005). Kallias and Rafiq (2010) employed FEA to investigate the effect of corrosion on regularly reinforced concrete beams and Walsh et al (2014) utilized finite element methods to identify damage effects on prestressed adjacent box-beam girders.

## 2.4 Finite Element Analysis – Damage to Prestressed Concrete

While the works discussed in the previous section studied the local effects of damage on the modeled reinforced concrete structures, they do not correlate those local damages to the bridge system's structural performance. The next step to improve this analysis approach is to integrate damage mechanisms common to this family of superstructures and model their effects on the performance of the entire bridge rather than just the affected components.

Some work has already been input towards resolving this challenge, albeit in different types of bridge superstructures. Gheitasi and Harris (2014a, 2014b, 2014c, and 2014d) explored the capabilities of finite element modeling to accurately understand and recreate the behavior of damaged in-service composite steel girder bridges. Some of their models integrated common types of damage into superstructures to determine their effects on the system's behavior, while others were promoted as supportive frameworks for maintenance practices. The rational approaches they developed revealed the extent of the residual structural capacity of bridge superstructures which were often considered limited by engineers.

Gheitasi and Harris (2014a) correlated structural damage to bridge system performance through collected data to infer a characterization of critical behavior stages and their relationship to failure, safety, and serviceability. Common types of deterioration such as corrosion, section loss, and cracking were integrated into their models so that their detrimental effects could be recreated in the modeled bridge. Similar objectives were set for this research in efforts to help provide similar advancements in the design, maintenance, and rehabilitation practices of prestressed concrete girder bridges.

This thesis builds from this strong foundation of research in efforts to recreate the full-scale linear and nonlinear behavior of a varied sample of prestressed concrete bridges. The goal of this

study is to provide accurate representations of system-level performance and structural capacity through numerical models. The rational foundation used to create the models should also allow for the accurate incorporation of damage to structures and understanding its effects on system-level performance. Further successful uses of these models may also help guide further understanding of system-level behavior, and in turn, both condition-rating and load-rating decisions. With continuous improvement in software and computing power, the application of this method to other families of bridges may have wider implications for the bridge industry, if further research efforts are directed toward computer simulation and analysis.

# 3.0 INVESTIGATION APPROACH

A defined investigation approach was to be followed to evaluate the performance of bridges of interest. The methodology, shown in Figure 2, would allow the available geometric and material properties to be used efficiently to create a suitable model, which in turn provides accurate results on full-capacity structural response. Prestressed concrete bridges loaded to their ultimate capacities were modeled using FEA software and validated against reported experimental results from referenced case studies. Damage conditions played an important role in this approach as well. Determining the effects of damage on the overall response of a prestressed concrete girder bridge constitutes one of the core expected outcomes of the proposed research. A comprehensive framework that can relate structural damage to a measure of system performance reduction can help support inspection practices and facilitate the decision-making process for maintenance of in-service bridge superstructures.

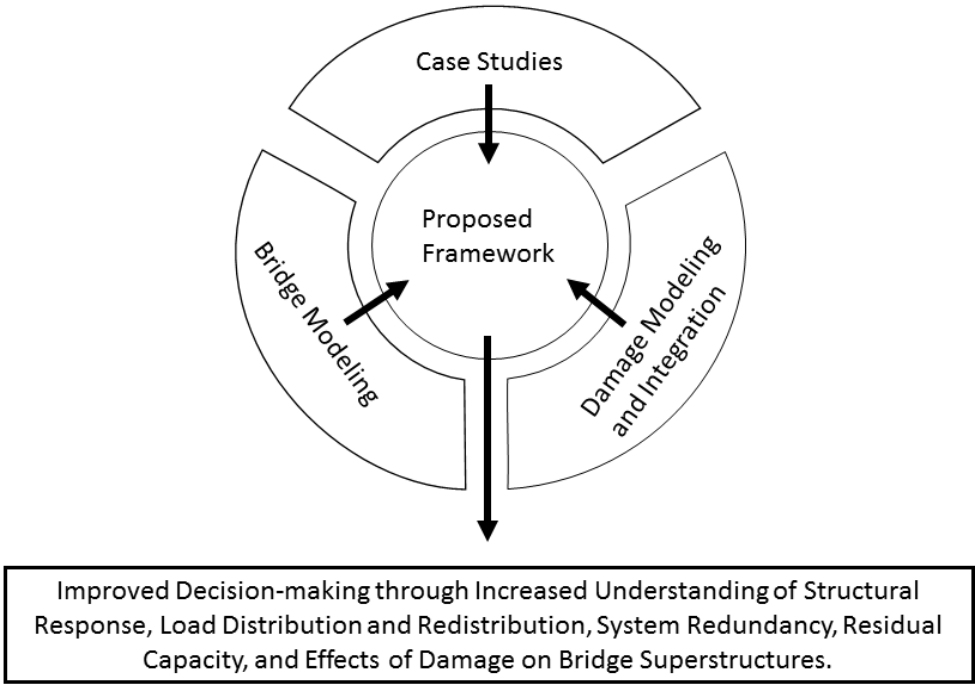


*Figure 2 - Investigation Approach Layout*

## 3.1 Proposed Framework

The framework developed by Gheitasi and Harris (2014a) was employed in this study due to the similarities in the problem statement and the overarching objectives. Even though the developed framework was originally designed for composite steel girder bridge superstructures, the authors deemed it “generic, allowing for extrapolation across other bridge types”. Their contributions helped pave the road for the research conducted in this study as many of their findings and conclusions align with the objectives of this investigation, and their methodologies are also based on finite element platforms.

For this study, the target framework was to be based on an FEA platform as well. However, the model development, calibration, and validation processes critically depend on the availability of accurate data from bridge load tests. Ideally, a varied sample set of bridges would be instrumented and then tested to their full capacities to build a bank of bridge performance data with different types of damage under various load scenarios. This wealth of data would then serve as a reference to which for new load tests could be compared in order to evaluate their current structural status and predict future performance; however, this process is not feasible because of the tremendous time and financial costs required.

Another option would be to test existing bridges while keeping their constituent materials in their elastic range. The drawback of this procedure is that only a limited set of data from the elastic behavior would be extracted. The behavior in inelastic stages would not be captured, since such loading would cause irreparable damage to the structure. As a result, the most suitable method for our purposes was found to be numerical structural analysis tools. Even though this method can be very reliable and is very time and cost-effective, it is highly dependent on the accuracy of reported information on material properties, geometric dimensions, and boundary conditions.

Therefore, acquiring accurate information of these variables was crucial and this step posed one of the biggest challenges associated with this method.

The software package used as a platform for FEA was the 15.0 version of ANSYS, a program developed by Swanson Analysis Systems, Inc. This commercial, multi-purpose, finite element software is capable of solving a wide variety of static, dynamic, mechanics, electromagnetic, fluids, and thermal problems. Within the structures discipline, ANSYS has been frequently used in the evaluation of bridges, buildings, and other structural components. The program allows the operator to model any structure (or part of a structure) to analyze the performance of a wide variety of products such as mechanical components or structural elements. Model solutions include a vast amount of information including stress, strain, displacement, heat flow, magnetic flux, etc. (Stolarski et. al, 2006).

With the goal of creating a numerical framework, the modeling of structural components was developed through multiple stages to optimize the procedure needed to efficiently model a damaged bridge. The investigation approach developed by Gheitasi and Harris (2014a) was reorganized into three distinct phases of increasing complexity, which range from the intact girder level to the intact bridge level and finally to the damaged bridge level. A schematic is shown in Figure 3 to explain the layout and progression of the three phases. Multiple case studies on prestressed concrete girder bridges were referenced to develop the simulations. That was necessary for the developed simulations to be progressively evolved to yield a rational final system-level model with integrated damage mechanisms, and to build a strong case for a validated, accurate framework.

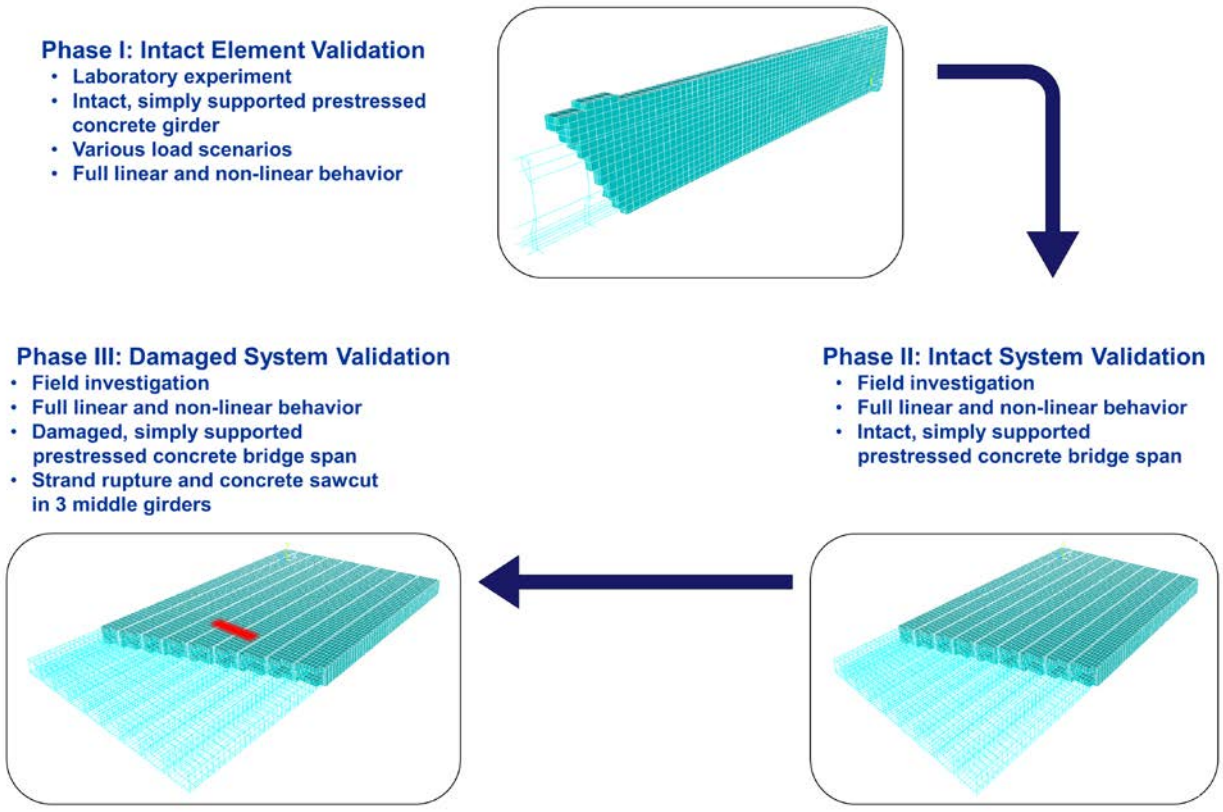


*Figure 3 - Schematic of Proposed Framework*

The first phase aims to accurately recreate the behavior of a single undamaged prestressed concrete girder by utilizing the numerical approximation strength of the finite element method. Through the completion of Phase I, proper modeling techniques and response recreation allows for the progression to a more complex bridge-level model in Phase II. The Higgs (2013) study on the full-scale test of four prestressed concrete girders under four different loading scenarios was referenced for the first phase of the study. His work included capturing the full behavior of prestressed concrete girders at their ultimate capacities; this study served as a suitable reference for the element-level validation step. The results extracted from his tests allowed for the comparison of the beam's experimental destruction to its equivalent in the model. Advantages of

this study include the comprehensive instrumentation and the load application at various locations on the four prestressed concrete girders, which allow for more rigorous validation procedures.

The second phase consists of the intact system-level validation, where an FE model is created to capture the complex behavior of the entire intact bridge system. Lessons learned along the development of Phase I would be applied to create an effective intact bridge model. The Phase II model must then be validated through comparison to experimental results from full-capacity load tests. After creating a strong, well-understood foundation, the third and final phase can be tackled. This phase of the study deals with the recreation of damaged system behavior. The successful validation of the Phase III model against experimental results verifies that the effects of damage can be accurately incorporated into FE models. Even though a single form of damage will be incorporated into the Phase III model, the same process can be extrapolated to other common damage mechanisms, such as corrosion and section loss. The resulting model would have the ability to determine the effects that different types of damage have on the overall performance of the structure.

Huffman (2012) and Steinberg (2011) were other heavily referenced studies where the investigators tested two bridge spans under truck and full-capacity loadings. For this set of experiments, one span was left intact, while the other was damaged. The investigators supported the results of their study by creating a numerical model of the fully instrumented, damaged span. Performance data extracted from these studies were used to calibrate models so that they best replicate experimental behavior. The validated models are then used to quantify the effects of common types of damage on the performance of bridge systems. The results of the tests helped better understand how prestressed adjacent box-beam bridges behave as a system and how damaged beams affect the overall behavior of the bridge.

In this chapter, each case study is described along with the steps of the model evolution. However, there are some baseline modeling techniques that were employed for all models. The following section describes these common initial stages.

## 3.2 Finite Element Modeling Process

Fundamentally, the modeling process consists of numerous steps divided into three major stages: pre-processing, solution, and post-processing. Each of these stages are necessary for the FEA models to reproduce the structure and extract accurate response behavior. Pre-processing, the first stage in FE modeling, sets up the model by defining its geometric properties, boundary conditions and loading pattern through element and material property definition. The solution phase takes place after design of the restrained structure is complete. The solution convergence criteria are defined in this stage. These criteria are selected to be based on displacement, rotation, moment or force. The post-processing stage consists of revisiting the solved model and extracting information of interest. The results can range from displacements of specific nodes at certain locations to a multitude of element properties along the accumulation of load.

### *3.2.1 Pre-processing*

The proper selection of element types is a vital first step for a functioning FE model. The element type selection process was straightforward since only 3 types of elements were needed in all case studies modeled along the development of this thesis. Eight-node, SOLID65 3-D reinforced concrete solid elements were used to model concrete. This type of element has the ability of simulating cracking in tension and crushing in compression along either of its three axes in nonlinear stages of loading. 8-node SOLID45 3-D structural solid elements allow for the modeling of bearing pads and steel supports. Instead of cracking and crushing, this element can

capture plasticity, creep, large strain and deflection, and other material-specific phenomena. Uniaxial 2-D LINK180 spar elements were used to model the prestressing strands, longitudinal mild reinforcement, as well as shear reinforcement. As expected in steel reinforcement, no element bending is considered, and plasticity, creep, and large strains can be captured. Every node in all elements described before can translate along three degrees of freedom, allowing for rotation and axial displacement (ANSYS 2011).

The next step consists of determining the material and geometric properties for all bridge and experimental setup components. All properties were extracted from available experimental data and integrated into classical constitutive relationships for each material (mild steel, concrete, prestressing strands, bearing pads, etc.). Some properties such as concrete moduli of elasticity and tensile strength are not explicitly available so certain estimation equations were utilized. For example, the work of Wolanski (2004) allowed for reasonable approximation of linear and non-linear material properties necessary to define the behavior of girder and deck concrete (specifically the stress-strain relationships). His material models use the William and Warnke (1974) model and the von Mises failure criterion to define the compressive uniaxial stress-strain relationship for the SOLID65 concrete elements. The following equations were used to accurately estimate the states of stress and strain in the concrete at different stages of loading:

$$f = \frac{E_c \varepsilon}{(1 + \left(\frac{\varepsilon}{\varepsilon_0}\right)^2} \qquad (Eq.\ 3.1)$$

$$\varepsilon_0 = \frac{2f'_c}{E_c} \qquad (Eq.\ 3.2)$$

Where $f'_c$ and $\varepsilon_0$ are the stress and strain of concrete respectively, at ultimate compressive strength, and $f$ and $\varepsilon$ are the stress and strain values under any load. A sample modeled concrete stress-strain curve created using these equations is illustrated in Figure 4.

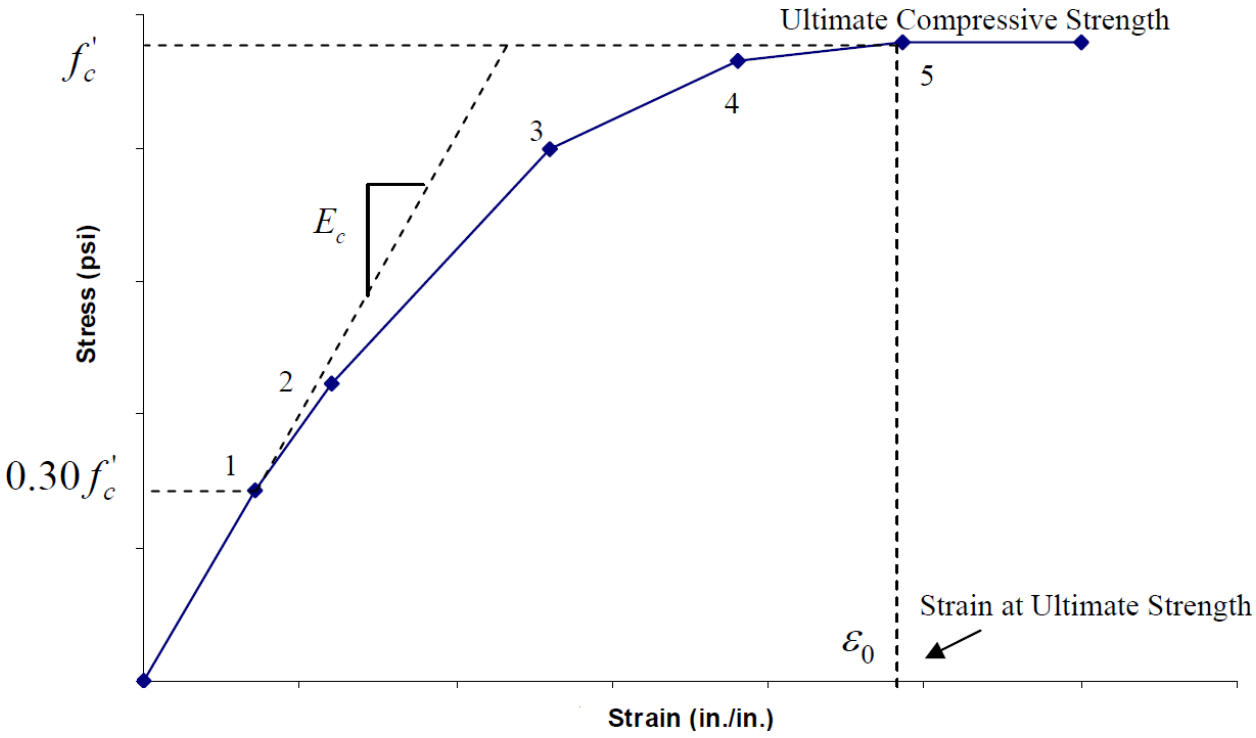


*Figure 4 - Concrete Stress-Strain Curve*

The behavior of steel reinforcement and prestressing strands was modeled using their corresponding stress-strain curves to create a simplified, but generic material performance model which was assigned to various elements in the FE model (Gheitasi, 2014). A multiline graph representing the stress-strain behavior of both types of steel reinforcement was input into the model to simulate the stress-strain relationship in steel. Figure 5 (a) and (b) illustrates the graphs taken as reference for the stress-strain behavior of strands and rebar respectively.

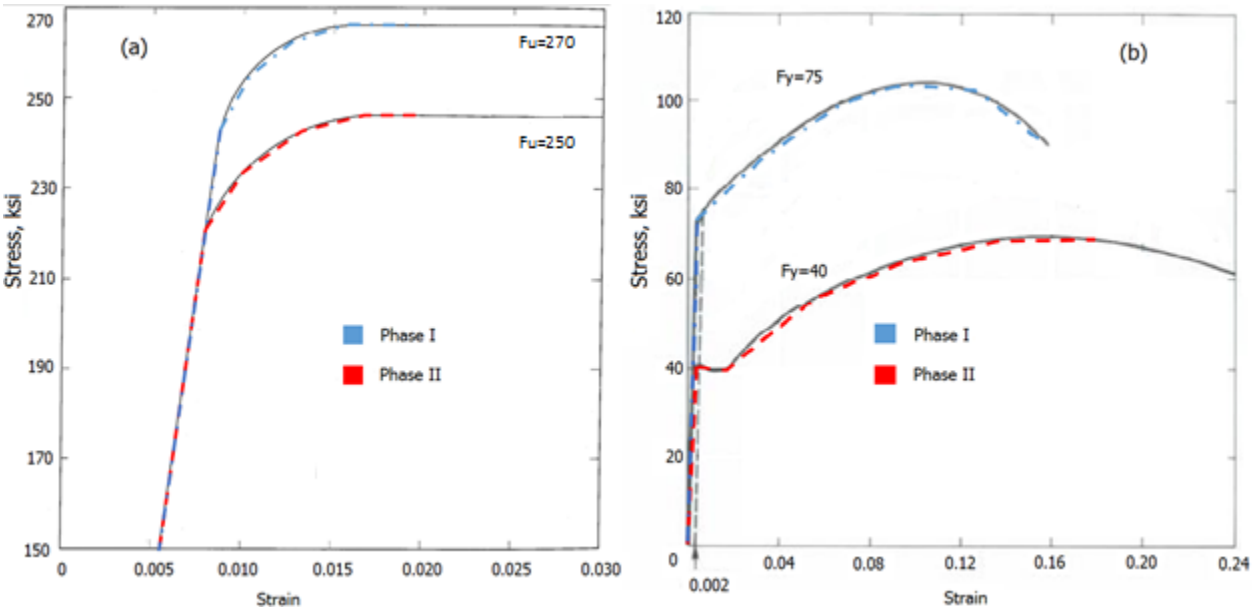


*Figure 5 - (a) Prestressing Strand and (b) Mild Reinforcement Stress-Strain Diagram*

Boundary conditions are usually not as easily replicated as the material models described above, since those conditions are rarely equivalent to idealized restraints. In the case studies selected, each set of boundary conditions was modeled differently, then refined through multiple analyses to converge on the most accurate setup. As the support mechanisms become more complicated, correctly modeling the boundary conditions becomes more difficult. Pin-roller assumptions must be refined by coupling stiffening springs, for example, to converge on an appropriate simulation.

Along the modeling process, challenges usually arise whenever information is lacking or inaccurate. In most cases, available data do not perfectly represent the status of the entire structure due to natural material variations, vague boundary conditions, and connection integrity between components. Model calibration through comparison of simulation results with experimental data allows for convergence on a suitable version that accounts for the unknown variables. Even though the model may include assumptions and simplifications, the resulting calibrated framework allows for the logical correlation of data for the validation and evolution of the three phases.

### *3.2.2 Solution*

For the numerical investigation of the structures, static analyses with the full Newton-Raphson method was selected as the model nonlinear solver. In accordance with Wolanski's (2004) and Gheitasi's (2014) solver recommendations, the convergence criteria were set for displacement values only at reference and tolerance amounts of 5 and 0.05 respectively. The load application process was force-controlled, so the loads were applied incrementally using automatic time-stepping. A script section was included in the early models to control the load through displacement rather than force; that section of code is attached in the appendix. However, that script was later omitted from the models, since there was no accurate information on the displacement rates used by investigators in some of the case studies, and its setup was more complicated than the force-controlled process. Note that displacement-controlled load application does allow capture of softening behavior if that is of interest for inspectors. For this study however, there was no significant advantage for its use since the behavior of the structure prior to its ultimate capacity is of the most interest.

Model analysis was interrupted, and the ultimate capacity of the simulated bridge was deemed to be reached, when the qualitative failure stages described by investigators at failure are recreated. Numerical non-convergence was another one of the criteria adopted as the simulated structures' failure standard. Model non-convergence is triggered by numerical instability in the matrices, which directly translates to excessive imbalance in the system. By definition, this system imbalance occurs when the aggregate reaction forces do not match the total applied loads on the structure. This imbalance can be delayed, and sometimes even averted, with the use of smaller loadsteps (smaller incremental increase in loading), as that helps the software overcome these imbalances. Figure 6 shows a sample graph produced by ANSYS as the software works on solving

the designed model. As the load increments increase over numerous iterations, the software attempts to converge each substep (marked by a green vertical dashed line). When loads do not converge after several tries, the software bisects the load (marked by a red vertical dashed line) and attempts to reach convergence again. This process goes on until the maximum amount of attempts specified by the user is reached.

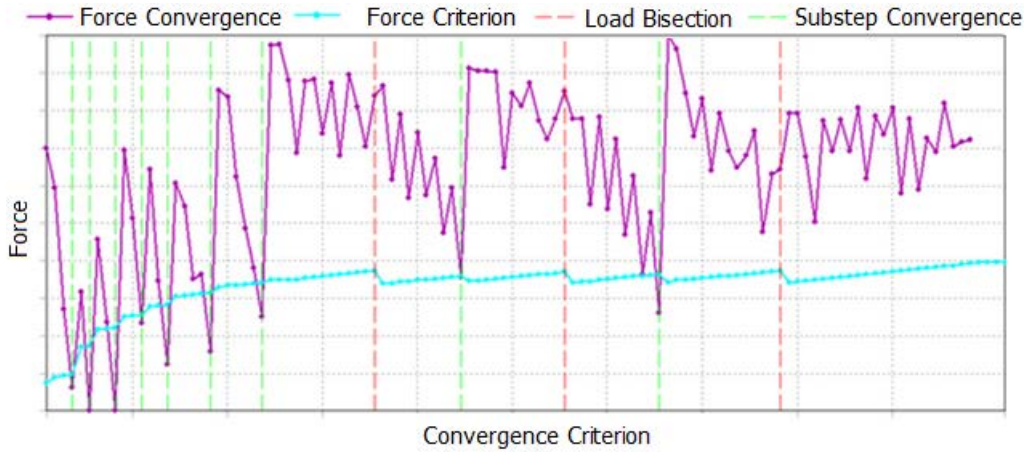


*Figure 6 - Sample Newton-Raphson Solution Plot*

### *3.2.3 Post-processing*

After model completion and successful solving, information on the behavior of various structural components at certain locations was to be extracted. This dataset was necessary to compare the model's deflection pattern to the load-deflection curves reported by the case study investigators. In addition to deflection, data on crack pattern, reinforcement stress, and failure features are taken from the model in this stage.

## 3.3 Case Studies

As described in section 3.1, the implementation of the proposed framework requires the validation of developed models using reported data from experimental results. The following sections explain the referenced case studies while focusing mostly on the test specimens, test

setups, and result output. Modeling assumptions and techniques adopted to create the FE computer models was also listed and clarified.

### *3.3.1 Phase I*

The first phase served to validate the intact element-level behavior of the bridge. For this study, an intact element translates to a single undamaged prestressed concrete girder. This phase serves to verify the procedure followed for the accurate establishment of the model and the recreation of a single girder's behavior. Starting from the small undamaged state allows for the transition to more complicated scenarios based on a strong, well-understood foundation. Due to the common use of prestressed concrete girders in bridges all over the United States' transportation network, much experimental data is available in the literature on the full-scale testing of those specimens. In most cases, investigators would remove girders from out-of-commission bridges and load them to their full capacities on-site or in a laboratory setting. Since undamaged specimens were the ones of interest, however, the inventory of suitable specimens was more exclusive. Newly constructed bridges that were not damaged or exposed to the elements for extended periods of time are rarely taken apart.

#### *3.3.1.1 Bridge Description*

Phase I commenced after an extensive search on possible test bridges. The selected candidates were a set of 4 girders extracted from the 400 South Bridge on I-15 in Orem, Utah, a prestressed concrete I-girder bridge (Higgs, 2013). There were several reasons behind the selection of these specimens, the first of which is the excellent condition of the girders. Even though the bridge was 52 years old at the time of the test, the tested girders were only 8 years old, since they were removed from a more recently added section of the structure. The entire bridge was decommissioned prematurely due to its replacement as part of UDOT's south I-15 core project.

The creation of the FE model began with the quantification of the geometric and material data of the test specimen. The bridge was originally constructed along the 400 South roadway in Orem, Utah in 1960 and it was then expanded by two lanes in 2004. The bridge was later decommissioned to be replaced during the I-15 core project in 2011. The four studied girders were extracted from the 2004 section of the bridge as shown and highlighted in Figure 7. The other four girders were used for a different study.

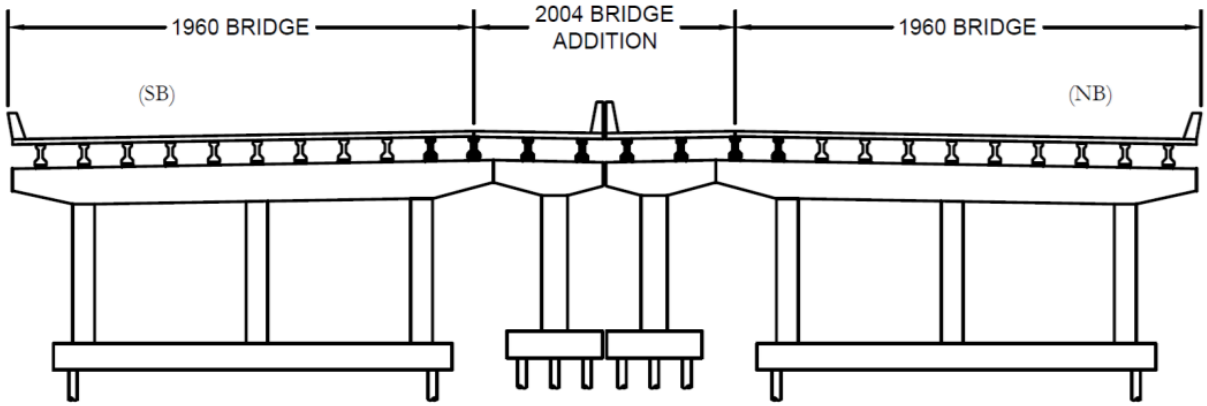


Figure 7 - Section Drawing of 400 South Bridge

Another advantage of this experiment was the availability of multiple girders, which allowed for various loading scenarios. Flexural, shear, and combination loading scenarios were applied on the four girders to trigger failure in different forms. This assortment of scenarios creates various opportunities for more comprehensive model validation. Moreover, each girder, except for the one loaded at midspan, was loaded twice. For example, for the shear loading scenario, the first load would be applied on one end of a completely intact girder; for the second test however, the other end would be loaded and the sheared end would be used as support. For reliability purposes, this phase's models were validated using data from the first test only.

All beams were thoroughly instrumented with a variety of strain gauges and string potentiometers to capture performance data and create moment-deflection and shear-deflection curves. For one of these load conditions, the girder under flexural loading, the authors created an FE model to replicate their experimental results. The script or input code generated from their work proved to be helpful in the early stages of modeling, but it was not used for this study. The provided model did serve as a benchmark to which the new model could be compared.

One last advantageous aspect of this case study was the inclusion of residual prestressing tests on the girders. This vital parameter, which determines the effective remaining force in the strands, is a key component for the efficient development of the model, as its absence requires a multitude of model iterations to converge on a reasonable value.

Initial inspections deemed the girders to be in excellent condition because of their relatively short service life. Therefore, the girders qualified to be used in the intact element-level validation phase. The test setup used to fully load the girders is shown in Figure 8. The investigators aimed to make support and boundary conditions in the laboratory as similar to the actual field conditions as possible. As part of the test setup, a steel plate was greased and placed between the load and the girder to ensure a pure vertical load was applied on the top of the girder and elastomeric pads were inserted under the beams to allow beam rotation at the ends. As shown, elastomeric pads were sandwiched between the beam and the steel supports.


*Figure 8 - Phase I Test Setup (Higgs, 2013)*

The geometric properties of the salvaged girders were readily available in the structural plans. The AASHTO Type 1 girders were cast from high-strength self-consolidating prestressed concrete and they were simply supported by either piers or abutments. They each spanned 36.25 feet and had a height of 28 inches. Six additional inches of concrete were present on top of the girder as part of the deck. At the time of the test, girder concrete and deck concrete had a compressive strength of 11.3 ksi and 8 ksi, respectively. The girders were prestressed using 13 straight ½ inch diameter seven-wire strands in the pattern shown in Figure 9. Further longitudinal reinforcement consisted of four #3 rebar and shear reinforcement consisted of #3 rebar at varying locations along the length of the beam. Figure 10 shows the shear and mild reinforcement configuration within the beam. As shown, the investigators left the deck integrated with the girder so that the behavior better simulated the in-service behavior of the girder. To conserve continuity and composite action between the girder and the deck, shear reinforcement along the length of the beam extends from the girders into the deck and connects both components.

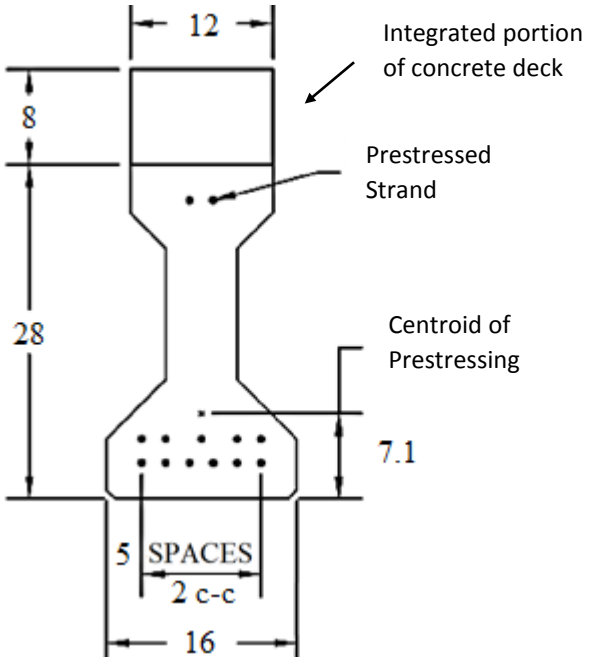


*Figure 9 - Girder Cros- Section and Strand Configuration (dimensions in inches)*

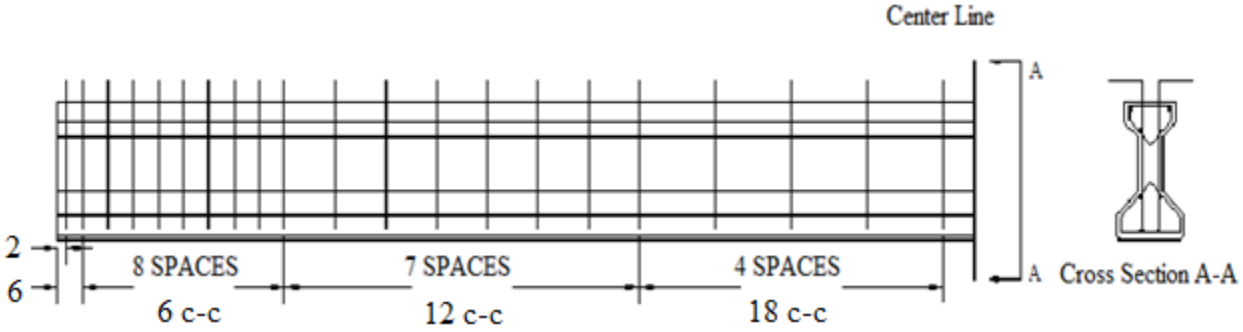


*Figure 10 - Shear and Mild Reinforcement Configuration (dimensions in inches)*

*3.3.1.2 Material Models*

Material properties for the specimens were available as well. Multiple concrete cylinder samples were cored at the time of the test to determine the actual concrete compressive strength in the girders as well as in the deck. Even though information on the design strength of concrete was available, the average compressive strengths determined from the core tests were used in this model, since they best describe concrete properties at the time of the test. The tensile strength of concrete was taken as $12\sqrt{f'_c}$ as it falls within the acceptable range define by ACI. The grades

and design modulus of elasticity of the prestressing strands and the mild reinforcement were both given in the structural plans. Information on the modulus of elasticity of concrete was not explicitly available, so approximation equations were used. Several modulus of elasticity equations were suggested in the ACI committee report on high-strength concrete (ACI 363-10). Table 1 lists the considered equations. After numerous model iterations, the equation proposed by Martinez et al. (1982) proved to be the most suitable for modeling purposes. The report states that this formula has proven to be a reliable expression, but it somewhat underestimates concrete modulus of elasticity.

*Table 1 - Modulus of Elasticity Design Estimate Equations*

| Source | Equation for E (psi) |
|---|---|
| Radain et al. (1993) | $2{,}101{,}775 + 26{,}200 * \sqrt{f'_c}$ |
| ACI 318-05 | $57{,}000 * \sqrt{f'_c}$ |
| Martinez et al. (1982) | $40{,}000 * \sqrt{f'_c} + 1{,}000{,}000$ |
| Cook (1989) | $w^{2.55} * {f'_c}^{0.315}$ |
| Ahmad and Shah (1985) | $w^{2.5} * {f'_c}^{0.325}$ |
| NS 3473 (1992) | $309{,}500 * {f'_c}^{0.3}$ |

Creating the model for the elastomeric pad was more challenging than other components since the study lacked any material or geometric information on the used pads. Because of that, various values for Poisson's ratio and the modulus of elasticity of the wide variety of commercially available bearing pads were used as reference. Assuming the pad is 8" x 12", and according to the FDOT-FHWA report (2007), the range of a pad's effective stiffness can range from 14 to 56 ksi, depending on the number and thickness of the elastomeric layers. This range was calculated by changing the thickness of each elastomeric layer from 0.25" to 0.5". Through multiple model iterations the most appropriate pad properties included a Poisson's ratio of 0.48 and a modulus of

elasticity of 20 ksi. Pad dimensions were not reported by investigators, the test setup image shown in Figure 8 was taken as reference for information on dimensions.

Properties of mild steel and prestressing strands were simpler to model as the grades of steel used were clearly defined in the study. Information on stress and strain was readily available in AASHO and ASTM codes and documentation in effect at the time (ASTM A615, ASTM A416). Because of the available information on geometry and modulus of elasticity, no assumptions were made for mild and prestressing steel reinforcement. Figure 5 compares the steel models to their actual behavior.

Next, the material properties summarized in Table 2 were integrated into the model and assigned to the various elements. Multiple versions of materials were created to allow use of the same elements for various purposes. An example is the use of SOLID65 elements for both girder and deck concrete which have different material properties. Another example is the longitudinal, prestressing, and shear steel reinforcement which are all made from LINK180 elements; but have different geometric and material properties.

*Table 2 - Phase I Material Properties*

| | | |
|---|---|---|
| Girder Concrete | Compressive Strength | 11.3 ksi |
| | Modulus of Elasticity | 5.25 ksi |
| | Tensile Strength | 1.275 ksi |
| | Poisson's Ratio | 0.2 |
| Deck Concrete | Compressive Strength | 8 ksi |
| | Modulus of Elasticity | 4.57 ksi |
| | Tensile Strength | 1.07 ksi |
| | Poisson's Ratio | 0.2 |
| Prestressing Strand (Seven-wire, Low Relaxation) | Grade | 270 ksi |
| | Modulus of Elasticity | 28500 ksi |
| | Ultimate Strength | 266 ksi |
| | Cross-sectional Area | 0.153 $in^2$ |
| | Poisson's Ratio | 0.3 |
| Mild Reinforcement | Grade | 75 |
| | Modulus of Elasticity | 29000 ksi |
| | Ultimate Strength | 104 ksi |
| | Cross-sectional Area | 0.31 $in^2$ |
| | Poisson's Ratio | 0.3 |
| Shear Reinforcement | Grade | 75 |
| | Modulus of Elasticity | 29000 ksi |
| | Ultimate Strength | 104 ksi |
| | Cross-sectional Area | 0.31 $in^2$ |
| | Poisson's Ratio | 0.3 |
| Elastomeric Pad | Modulus of Elasticity | 20 ksi |
| | Poisson's Ratio | 0.48 |

*3.3.1.3 Model Design*

After finding all necessary geometric and material properties, the next modeling step consisted of designing the mesh pattern of the cross-section. The locations of the nodes needed to match key features in the cross-section such as prestressing strands and mild reinforcement. The overall pattern was divided into quadrilateral shapes with similar-sized areas, as shown in Figure 11, so that the more erratic "free" mesh configuration option could be avoided. For model stability purposes, the areas could not have any excessively obtuse or acute angles, and for refined results and efficient modeling, a balance must be created for area size. Large areas do not provide accurate and smooth depiction of girder performance, while areas that are too small create a mesh pattern that is too dense and a model that is computationally too expensive. After multiple design iterations, a mesh pattern was selected and the element size along the length of the beam was selected to be 3 inches, since that correlates well with the variable spacing of shear reinforcement and it strikes a suitable balance between mesh density and efficient computation.

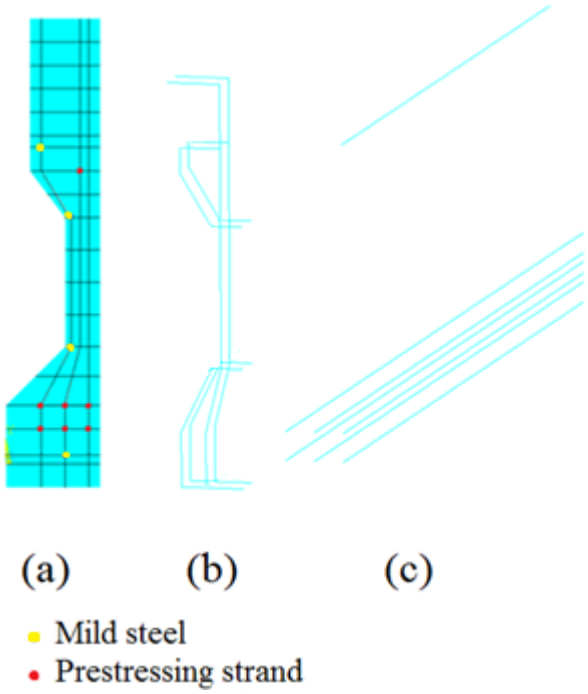


*Figure 11 - Phase I – (a) Mesh Pattern – (b) Shear Reinforcement – (c) Prestressing Strands*

Since the beam was fully symmetric, in both geometry and boundary conditions along its vertical axis, it was possible to only model half of the beam without affecting the results, as shown in Figure 11. This is due to the application of symmetric boundary conditions on the face of symmetry. These symmetric conditions partially restrain all the nodes on the face of symmetry in all three dimensions. This allows for substantial reduction of the number of nodes and elements, which in turn reduces the computational time of the model. A necessary modification due to this process was the division of one prestressing strand into two equal smaller strands. This is due to the location of that strand exactly at the vertical face of symmetry. Dividing the strand in half while keeping it on the same vertical level maintains the correct distribution of prestressing force while allowing the section to be split in two without causing any lateral moment due to asymmetric prestressing.

Shear reinforcement modification was another aspect of the model which was modified for efficiency. As shown in Figure 12, the reinforcement pattern for shear rebar was slightly modified so that the bars align with the predesigned mesh pattern. These modifications are marked in red in Figure 12.

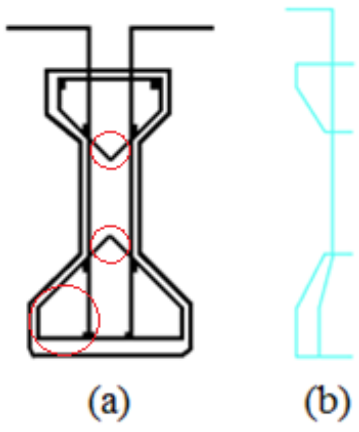


*Figure 12 - (a) Actual Shear Reinforcement vs. (b) Model Shear Reinforcement*

The initial prestressing force was known at the time of construction but over time, accumulated short-term and long-term losses reduced this initial force. For accurate modeling, an approximate value of prestressing force must be known. Prior to all destructive experiments, the investigators conducted moment cracking tests to calculate a theoretically sound estimate of the residual prestressing force in the test specimens.

The moment cracking test consists of the application of small midspan loads on the girders. The applied load steadily increased until a visible transverse crack appeared along the bottom of the beam. Upon crack appearance, the load would be removed and a strain gauge would be mounted at the location of the crack. Loads would be applied again to capture strain data while not exceeding any load that would result in permanent damage to the girders. After determining the cracking load and strain, the internal stress at the location of the strands can be calculated by summing the total stresses present at that location due to the effective prestress compressive stress, the bending stress due to prestress eccentricity, the moment due to self-weight, and the moment due to the cracking load. Figure 13 illustrates this concept of stress accumulation in prestressed concrete beams.

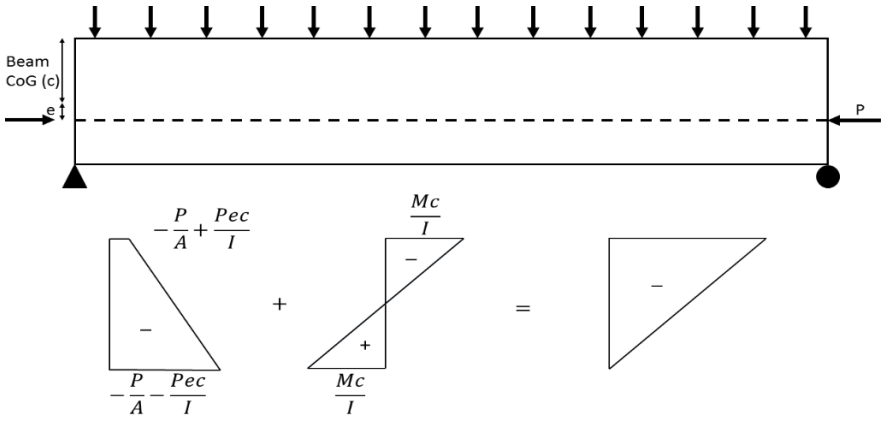


*Figure 13 - Stress Distribution in Prestressed Concrete Beams (Nawy 2009)*

Since the loads and geometric information are known, the only unknown variable in that formula would be the residual prestressing force. Through this procedure, the investigators

determined that 309 kips was the average remaining force between the beams with a 2% variation. The following equation was used to calculate the residual force in the strands, where $\sigma$ is the stress at the bottom of the girder. Information on the other variables and calculation process can be found in the appendix. Equation 3.3 is manipulated to form equation 3.4 by placing the unknown (P, residual prestress force) alone on one side of the equation.

$$\sigma = -\frac{P}{A_g} - \frac{P e_p C_g}{I_g} + \frac{M_{sw} C_g}{I_g} + \frac{M_{xt} C_g}{I_g} \qquad (Eq.\ 3.3)$$

$$P = \frac{\frac{M_{sw} C_g + M_{xt} C_g}{I_g}}{\frac{1}{A_g} + \frac{e_p C_g}{I_g}} \qquad (Eq.\ 3.4)$$

In the model, there were two different options to apply the prestressing force onto the girders. The first was the use of point loads at the ends of the girders; however, that setup resembles more the behavior of post-tensioned beams rather than pretensioned ones. Another possible option consisted of the application of initial stress or strain values to the strand elements directly. This option was selected in lieu of the first one since it best represents the mechanisms of prestressing in strands. Unfortunately, the LINK180 element does not have the option to input an initial stress in the element. Therefore, the use of a separate initial condition function was necessary to input the prestressing force in the strands. To determine the initial strain values, the 309-kip residual force value was divided by the area of the strands then converted to residual strain by dividing the stress by the strand modulus of elasticity. The following equation displays how the maximum prestressing strain along the length of the beam was calculated:

$$\frac{309\ kips}{\left(13\ strands * 0.153 \frac{in^2}{strand}\right) * 28500\ ksi} = 0.00545\ in/in \qquad (Eq.\ 3.5)$$

To correctly model strain accumulation in the prestressing strands, the transfer length must be taken into account. Transfer length is defined as the length over which the prestressing force is transferred from the stressed strands to the concrete by bond. Along this length, stress increases from zero at the end of the beam to full stress at the end of the transfer length. In this model, it was convenient, yet still accurate, to assume that stresses increase along a step function in 3-inch increments. The length of each step is equal to the length of each element along the length of the beam. The transfer length used was $50 * d_b$, where $d_b$ is the diameter of the prestressing strands. Since the strands' diameter is 0.5", transfer length was calculated to be 25". Since the beam length was divided into 145 3-inch long elements, the increase in prestressing took place over 8 stages before reaching full stress over a total length of 24". Table 3 summarizes this accumulation of strain as a function of distance. Figure 14 shows the contents of Table 3 graphically.

*Table 3 - Stress Accumulation in Strands along Beam Length*

| Distance along the beam (in.) | 0-3 | 3-6 | 6-9 | 9-12 | 12-15 | 15-18 | 18-21 | 21-414 |
|---|---|---|---|---|---|---|---|---|
| Strain (in/in) | 0.0007 | 0.00136 | 0.00204 | 0.00273 | 0.00341 | 0.00409 | 0.0048 | 0.0055 |
| Distance along the beam (in.) | 414-417 | 417-420 | 420-423 | 423-426 | 426-429 | 429-432 | 432-435 | |
| Strain (in/in) | 0.0048 | 0.00409 | 0.00341 | 0.00273 | 0.00204 | 0.00136 | 0.0007 | |

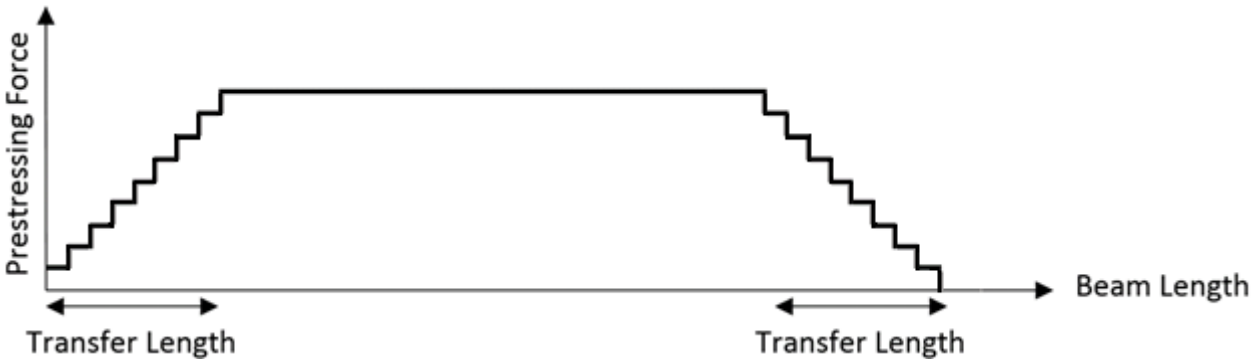


*Figure 14 - Prestress Force along Beam Length*

*3.3.1.4 Loading and Boundary Conditions*

As stated before, this study tested four girders each in a different load pattern. Load tests were completed at midspan, and at 4D, 2D, and 1D from the support, where D is the depth of the beam and the preceding number denotes the multiple of D. The character combination denotes the total is distance from the end of the beam to the point of load application. Figure 15 illustrates the 1D and midspan load cases as examples. This variety in loading scenarios allows for broader testing of the model and would help determine whether or not the latter has the capability of capturing accurate data for different failure mechanisms. A generic model was created for all 4 different load scenarios where the only difference between them was the location of the 12”x12”x2” (30 cm x 30 cm x 5 cm) steel loading plate on which the load was applied. Having a steel plate, rather than direct load application on the elements, ensures surface-to-surface load transfer and agrees better with the experiments.

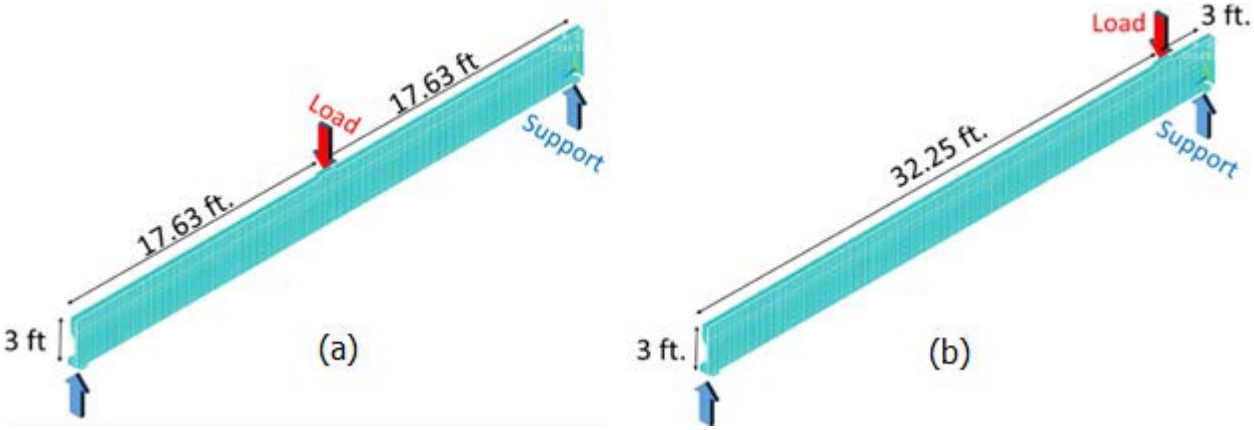


*Figure 15 - Phase I Finite Element Model Geometry – (a) Midspan Load – (b) 1D Shear Load*

After the completion of the model, the boundary conditions were defined. Since the inspectors stated that the beams were allowed to rotate at the ends on-site, the model recreated those conditions by applying simply supported conditions on the beams. With pin-roller supports to model the elastomeric pad under the beam, the boundary conditions best match the actual ones

applied in the laboratory experiment. The exact location of the lines of support were determined after several calibrating runs of the model. Figure 16 displays a view of the Phase I beam, some of its steel reinforcement, the loading plate, and the elastomeric pad.

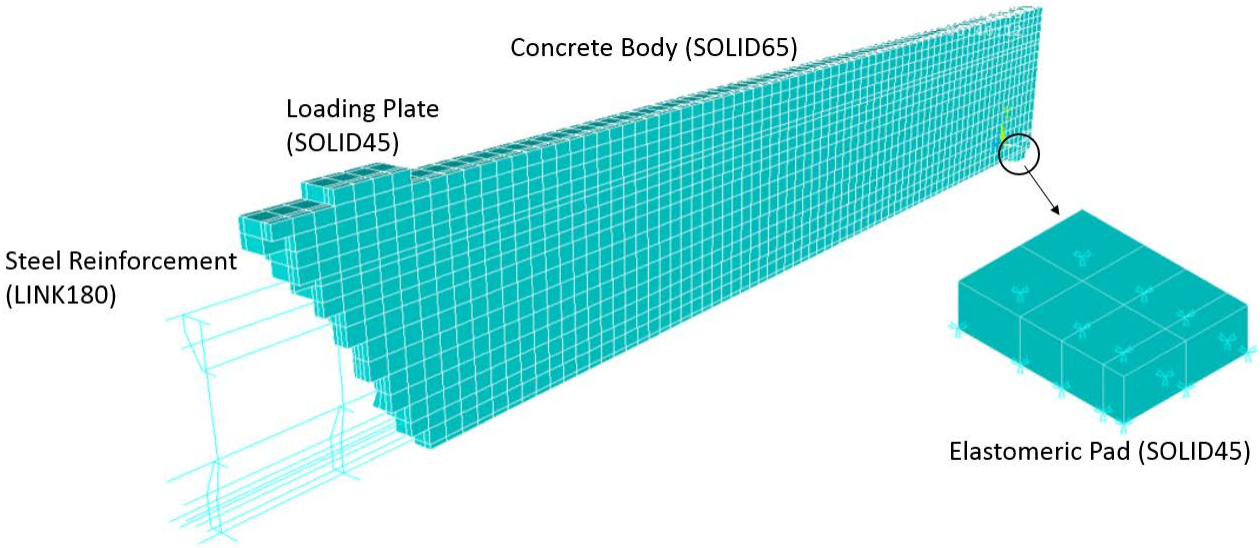


*Figure 16 - Phase I Beam Model*

### *3.3.2 Phase II*

Phase II focused on the development of a new system-level model to recreate the behavior of an intact bridge span. The successful validation of the Phase II model will allow for the capture of the various failure mechanisms of a more complicated, composite bridge system. Few documented ultimate capacity case studies on full prestressed concrete girder bridges were available in the literature. It is unlikely for entire bridge spans, still in good condition, to be removed from service and loaded to failure. Another obstacle was the vital need for sufficient material and geometric properties for model creation. The exclusive list of requirements made finding a suitable case study even harder to find in the literature.

*3.3.2.1 Bridge Description*

Bridge 35-17-6.80 located in Fayette County, Ohio failed its inspection due to the deteriorated conditions of one of its spans, and it was scheduled for replacement in 2012. At the time, it was 43 years old and it consisted of three equal spans supported by piers or abutments. Overall, the structure's other spans were deemed structurally sound enough to be suitable candidates for full-scale destructive testing. Through these tests, investigators aimed to better understand the ultimate capacity behavior of this type of structure. The investigators also chose to input damage onto the west span while keeping the center span intact to act as a control. The west span was damaged through a 2" deep sawcut into the bottom of the three interior beams, severing 14 strands per beam, or a total of 42 strands. For this phase, the intact system level behavior is to be captured through modeling. Since structural inspection concluded that there was minimal degradation of the center span of the bridge, shown in Figure 17, the candidate was taken to be in an undamaged state.

*Figure 17 - Phase II - Center Span (Steinberg, 2011)*

The adjacent box-beam bridge was tested to full capacity on-site to obtain experimental data on the overall performance of the system. The bridge had three spans, each consisting of 9 adjacent concrete box-beams made transversely composite through shear keys and transverse tie

rods. Each bridge span was 47’ 10” long with a 15º left forward skew. The spans were initially continuous, as they were connected together through overlapping reinforcement in a field pour joint, but those bars were cut prior to testing. The bridge’s connection to the piers was provided through the combination of dowel bars and mortar beds. Modeling boundary condition is discussed in more detail later in this section. Figure 18 shows a plan view of the bridge, along with some of its internal lateral reinforcement.

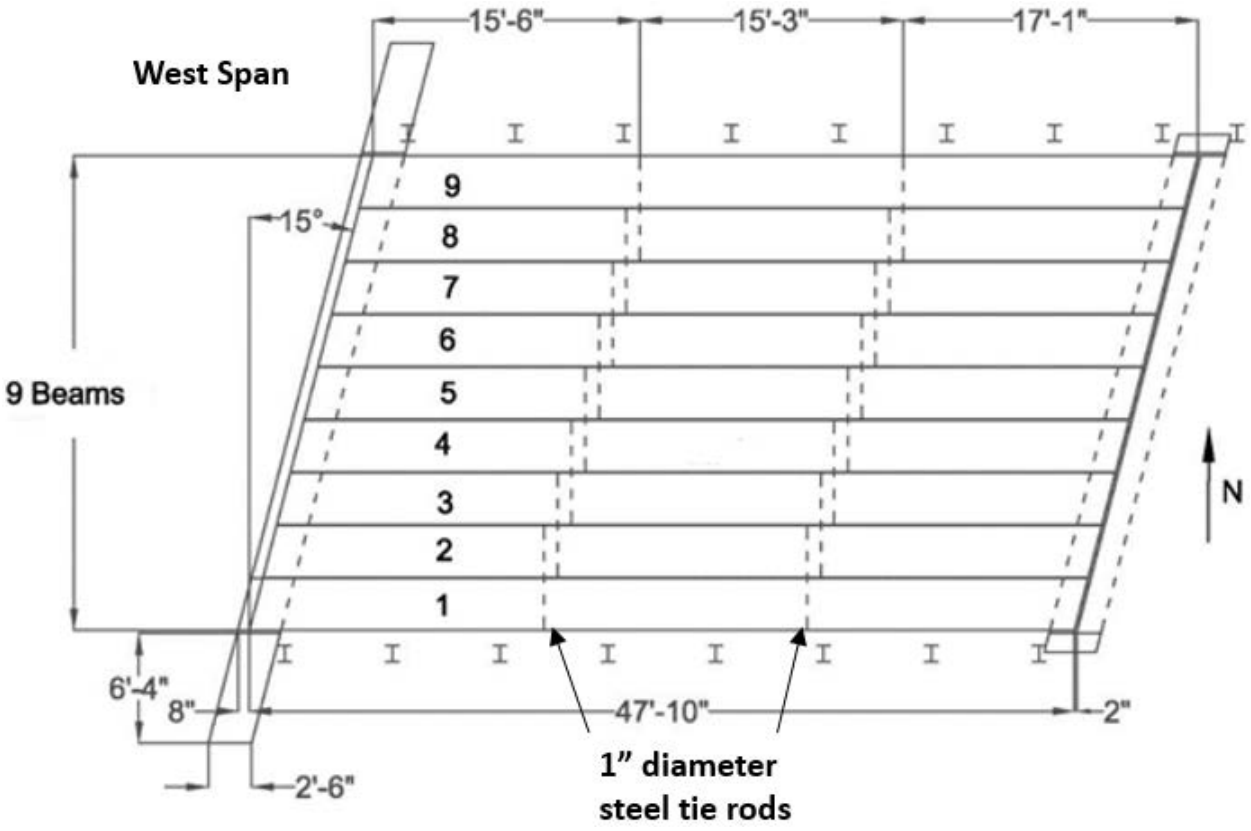


*Figure 18 - Bridge Plan View*

This work is one of the few suitable case studies that considered the full-scale destructive testing of a prestressed concrete beam bridge, and reported enough information on the test setup and response results. The graduate thesis, papers, and referenced reports (Steinberg et al. 2011, Huffman 2012, and Huffman et al. 2012) provided information on the extensive case study which consisted of the on-site, full-scale destruction of a prestressed adjacent box beam bridge whose

cross-section is shown in Figure 19. Figure 20 shows the structural details of the box-beam in greater detail.

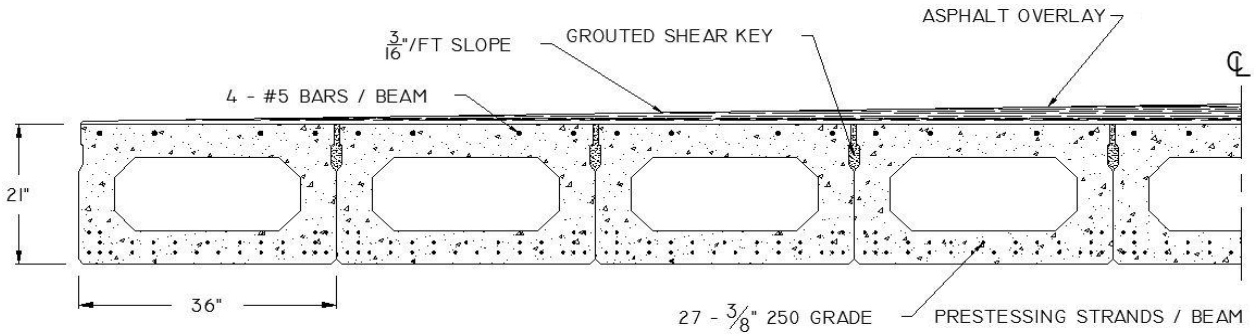


*Figure 19 - Phase II Cross Section (Huffman, 2012)*

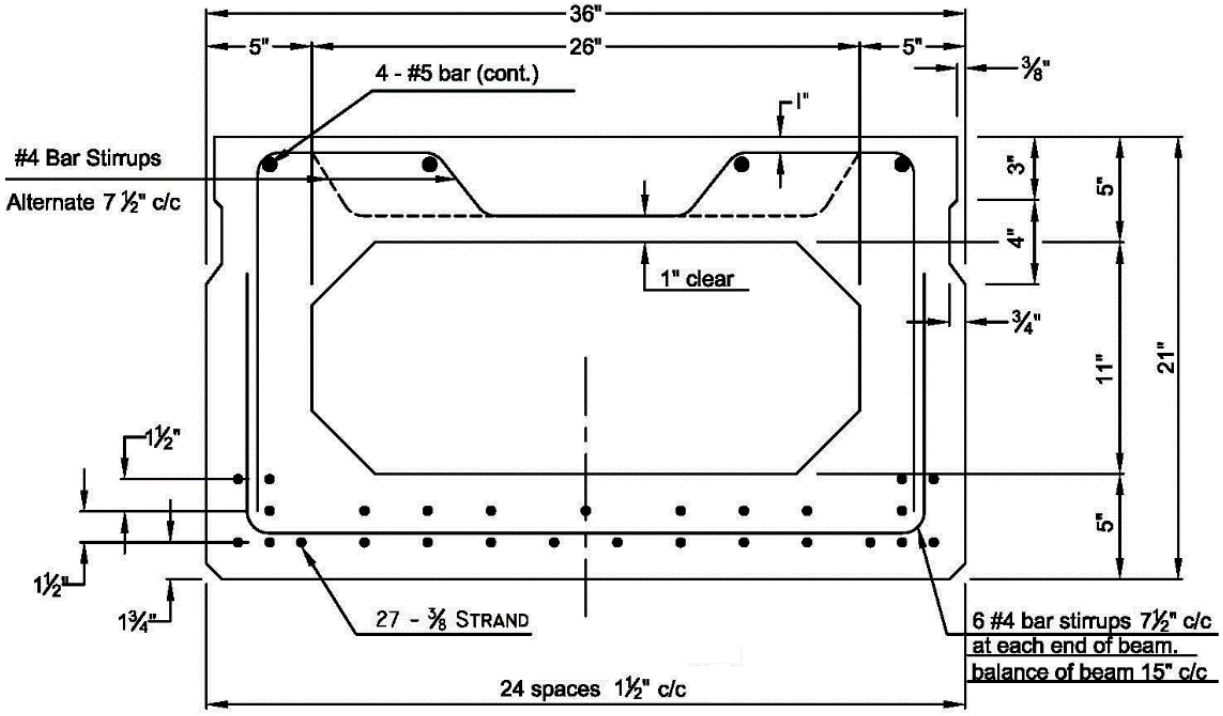


*Figure 20 - Box Beam Cross Section (Huffman, 2012)*

*3.3.2.2 Bridge Instrumentation and Testing*

The bridge was instrumented along its midspan and one of its quarterspans with strain gauges and string potentiometers. Every beam was instrumented with 4 strain gauges along the midspan and quarterspan on the bottom and top faces of the beams. The asphalt wearing surface was ground down and thoroughly cleaned so that the gauges could be applied directly on the

concrete beams. String potentiometers were also mounted at the same location as the gauges. Figure 21 shows the layout of the sensors.

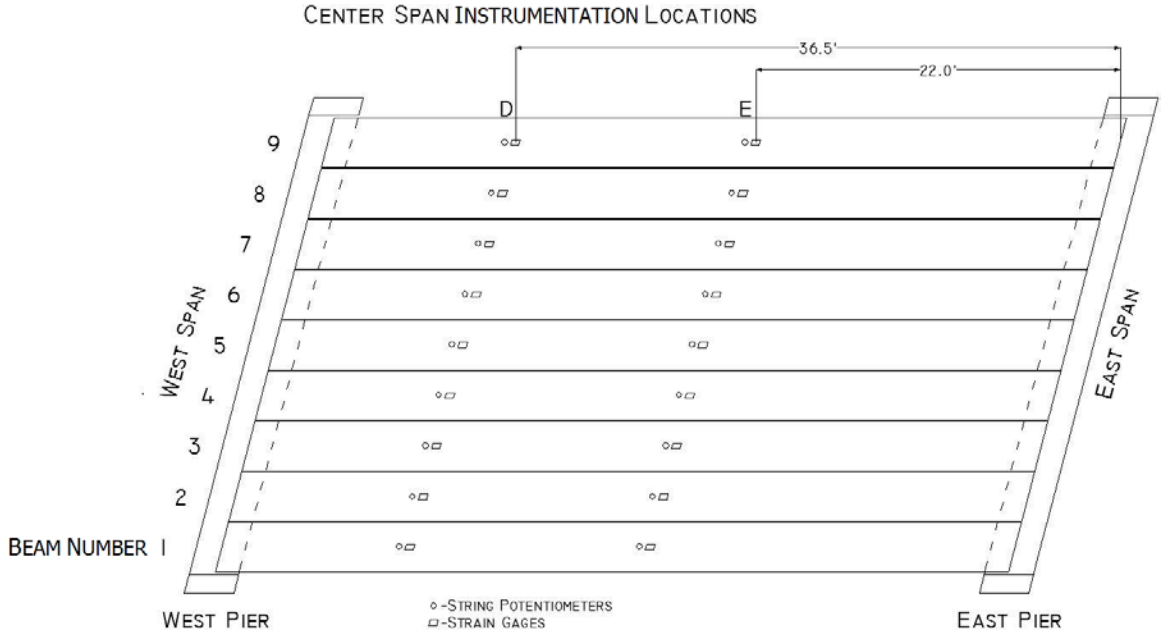


*Figure 21 - Instrument Layout (Huffman, 2012)*

Three steel structural test frames were designed, then installed on-site to withstand a force sufficient to load the structure to failure. Three hydraulic cylinders, each with a capacity of 350 kips, were used to load the bridge span in the configuration shown in Figure 22. Two 4-foot long sections of W6x25 spreader beams were placed side-by-side between the cylinder and the bridge to ensure that the hydraulic jacks did not punch through the box flanges. Each pair of spreader beams was large enough to apply loads on three beams at a time, but due to the spreader beam configuration, the middle of the three beams were assumed to carry a much more significant part of the load than its counterparts.

The three hydraulic cylinders were loaded equally as investigators loaded the bridge spans to their ultimate capacities. Each of the three cylinders were simultaneously loaded up to a

maximum of 150 kips. Loads in all cylinders were increased steadily in 50-kip increments until span failure was reached.

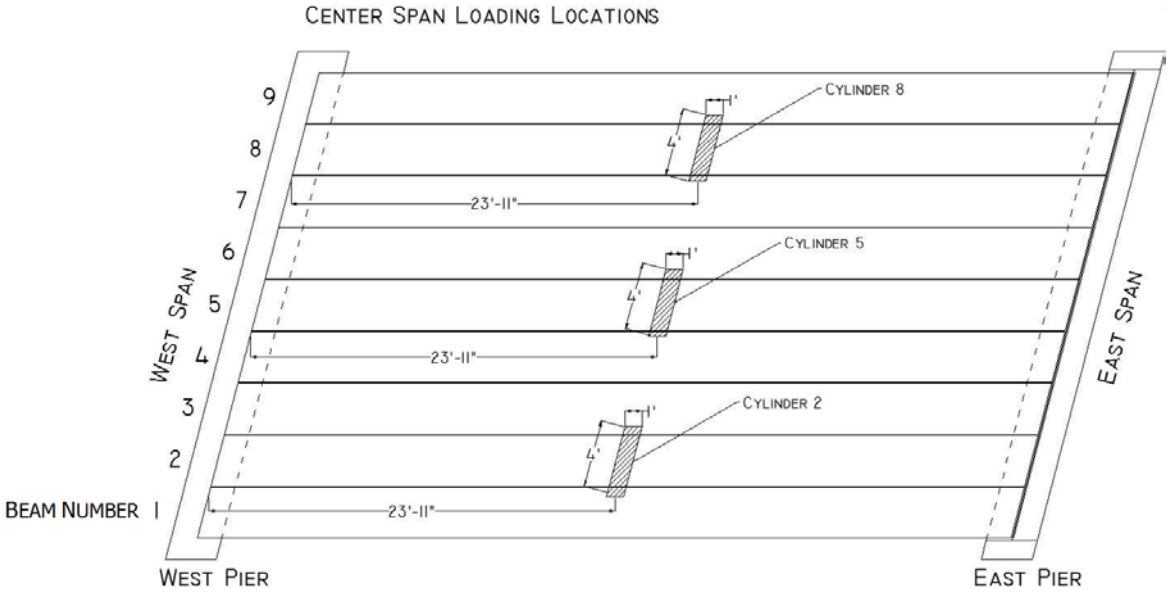


*Figure 22 - Load Configuration (Huffman, 2012)*

*3.3.2.3 Material Models*

Most material properties for the structure at the time of the test were available in the study. The investigators took concrete samples from the bridge and determined that compressive strengths of beam and shear key concrete averaged about 10 ksi. Wolanski's work (2004) was used again to model the stress-strain behavior of the both types of concrete used. Even though concrete strengths for both the shear key and the beams themselves were the same, shear keys were modeled to have lower strengths than the beams. The following section further discusses the rationale behind that modification.

Material properties for mild steel were challenging to determine since the study does not specify which grade steel was used for longitudinal and shear reinforcement. The AASHO Standard Specifications for Highway Bridges (1961) was most likely used at the time of the bridge design since the bridge was built in 1969. The AASHO specification referenced ASTM standard

A15 for mild reinforcement steel. However, that standard was withdrawn and replaced by A615 in 1969 so that version of the standard was reference. The A615-69 reference states that steel yield can either be 40 ksi or 60 ksi with tensile strengths of 70 ksi and 90 ksi respectively. Since no information was provided by the authors, both were modeled and it was eventually determined that the grade 40 version correlated better with the results. Similarly, properties of prestressing strands were readily available in documentation in effect at the time (ASTM A615-69, AASHO 1961). Material properties used in Phases II and III were summarized in Table 4.

*Table 4 - Phase II Material Properties*

| | | |
|---|---|---|
| Girder Concrete | Compressive Strength | 10 ksi |
| | Modulus of Elasticity | 5 ksi |
| | Tensile Strength | 0.75 ksi |
| | Poisson's Ratio | 0.2 |
| Shear Key Concrete | Compressive Strength | 2 ksi |
| | Modulus of Elasticity | 2.79 ksi |
| | Tensile Strength | 0.27 ksi |
| | Poisson's Ratio | 0.2 |
| Prestressing Strand (Seven-wire, Low Relaxation) | Grade | 250 ksi |
| | Modulus of Elasticity | 27500 ksi |
| | Ultimate Strength | 246 ksi |
| | Cross-sectional Area | 0.16 $in^2$ - 0.32 $in^2$ |
| | Poisson's Ratio | 0.3 |
| Mild Reinforcement | Grade | 40 |
| | Modulus of Elasticity | 29000 ksi |
| | Ultimate Strength | 70 ksi |
| | Cross-sectional Area | 0.31 $in^2$ |
| | Poisson's Ratio | 0.3 |
| Shear Reinforcement | Grade | 40 |

| | | |
|---|---|---|
| | Modulus of Elasticity | 29000 ksi |
| | Ultimate Strength | 70 ksi |
| | Cross-sectional Area | 0.2 $in^2$ |
| | Poisson's Ratio | 0.3 |

Similar to the Phase I model, all material properties were input into the model and multiple versions of the same element were created to be used under different conditions. Most real constants were reserved for prestressing strand elements with initial strain variation.

*3.3.2.4 Model Design*

The model's cross section was meshed in the same process followed for Phase I. A mesh pattern was designed to create a simplified cross-section while taking optimum mesh density and all structural key features in the beam into account. For this bridge, the element sizes along the length of the beam were all 7.5" long except for the first and last elements, which were 2" long. This is due to the location of shear reinforcement, as the first set of shear reinforcing bars were 2 inches away from the end of the beam. After the first line of support, spacing varies in increments of 7.5". Also, in accordance with the specified beam geometry, the interior of the beams was voided throughout the entire section except for 17" in from either ends. Figure 23 displays both bridge model features.

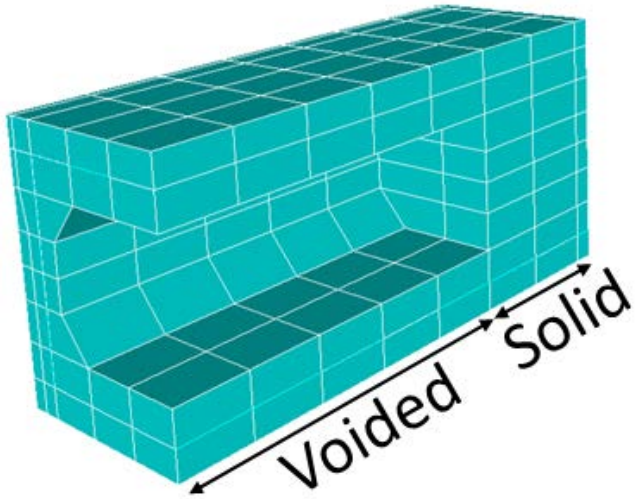


*Figure 23 - Inner View of Box Beam near a Support*

The model incorporated several minor simplifications, including modification to its geometry and shear reinforcement, grouping of prestressing strands, and transverse tie reorientation to help reduce model complexity and streamline the modeling process. Moreover, the asphalt overlay was not included in the model due to its low stiffness and expected limited relative contribution to the system's structural behavior (Huffman et al. 2012).

Since the structure was prestressed using multiple small-diameter strands, it was necessary to group multiple strands and form larger ones. Exact modeling of the strand pattern would create an extremely dense mesh in that area. An equivalent strand pattern was created to reduce the number of nodes and elements to a numerically efficient level. To relocate and regroup the strands without altering their effects on the system, symmetry must be maintained about the vertical axis and the height of their center of gravity must remain unchanged. Strands were grouped in numbers of 2 to 4. This reduced them from 27 individual strands to 9 strand groups that have the same prestressing effect on the system. Figure 24 (a) shows the actual layout of prestressing strands in the box-beam, and the red circles mark how each set of strands was grouped. Figure 24 (b)

illustrates the modeled FEA mesh pattern. Comparing strand locations in both versions shows how the centers of gravity of the actual strand pattern and the reorganized pattern are equal.

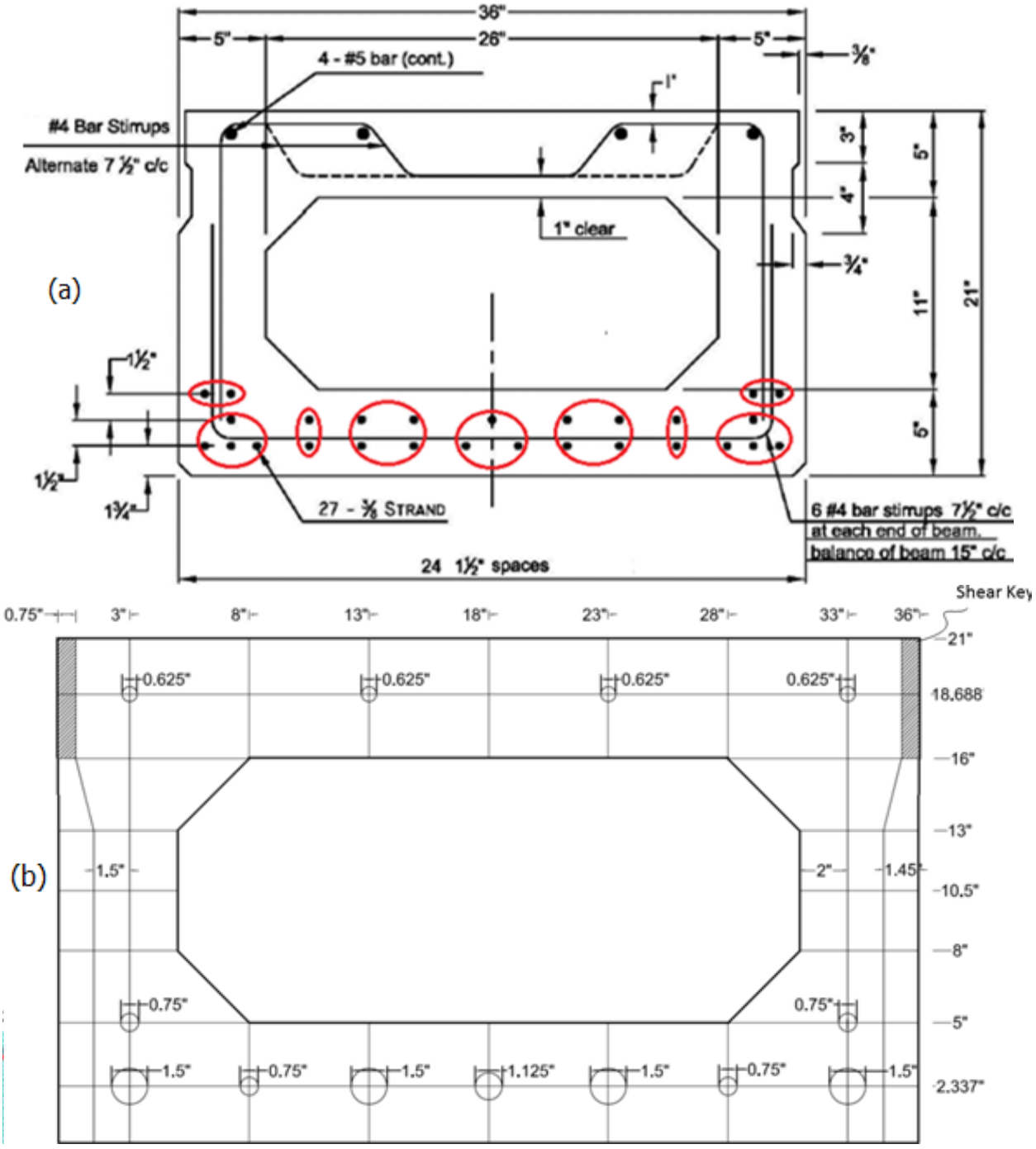


*Figure 24 - (a) Strand Grouping, (b) Mesh Pattern*

Aside from the strand reconfiguration, slight geometric variations can be observed between the model and the actual beam, the most prominent of which being the shear key. An exact model of the shear key created model convergence problems as element shapes became too small or irregular. The simplified shear key design has a cross-sectional and a contact area similar to that of the actual key. To ensure the contact area is correct, the beam was modeled to have a small difference in widths of the top and bottom flanges. The reasoning behind this simulation is to keep the beams from merging and acting monolithically along the entire depth. Figure 25 shows an exaggerated illustration of the modified shear key design, as the clear distance between the beams is much smaller than what it shown.

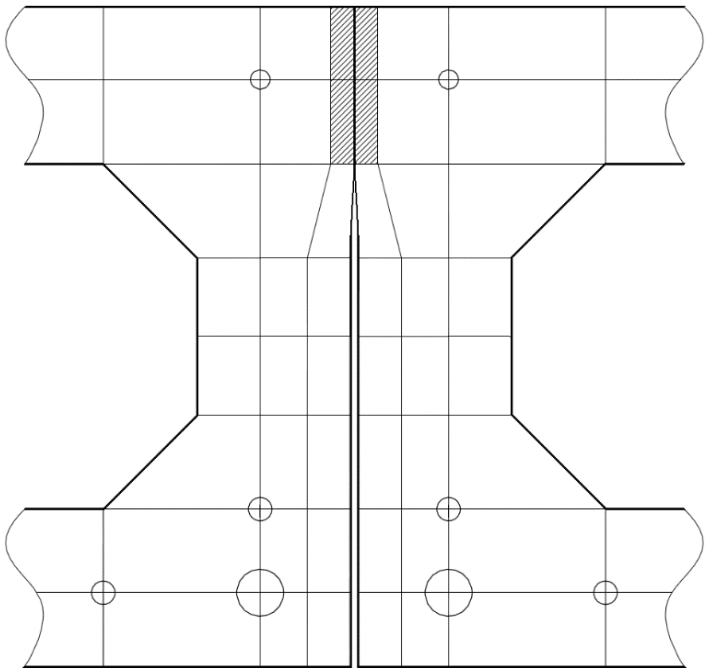

*Figure 25 - Shear Key Model*

When multiple beams are created along the width of the bridge, the top 5” (top two elements) are in full monolithic bonded contact. The concrete below the 5” mark from the top starts to diverge away from adjacent beams by a miniscule distance of 0.05”. This would allow the beams to merge along that 5” deep area but remain unmerged for the bottom 16”. This

simplification takes into account the geometric shape of the shear key, and the bonded area between beams. To take into account the weakness along the bond between the concrete and the shear key, other measures were taken.

Since the bond strength between the shear key and the beams was unknown and difficult to estimate due to both mechanical and chemical contributions, this issue was tackled from a different perspective. The authors reported that the shear keys had the same compressive strength as the beams. However, the bond strength between the shear key and the beam's concrete is likely significantly weaker than the internal strength of concrete itself (Carbonell, 2014). In the developed model, the bond was made to be monolithic but the connection strength was compromised by reducing the strength of the shear key. The strength of the shear key was then calibrated through several model runs until the performance was matched.

Two other designs were considered along the progression of the shear key modeling process. The first method disregarded the presence of a shear key altogether and connected the beams monolithically through the top 5". It was found that this design oversimplified the connection and it produced overly stiff results, which required much revision. The second design consisted of the incorporation of contact elements between the beams to act as shear keys. These special elements are defined by a modulus of elasticity and a coefficient of friction. These elements had options that can be altered to restrict movement along certain axes. These contact elements triggered a lot of convergence issues and took a significant time to overcome. After much model refinement, the elements worked and produced the expected load-displacement behavior. However, some overall system failure characteristics, such as shear key cracking along the span length, could not be captured. The deflected contour shape near the supports did not match the experimental case either, so the endeavor to utilize contact elements in the model was abandoned.

The final design approach worked as somewhat of a functional representation of the connection between the beams. The combination of weaker shear keys and monolithic bonds, equated to the combination of strong shear keys and weak bonds best simulated the effects of shear keys on the bridge system. Figure 24 (b) displays the box-beam cross-section's final design (Stolarski et. al, 2006).

Another assumption was the transformation of the irregularly shaped shear bars into straight hoops since modeling exact angles and dimensions of the bars would cause a minimal difference in the scope of the entire bridge. It would also require much model refinement and would result in an excessively dense mesh pattern. The bar overlap and variable spacing were taken into account by varying the cross-sectional area of the bars through real constants. Figure 26 displays a section of a single beam's mild reinforcement cage.

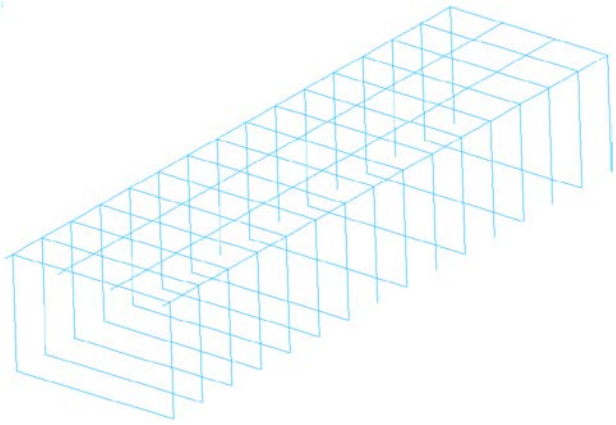

*Figure 26 - Phase II Beam Mild Reinforcement Cage*

The prestressing strands were modeled in a fashion similar to that of Phase I, where the strain in the strands gradually increased in step increments from the beam's edge until the end of the transfer length. In contrast to the study in Phase I, where the amount of prestressing was known, a challenge faced in this phase was the lack of any information on the residual prestressing in the strands at the time of the test. Without a specific value for prestressing forces, residual strain values

had to be estimated. This task can be somewhat challenging as described by Osborn et al. (2012); nevertheless, there are several techniques that may be used to converge on a rational estimate.

Initially, the jacking force input in the strands at the time of construction was estimated to be the maximum allowable prestressing force. Since the type of strands used at the time of construction (1969) is likely to have different properties than strands in use today, historic versions of ASTM standards used at the time were referenced to find strand material properties and proper allowable initial prestressing forces (ASTM A615-69, AASHO 1961). Even though this value may not represent the actual amount of stress in the strands, it provided a theoretical upper bound. Initial prestressing was later calibrated through the creation of a Magnel (Allowable prestressing - eccentricity) diagram for the box-beams. Since the actual eccentricity is known, the diagram provides a range of acceptable prestressing forces that would not violate the beam's capacity at any time, as shown in Figure 27. The safe range, shown in green, turned out to be larger than the ultimate strength of the strands, but multiple iterations of the model using a variety of prestressing values within the acceptable range helped converge on the most likely value at the time of the test. (Nilson, 1987). The equations and calculations used to create the diagram are included in the appendix.

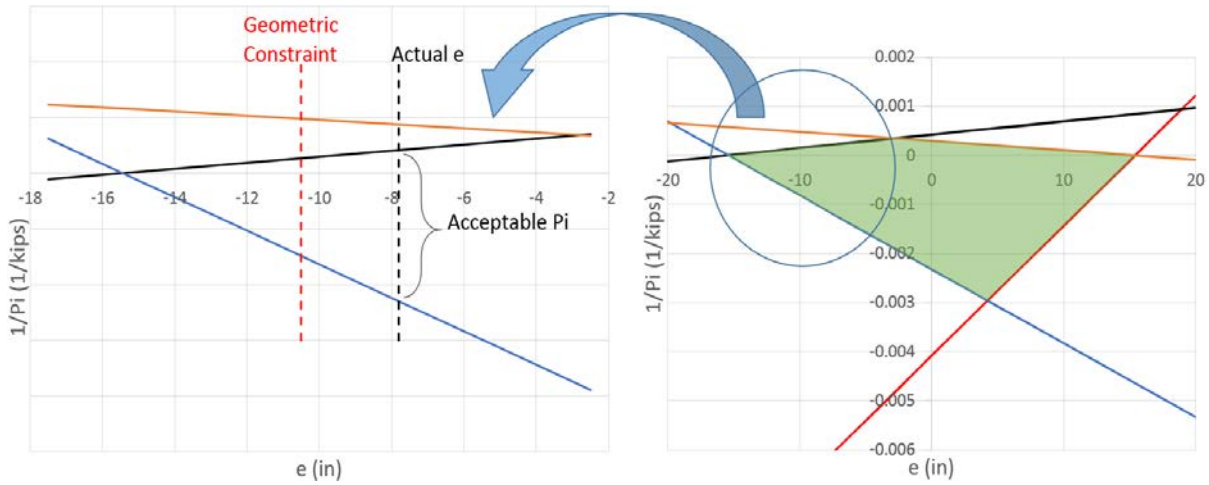


*Figure 27 - Magnel Diagram*

To find residual prestressing at the time of the test, the total accumulated losses over 43 years of service were then subtracted from the initial prestressing force in the strands after short-term losses, including elastic shortening and long-term losses such as steel relaxation, creep and concrete shrinkage were estimated.

It is well-established that as soon as prestressing loads are applied to concrete elements, instantaneous and long-term effects reduce this initial force input. It is important for engineers to determine the extent of those losses as they may have some significant detrimental effects on their designed structures. Finding out the exact magnitude of those losses without direct measurement is not achievable, as system losses are highly sensitive to a number of external and internal factors. Various institutes and organizations have suggested recommendations for prestress loss estimation. The approaches and rigor of these equations vary widely, but they are divided into two main categories: lump-sum losses, and approximation equations for each source of losses. Nawy recommends that the lump-sum is more desirable for standard conditions, but detailed loss analysis is more appropriate if loading and exposure conditions are unknown. Due to the lack of information, detailed analysis was conducted to converge on the correct amount of prestressing loss. Calculations for these losses can be found in the appendix.

Transfer length was again taken into account in the prestressing strand modeling process. For this phase, elements were 7.5” long so stresses increased along a step function in 7.5-inch increments. The length of each step is equal to the length of each element along the length of the beam. The transfer length used was also taken to be $50 * d_b$, where $d_b$is the diameter of the prestressing strand. Since the strands’ diameter is 0.375”, transfer length was calculated to be 18.75”. The beam length was mostly divided into 2-inch and 7.5-inch long elements, so the increase in prestressing took place over 3 stages before reaching full stress over a total length of 17”. Table 5 summarizes this accumulation of stress as a function of distance. Similar to Phase I, Figure 28 illustrates stress accumulation in the strands graphically.

*Table 5 - Stress Accumulation in Strands along Beam Length*

| Distance along the beam (in.) | 0-2 | 2-9.5 | 9.5-17 | 17-559 | 559-566.5 | 566.5-574 | 574-576 |
|---|---|---|---|---|---|---|---|
| Strain (in/in) | 0.001 | 0.002 | 0.003 | 0.004 | 0.003 | 0.002 | 0.001 |

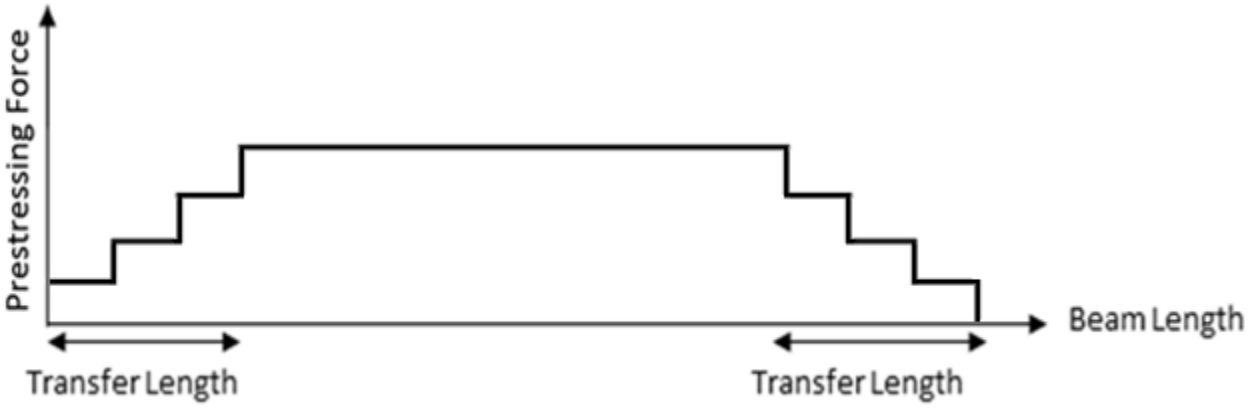


*Figure 28 - Prestress Force along Box-beam Length*

*3.3.2.5 Loading and Boundary Conditions*

The loading and boundary conditions for this phase were well described in the reports. Spreader beam dimensions and hydraulic cylinder loadings were accurately replicated in the model. The areas of load application on the bridge were input into the model direct load application on the respective nodes. The number of loaded nodes on each beam directly correlated with the loaded areas on the actual bridge. The boundary conditions were also well described through structural plans of abutment and pier connections. Anchorage to the supports was achieved through dowel bar and mortar bed action. Multiple modeling approaches were considered in the accurate replication of these conditions; the scenario which agreed the most with the reported results was that of a simply supported beam.

Pin-roller supports were input at the line of nodes along the width of the span at the locations of the dowel bars. Even though the connection is quite long, the dowel bars act as a fulcrum, providing rotation and translation restraint in early stages of loading. The assumed simply supported conditions are not completely accurate, as the mortar bed contributes some stiffness to the system. Figure 29 shows the cross-section of the beam's end.

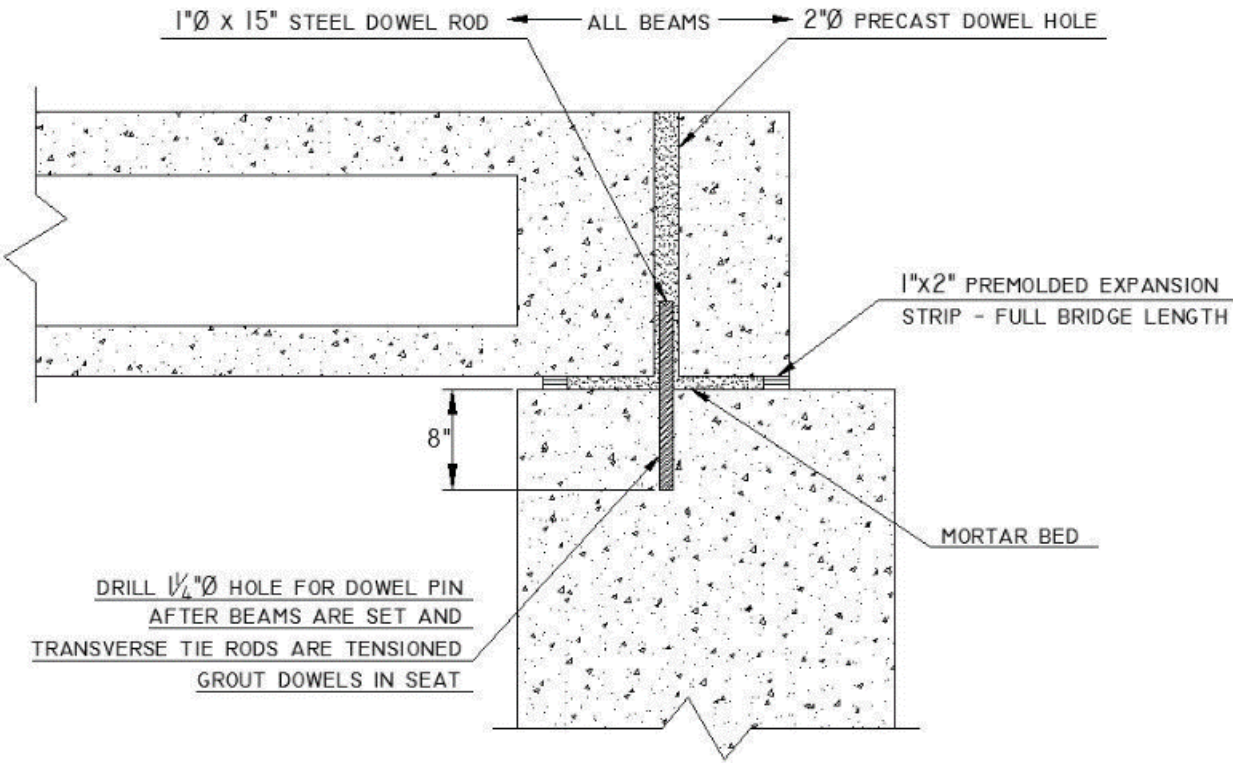


*Figure 29 - Phase II Support Detail (Huffman, 2012)*

The aforementioned material and structural properties were combined to create the model shown in Figure 30. Section (a) shows the final layout for the modeled beam while (b) shows the entire bridge.

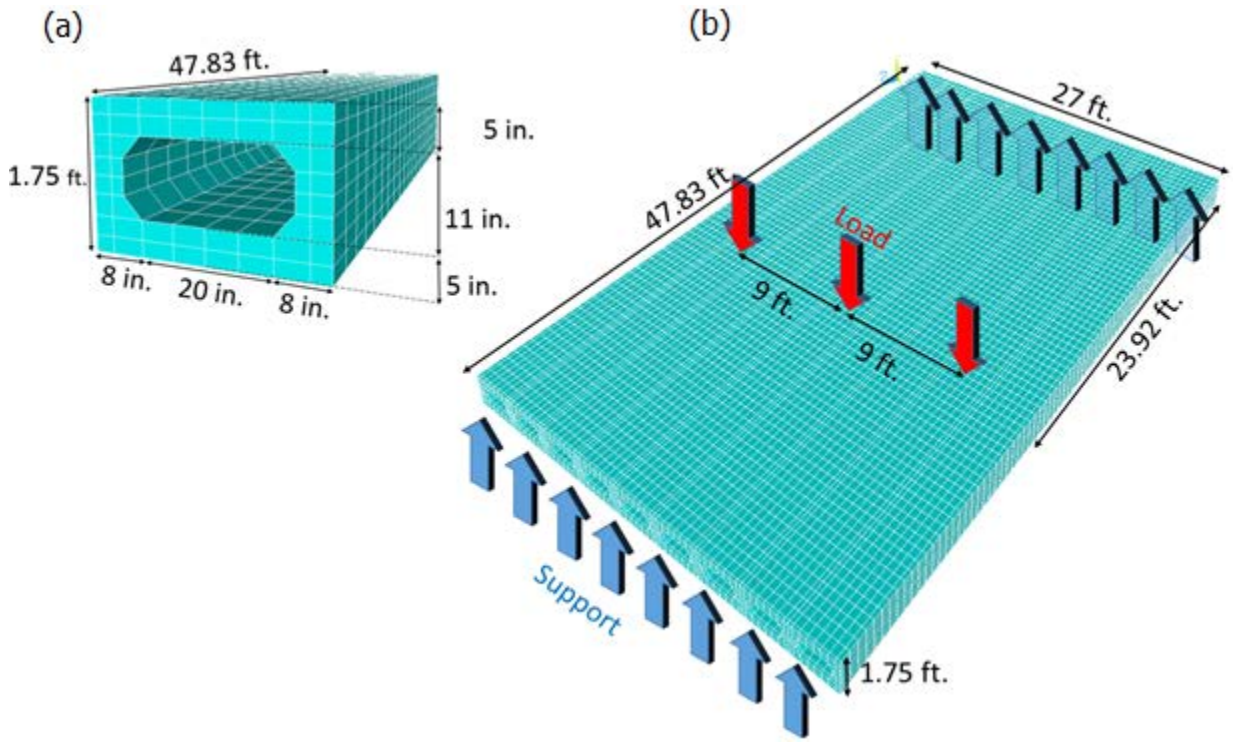


*Figure 30 - Phase II (a) Beam Cross-section - (b) Bridge Geometry*

### *3.3.3 Phase III*

The third and final phase of this thesis focuses on the integration of damage in the model, and correctly reproducing the experimental response. While the time-consuming part of model creation was averted, modeling the damage properly was not very straightforward. Phase III is implemented directly on the model created for the second phase. Since the Huffman (2012) case study tested damaged and intact versions of two almost identical spans, there was no need for the creation of a new model. Various common types of damage scenarios such as corrosion, strand rupture, and section loss could have their mechanisms input into the model in order to gauge their effects on the system.

In the experiment, damage was introduced to the west span of the bridge by sawing two 2" deep cuts, 3 feet apart, into the 3 middle beams, in effect rupturing 14 strands in 3 beams (for a

total of 42 severed strands). For Phase III, this damage was modeled on the FEA platform to capture the reduction in system capacity due to strand rupture and effectively recreate the system damage reported by the case study investigators. Figure 31 shows the actual cuts made in the bridge by the investigators. Concrete was chipped away at the location of the cuts to verify strand rupture.

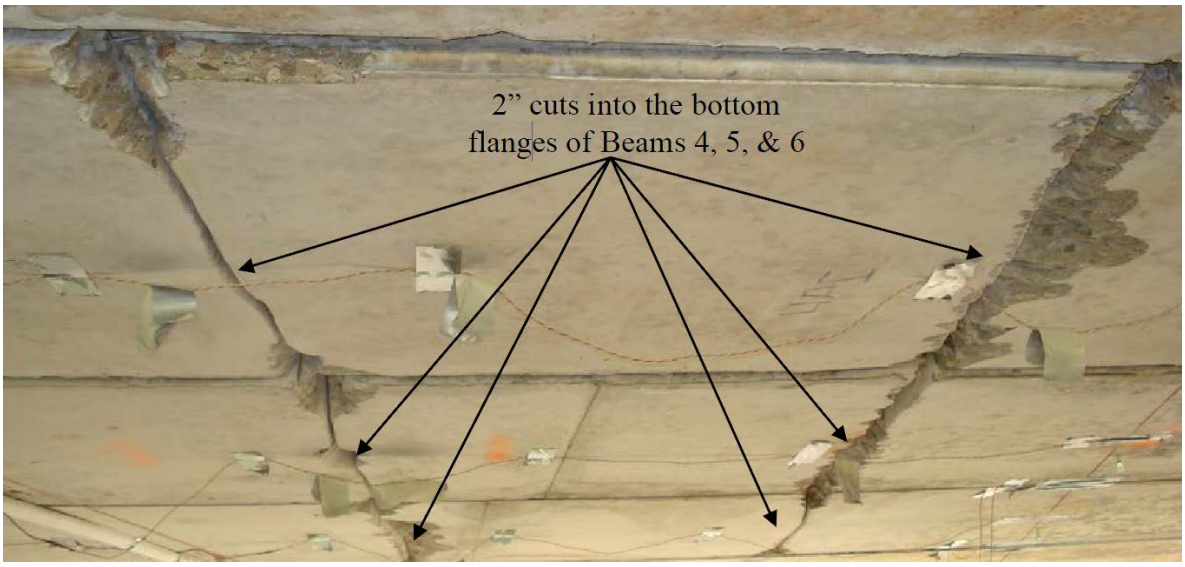


*Figure 31 - Phase III Bridge Damage*

To model the damage, the rows of severed strand elements were removed from the midspan along the width of the three affected beams. Since the strands were grouped in numbers of 2, 3, and 4, severing the exact number of individual damaged strands could not be achieved while maintaining symmetry. A total of 16 strands instead of 14 were ruptured as marked by the "X" in Figure 32. This damage configuration was found to be that most suitable as it avoided any structural deviations from the experiment. An alternative modeling approach would consist of the reduction of strand cross-sectional area so that the damaged section will have similar effective strand area as that of the intact strands remaining after sawcut damage.

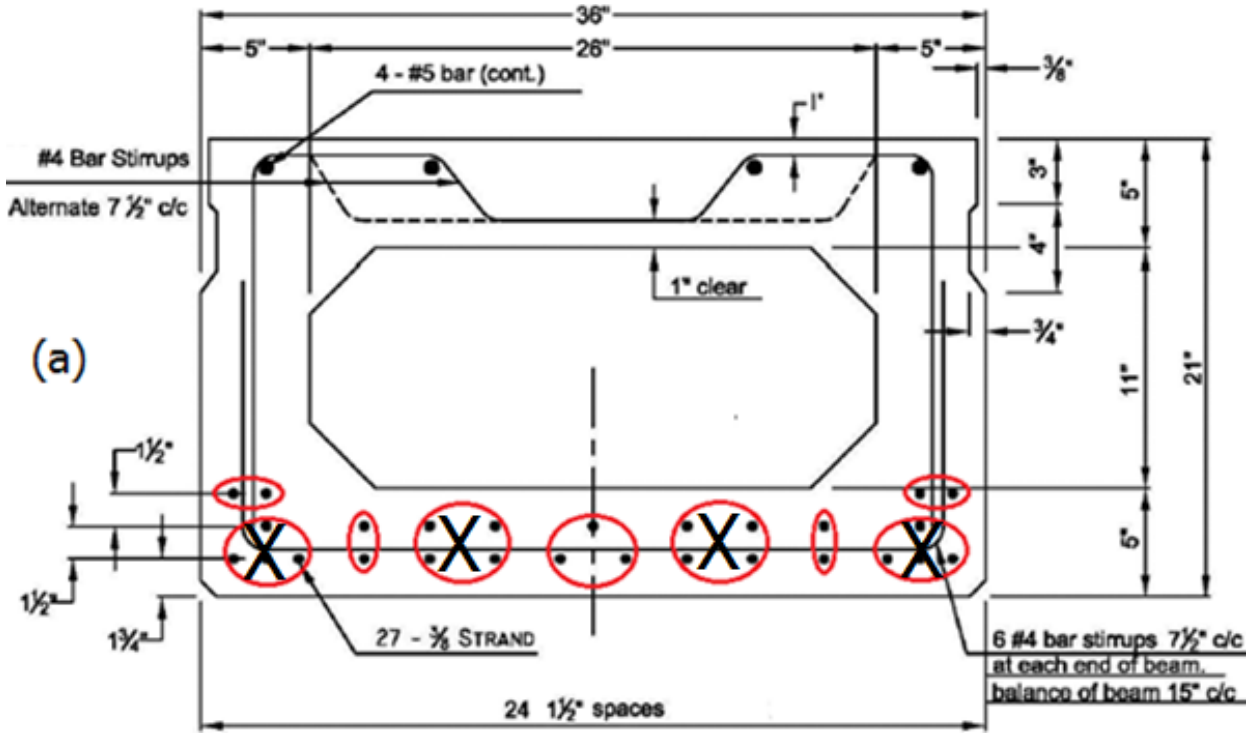


*Figure 32 - Phase III Strand Damage Configuration*

The amount of prestressing in the strands and its effective moment arm changes at the location of the damage as displayed in Figure 33. The strand centroid shifts upwards, and stress in the strands increases incrementally from zero at the location of the damage into the beam until full prestressing is achieved, similar to the transfer length behavior observed at beam ends. The transfer length was again considered to be $50 * d_b$, where $d_b$is the diameter of the strand or 0.375 inches.

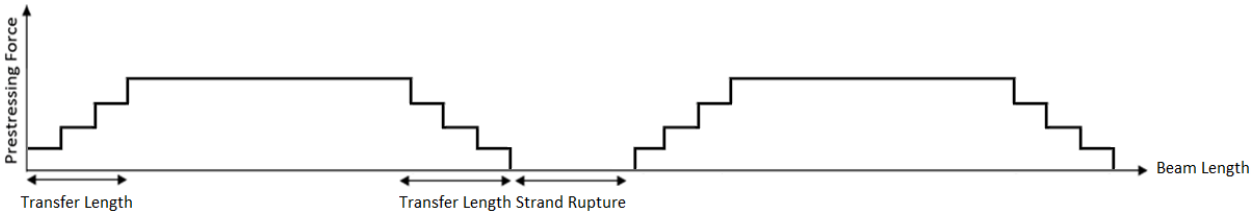


*Figure 33 - Phase III Prestress Evolution along the Length of the Bridge*

Furthermore, to model the section loss in the damaged concrete, the tensile capacity of the concrete was reduced to almost zero at the location of the cuts. This allows for cracking to happen

soon after the bottom of the beams decompress, thereby transferring the tension directly to the strands. Figure 34 (a) displays the sawcut concrete sections while Figure 34 (b) shows the severed strands.

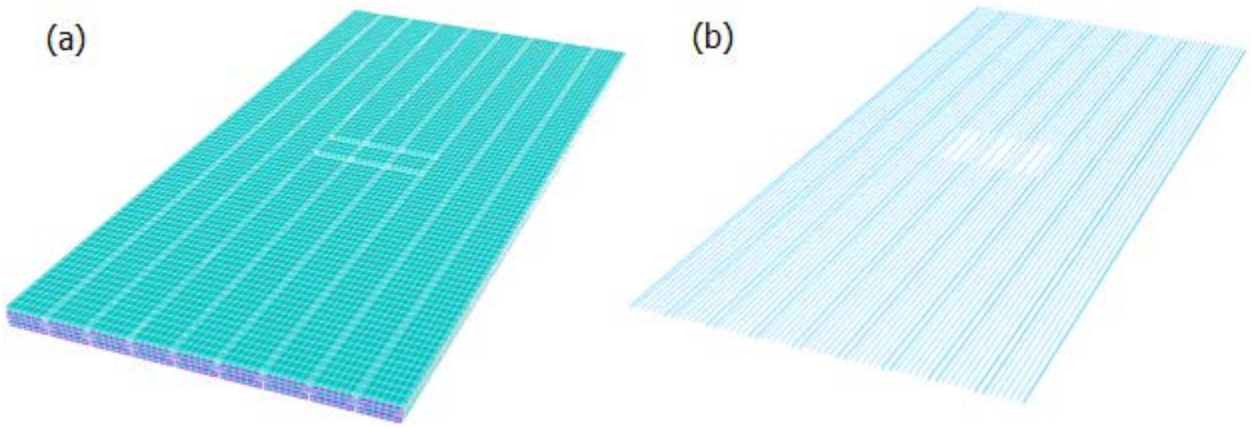


*Figure 34 - Phase III Model Damage*

While the sawcut damage input into the previously developed intact bridge model seems simple in practice, its local and global effects on the system were difficult to model. Simply removing the strand elements from the model to replicate damage did not reduce its capacity to the extent achieved by the inspectors. After several iterative models, transfer length effects at the location of the cuts, and a 10% reduction of tensile strains in the strands recreated the expected behavior. The exact amount of prestress loss is dependent on a multiple of factors such as bond-strength between the strands and the surrounding concrete and the gap thickness due to the sawcut. These factors may cause the strands to retreat into the beam or they may allow the beams to camber up because of the generated gap thereby reducing the residual strain by a significant amount. The works of Miller (2007), Rosenboom (2006), and Nguyen (2013) support this proposal by showing a reduction in tensile strains and prestress forces in undamaged strands after other ones are ruptured. The selected 10% value was an appropriate value found after multiple model iterations.

# 4.0 RESULTS AND DISCUSSION

The three calibrated models provided much data including element stresses and strains, system deflections and crack patterns. Qualitative structural features such as material plasticity, stages to failure, and system failure modes were also captured by the model. In order to validate each model and progress to the next phase, it was necessary to compare data extracted from the models to experimental results reported by the investigators. The three experimental studies had various criteria to which the models' output could be compared. Before comparing all available data, the load-deflection graphs were selected to act as the benchmark for initial comparison. In other words, if the model's load-deflection data were found to match those of the experiment, the model is checked to see if specific events that occurred during actual experimental system failure were replicated. Examples include cracking pattern in the concrete, deflection profile of the structure, and failure modes. Load-deflection curves were selected to be the initial evaluation standard since they compare overall structural performances as the specimens are loaded, and experimental data were readily available in all selected case studies.

Different modeling techniques and material model estimation formulas were tested on the Phase I models. Successful strategies employed in Phase I were used again in later phases to help create an optimized final framework. The simple model had a very small number of nodes and elements compared to that of Phases II and III. Since computation time is directly proportional to the number of elements, various modeling techniques could be tested very efficiently with short trial model runtimes. This testing methodology dramatically helped in converging on the proper methods to model features like boundary conditions, material properties, element type, mesh size, mesh pattern design, load and prestressing application, and solution convergence criteria.

*4.1 Phase I*

Because of the multitude of test specimens available as part of Phase I, the model was rigorously validated through four different load configurations. The model was created and validated for the midspan load first as it was the simplest to recreate. The model was then modified and fine-tuned until the point was reached where the relocation of the steel loading plate was the only modification necessary to produce the expected behavior for the other scenarios. Figure 35 through Figure 38 illustrate the behaviors of the FE models compared to those of the different experiments. For all cases, the deflection is measured at the location of load application, and in the midspan case, the design capacity was computed to gauge its prediction when compared to the experimental and modeled results. The calculated nominal capacity of 1135 k.ft was about 2.5% lower than the actual capacity of 1165 kip.ft and 3.8% lower than the modeled capacity of 1180 kip.ft. Calculations can be found in the appendix.

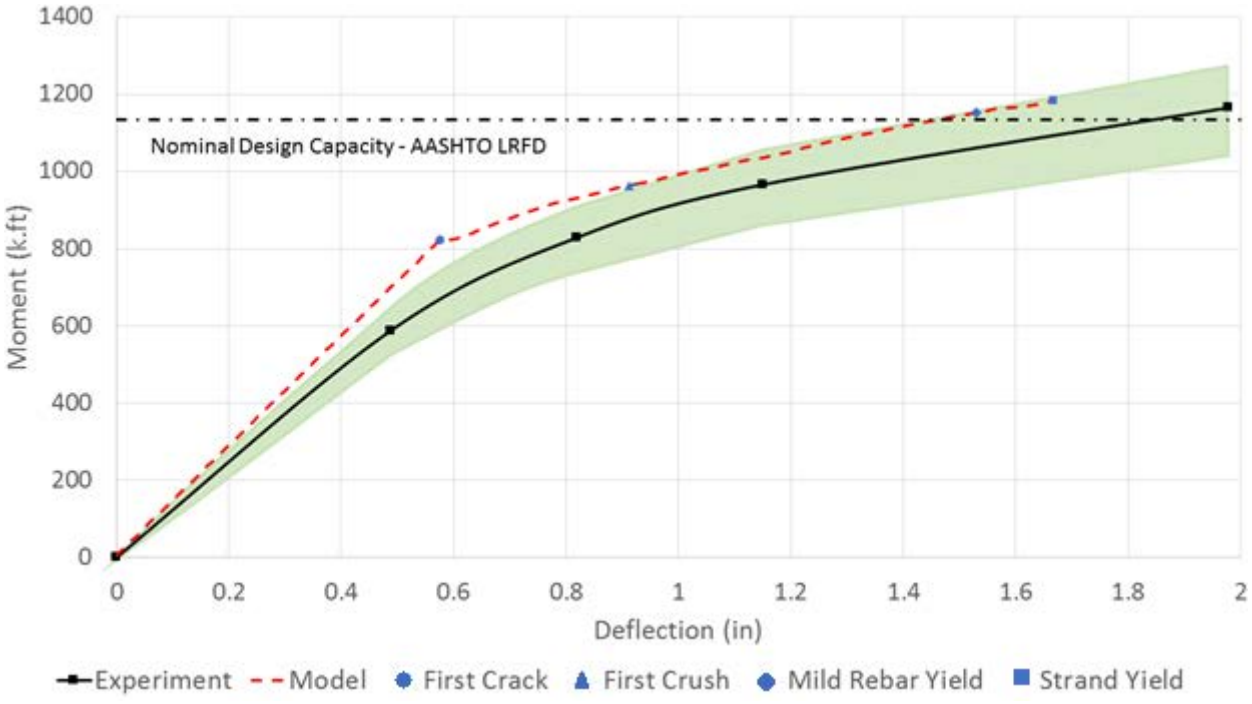


*Figure 35 - Phase I Load Deflection Curve Comparison for the Midspan*

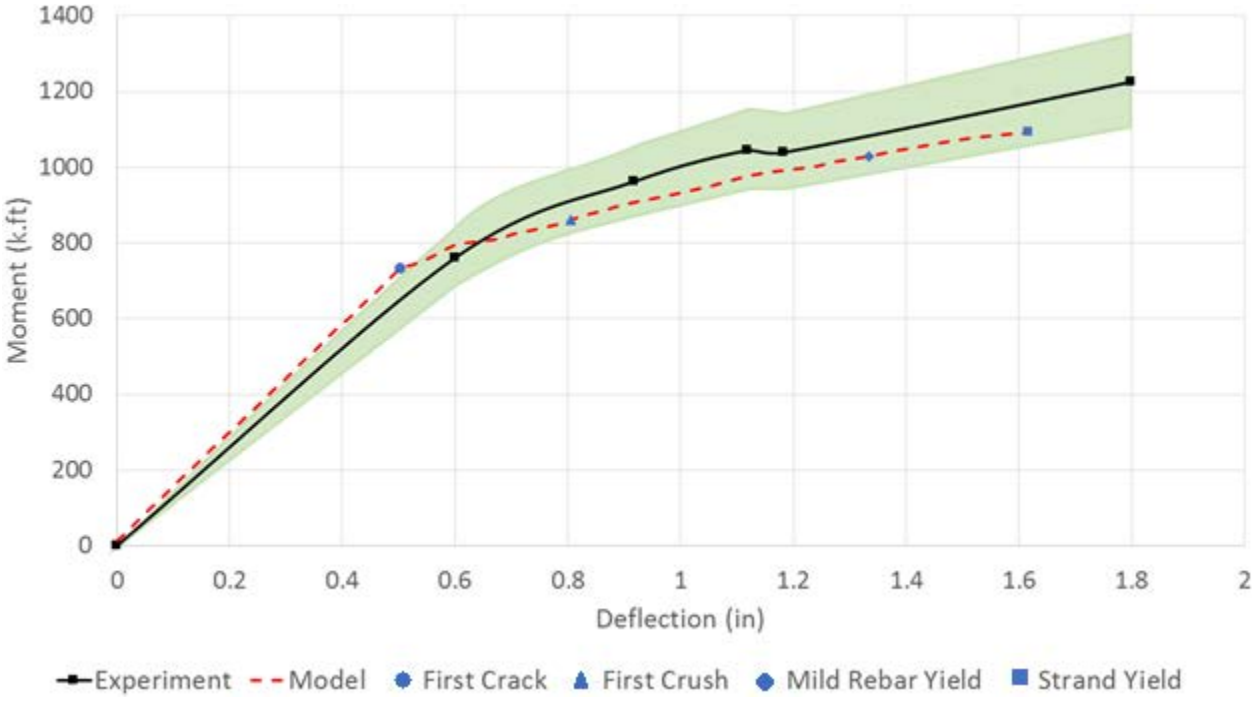


*Figure 36 - Phase I Load Deflection Curve Comparison for the 4D*

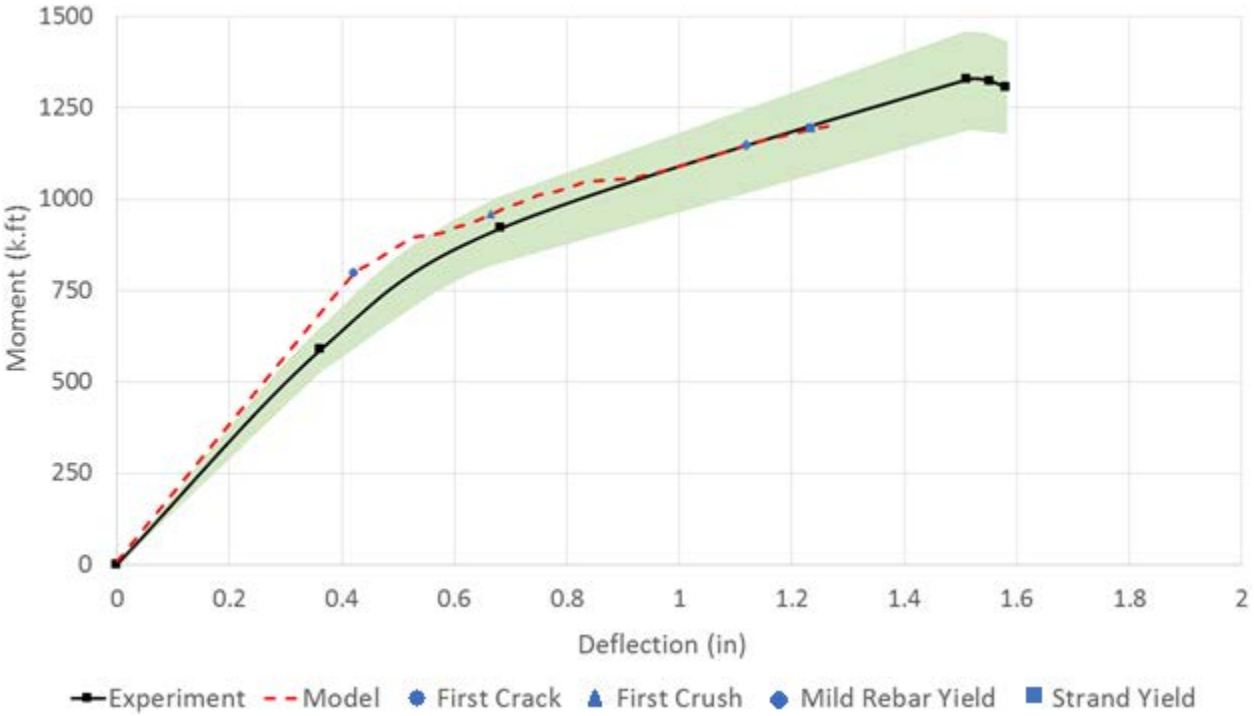


*Figure 37 - Phase I Load Deflection Curve Comparison for 2D*

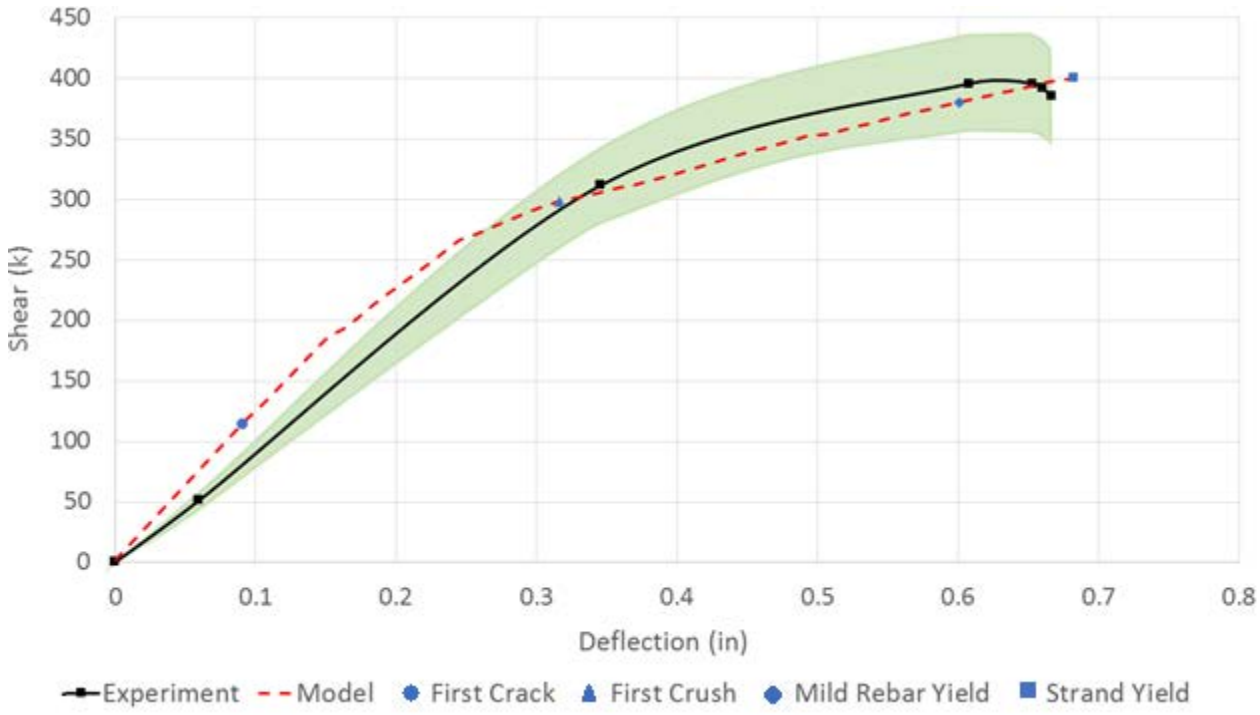


*Figure 38 - Phase I Load Deflection Curve Comparison for 1D*

In all cases, the initial response is slightly stiffer than experimental results. This variance could likely be minimized through further refinement of boundary conditions, as that can have a significant effect on the response in the elastic stage. The figures show how the models closely followed the deflection behavior obtained experimentally. The model does not match the experimental behavior perfectly, but that is likely due to the various model simplifications and assumptions. Overall, the responses are similar enough to deem the model quantitatively validated. At the four models' very worst, the simulation deviates from the experiment by 20% but in most circumstances, the model remains within a 10% band (shaded green in the result figures) along the experimental load-deflection behavior. This 20% variance between the two datasets equates to about 0.25 inches and it occurs in the midspan scenario at a moment of 820 k.ft.

The next step of model validation consists of checks for the qualitative response generated under the different loads. For all load scenarios, the crack patterns were very similar to the ones described by the investigators in the experiment. Figure 39 compares the 1D scenario's crack

pattern, while Figure 40 compares that of the midspan scenario. 1D cracks started off initially at a 45$^{o}$ angle from the support and gradually spread towards the loading plate. Midspan crack patterns started off vertically as expected, then accumulated and spread along the length of the beam while gradually tilting towards the midspan. Note that the cracking present near the location of load application in Figure 40 is due to local effects and do not significantly contribute to the system's behavior. Dashed red lines were superimposed on the experiment's cracks for easier visibility.

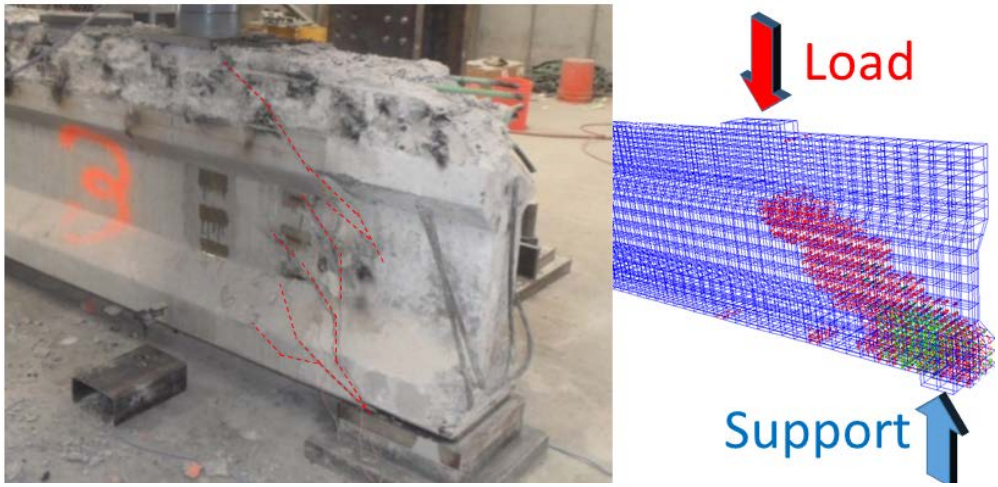


*Figure 39 - 1D Shear Crack Pattern Comparison*

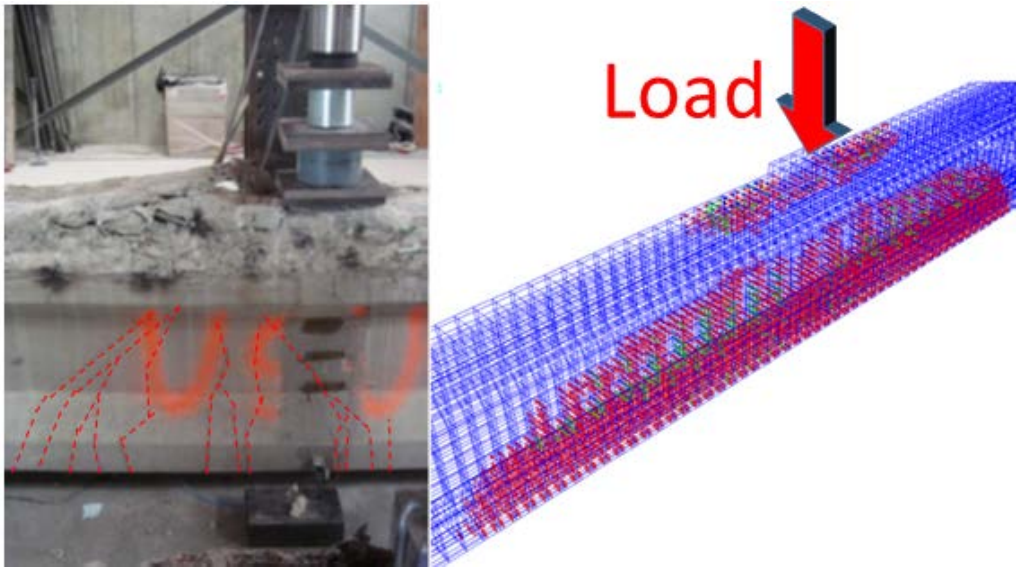


*Figure 40 - Midspan Flexural Crack Pattern Comparison*

As shown in Figure 39 and Figure 40, the models can accurately replicate crack initiation, propagation and final pattern in the concrete according to the location of the load. Moreover, the models were able to capture key failure stages as each beam was loaded to its maximum capacity. The analyzed model can be revisited to extract information on the exact structural status of the beam and monitor its evolution along each increment of loading. Tracking the progression of the beam's response allows for isolating the distinct stages that structures go through as their ultimate capacity is approached. While these stages are usually detected by the investigators (cracking, crushing...), stages like steel yielding are difficult to capture experimentally, but are readily available in the models. Unfortunately, investigators did not report the instance at which these stages first occurred in the girders. Therefore, the failure stages captured in the model cannot be validated, but they are still very useful pieces of information that can be referenced bridge inspectors and maintenance decision makers.

Beam failure modes were replicated in the models in all four scenarios. The investigators reported that the 1D loading caused a shear failure in the beam, while the three other beams failed by means of "concrete compression failure in the deck coupled with flexural cracking at the bottom of the girder". At high levels of loading, the compression block of the girder (specifically the weaker deck section with lower concrete strength) crushes. By then, extensive cracking in the tensile block of the girders would have occurred.

In all scenarios, the models behaved similarly to the experiments, as they usually remained within 10% of loads for a given deflection. Further refinement and less simplification in the models should continuously improve their performance. Ever-present uncertainties associated with the boundary conditions, for example, can be improved through further iterative models. Note that under certain conditions, effects of model inaccuracies are magnified. For example, as the location

of load application nears the supports, the inaccuracies in the model amplify, causing the behavior of the modeled structure to diverge from the expected outcome.

Phase I underwent a great deal of troubleshooting to create the final modeled product. Results achieved from initial models provided acceptable results for the 4D and midspan scenarios; however, the 1D and 2D results were inadequate due to premature cracking in the concrete. The appendix includes some figures on designed models found to be inadequate. Creating a model that worked for all four cases proved to be problematic. As the loads neared the supports, the divergence from the experimental results grew, which implied some inaccuracy in modeling the supports or boundary conditions. Not all features at the supports could be refined as some were well-defined by the investigators. The inaccuracies with the size and stiffness of the elastomeric pads allowed some room for modification. This proved to be key for convergence on a satisfactory common model for all four cases. The pad was redesigned according to report recommendations (FDOT-FHWA, 2007) to create the end-product.

While not exact, the element-level models were able to recreate the experimental behavioral characteristics. The FE results also replicated all of the failure stages and modes, so the models were deemed validated for the simple, single prestressed girder scenarios. The practices employed towards this phase's success allows for the evolution of this model to the more complicated, composite system-level bridge model.

### *4.2 Phase II*

The intact bridge phase had four load scenarios as well. These cases consisted of two asymmetric load scenarios, and two symmetric ones. Three of those loads kept the bridge in its elastic range while the final scenario loaded the structure to failure. The available data is not as extensive as that of Phase I, but it was still sufficient for validation purposes. Using the same

modeling techniques and analysis processes developed for the Phase I models, the bridge's response as it is loaded to its ultimate capacity was modeled.

### *4.2.1 Load-Deflection Comparison*

Load-deflection curves were again the benchmark for initial comparison with the experimental results. Data were compared for all nine girders in the bridge. Figure 41 and Figure 42 show the performance comparison for the middle girder and one of the exterior ones, respectively. According to AASHTO specifications, the elements of bridge superstructures govern the system's design. For the considered case study, the element is a single prestressed box beam. Figure 41 and Figure 42 include the calculated capacity of the single box-beam element within the bridge system. Because this design method does not account for the composite interaction between the girders and the continuous load-sharing and redistribution among them, the designed capacity of the structure is dramatically diminished.

The graphed results are limited to the region of interest, which begins with the bridge unloaded and ends when the peak load is reached. Softening behavior was outside the scope of this study and its incorporation into the model requires significant changes in the method of load application, material models, and bond-slip mechanisms.

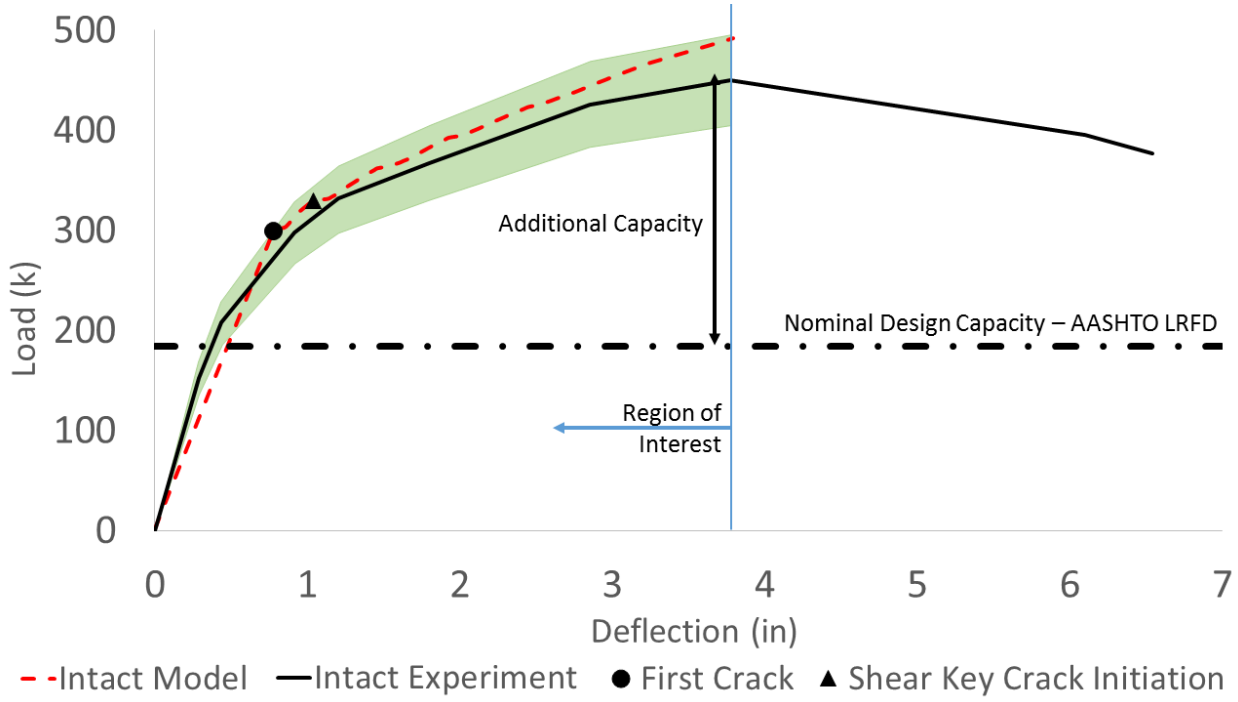


*Figure 41 - Load Deflection Curves for the Middle Intact Girder*

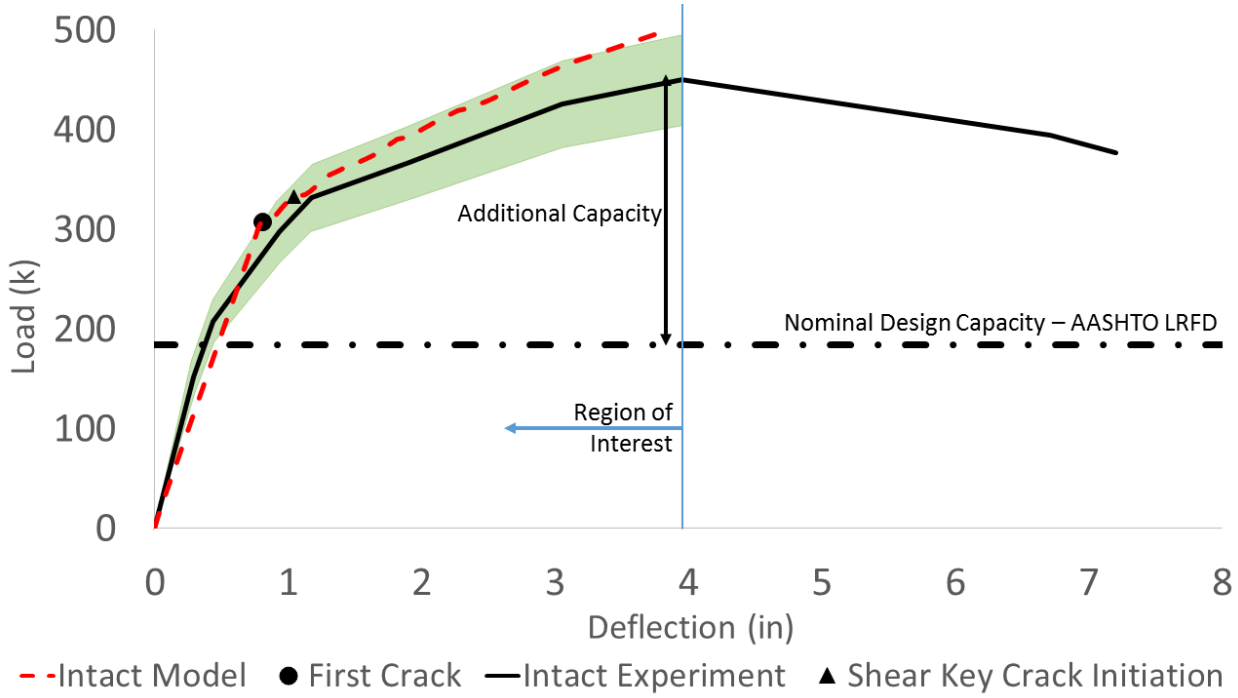


*Figure 42 - Load Deflection Curves for an Exterior Intact Girder*

For this phase, the results showed that the modeled structure correlates well with the experimental results. The most significant difference between the two datasets is found in the

elastic stage, where under a load of 208 kips, the model deflected about a tenth of an inch more than the experiment. While that difference is quite miniscule, it could be rectified with further model refinement. Another model deviation from experimental results arises in the post-cracking behavior. At this stage, the simulated slope of the model is slightly stiffer than that of the experiment. Since the concrete had already cracked by that stage, the slope of the graph should be mainly dictated by the stiffness of the strands and the residual prestressing. Other factors may come into play but with the available information, the displayed behavior was the most adequate after numerous iterations.

### *4.2.2 Qualitative Failure Comparison*

After quantitative validation, it was necessary to make sure that the bridge model replicates the behavioral stages and failure mode reported from the experiment. For all girders in this phase, flexural and shear key cracking were the only failure stages recorded by the model. To understand why that occurred, the published reports were referenced for their experimental procedures.

The investigators stated that the test was terminated when the top flange of one of the exterior beams crushed. Another contributing factor to the system's failure was the loss of composite action between the girders due to extensive damage to the shear keys. While shear key failure was captured in the model, the local crushing of the top flange did not occur. After further investigation, it was found that the beam that failed had some existing damage prior to the test. Figure 43 shows a view of the center span with some of the deteriorated locations. Even though the inspectors deemed the span to be in good condition, some localized damage was present. The locations marked in Figure 43 highlight the damaged areas.

*Figure 43 - Existing damage on the Center Span's Beam 1 (Steinberg, 2011)*

For the shear reinforcement to be exposed, 2.5 - 3 inches into the box beam must have been eroded over a length of at least 35 inches. In the reported image of the failure, the crushing of that beam occurred at the exact location of the damaged section closer to midspan. Therefore, this pre-existing damage likely played a large role in the crushing of the top flange of that specific member. Since all 9 beams were modeled as completely intact for this phase, the crushing of that top flange could not be recreated. In the model, the crushing phenomenon does not occur until higher loads are reached. With more information on the damage and further refinement, future models could reproduce this failure mode in the top flange.

Figure 44 (a) illustrates the intact bridge's overall deflection contour under full symmetric loading as reported by the investigators. Since the conducted experiments were displacement-controlled, the deflection contours reach a peak load then decrease as the bridge continues to deflect. The simulated color-coded deflection contour in Figure 44 (b) corresponds to the 450 kips load, since that was the peak load achieved by the structure before softening. As expected, the deflection remains somewhat constant along the width of the bridge.

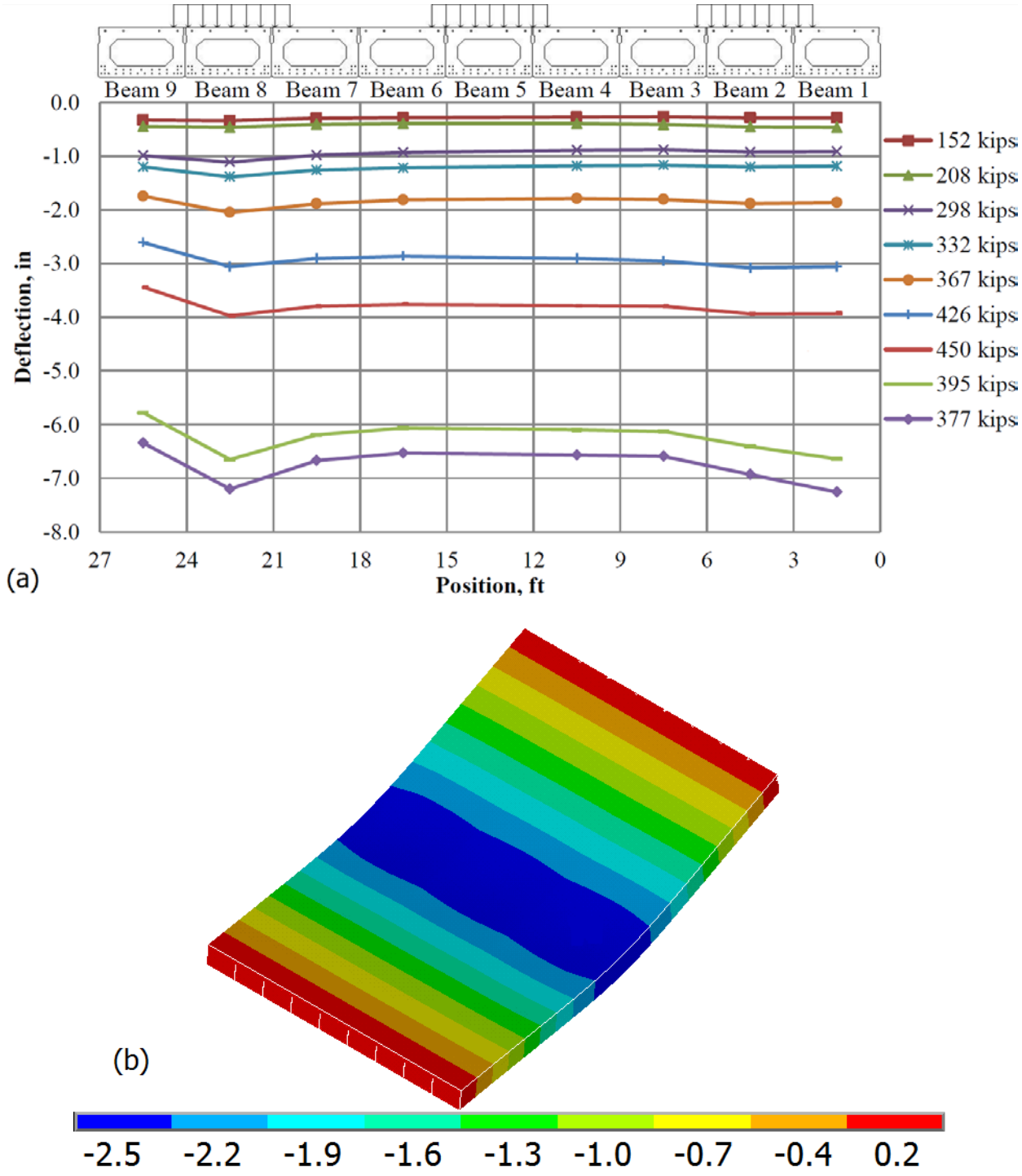


*Figure 44 - Phase II Cross-section Deflection Evolution (a), Deflection Contour at Peak Load (in)*

Another phenomenon that was replicated in the model was the cracking of the shear keys along the length of the bridge. As the applied load increases, the shear keys either crack or separate from the girder concrete. Figure 45 (a) illustrates the resulting crack pattern at the end of the simulation while Figure 45 (b) displays the extent of shear key cracking under high loads.

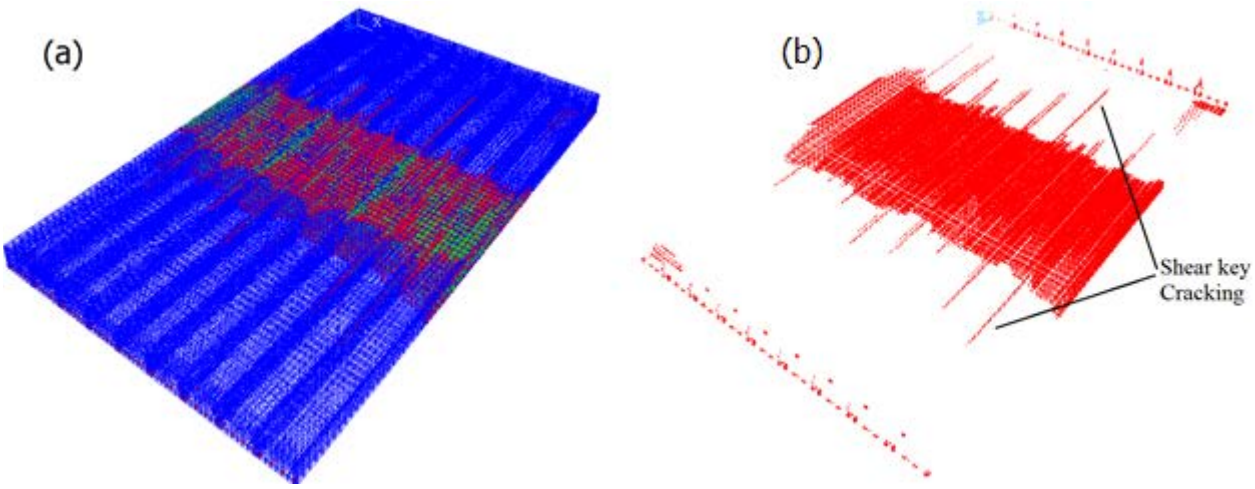


*Figure 45 - Phase II Failure Mechanisms (a) Flexural cracking (b) Shear Key Cracking*

Numerous challenges arose along the development process of the Phase II model. To achieve the discussed results, numerous model variations were tested to converge on a suitable combination of residual prestressing force in the strands, system boundary conditions, and shear key modeling. As discussed in section 4.1, the Magnel diagram allowed for setting a range of viable initial prestressing loads which were converted to residual loads at the time of the test by calculating theoretical accumulated losses. Appropriate support simulations were well defined by the structural plans in the referenced reports (Steinberg et al. 2011, Huffman 2012, and Huffman et al. 2012), leaving little room for model assumptions. The shear key model, on the other hand, had multiple vague components that were difficult to accurately recreate. Since the shear key grout is not monolithic with the box-beam, the bond between the two poses a significant local weakness.

To model this reduced bond strength at the concrete interface, multiple approaches were attempted. Modeling the exact geometry of the shear key proved to make the model too

computationally expensive, so, as described in section 3.3.2.4, a simpler shear key design was adopted to maintain high modeling efficiency. To model the bond weakness between the two components, contact elements were attempted at first. Contact elements are used to represent contact and sliding between surfaces (ANSYS 2011). CONTA173 elements were selected as they were 4-node 2D, which merge a selected surface to another target surface, allowing the user to define the properties of the small volume in between the two surfaces. Numerical convergence issues were faced with this method as the software could not load the structure to the intended loads without losing convergence and crashing. Research showed that the use of contact elements is sensitive and requires much time to set up correctly (Metrisin, 2008). After much time and effort spent on refining the incorporation of contact elements into the model, the method was discarded in lieu of an alternative approach. The other developed methodology described in section 3.3.2.4 was calibrated to produce the expected behavior by reducing the strength of the shear keys but maintaining a monolithic bond between the shear key and the concrete beams.

*4.2.3 Load Distribution Analysis*

The evolution of girder distribution factors is an important output from the models developed through this research. As shown in equation 4.1, distribution factors were found by dividing a single beam's deflection by the sum of the deflection in all beams along the width of the structure. These figures allow for a better understanding of the reasons behind load redistribution and the paths taken by the load as structural components successively fail.

$$DF = \frac{\Delta_i}{\Sigma\Delta_i} \qquad (Eq.\,4.1)$$

As the load applied on the structure increases, the composite girders work together by sharing the applied load, regardless of the point of application. Figure 46 illustrates how FEA can

model the distribution and redistribution of load as the structure approaches its ultimate capacity. Initially, the girders' distribution fluctuates due to lingering precamber effects and boundary condition assumptions. As loads increase, distribution factors settle until the first flexural cracks appear. By the end of the elastic stage, stress is relieved from some of the beams and transferred to the ones more directly loaded. This divergence increases as the shear keys connecting the beams fail, causing further losses in the integrity of the system's composite action. As expected, by the time loads reach the structure's maximum capacity, the three beams (2, 5, and 8) directly under the hydraulic jacks handle the largest portion of loads. The girders adjacent to them (3, 4, 6, and 7) resist less load, and the exterior girders (1, 9) provide the least contribution.

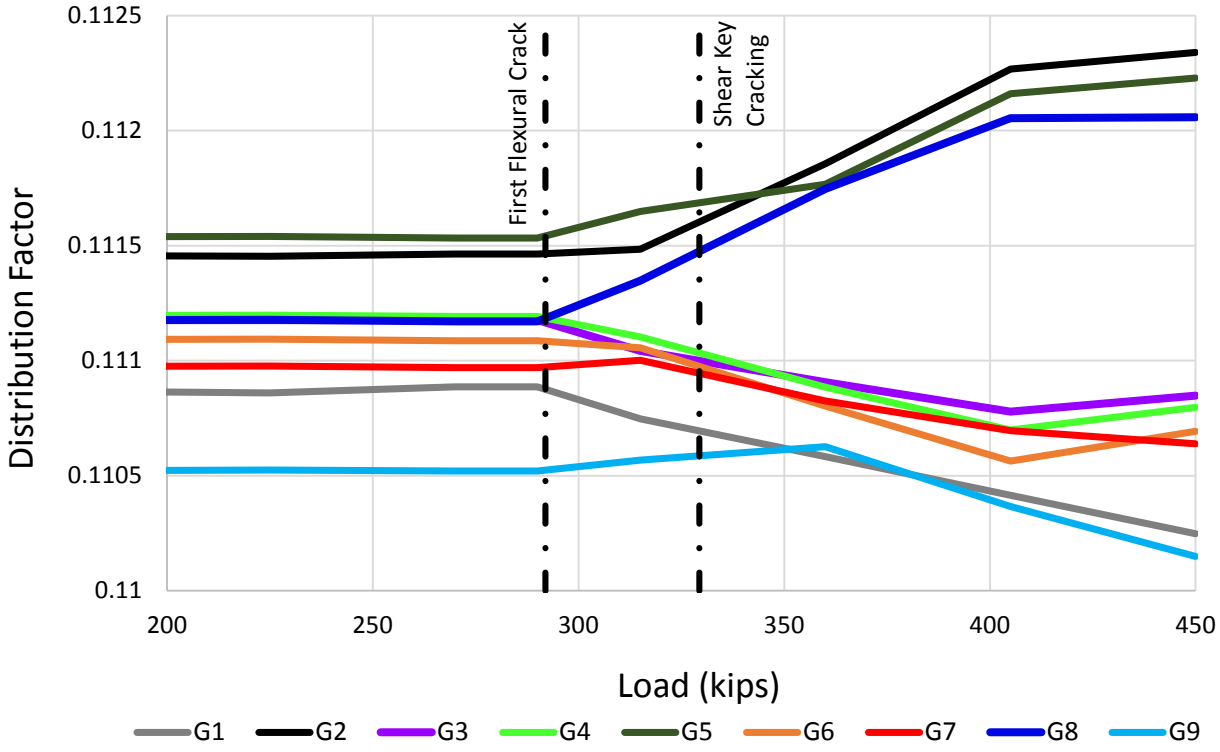


*Figure 46 - Intact Bridge Distribution Factors*

The trends observed in the figures above support the notion that overall bridge deflection and failure mechanisms could be replicated through FEA. All shown outputs replicate the reported

behavior on-site as the deflection along the cross-section was somewhat constant and shear key cracking was prevalent along the span length. The numerical model was able to recreate performance data in both linear and nonlinear regions, in addition to capturing some distinctive failure stages such as flexure cracks patterns and other local failures.

### *4.3 Phase III*

The final phase of this study consisted of integrating strand rupture damage into the modeled structure and studying its effects on the overall system behavior. Validating this phase involves recreating the results obtained by the damaged span scenario in the Huffman (2012) study. Successfully completing this stage verifies that the desired framework is capable of modeling damage and allows for the accurate comparison between an intact structure and a damaged one. A successful Phase III model would have the capability of illustrating the effects that different types of damage can have on the structure's ultimate capacity, redundancy, ductility, and reserve capacity. Because of the presence of reported experimental data, strand rupture was the damage mechanism selected for modeling in Phase III.

Figure 47 and Figure 48 show a performance comparison between both versions of the damaged and intact bridge or two different girders. Again, the modeled results remained well within 10% of the experimental results. The impact of cut strands on the behavior of the bridge system is apparent as the reduction in capacity was analogous for both datasets. In addition, Figure 49 shows the deflection pattern of the damaged span with the associated shear key crack pattern.

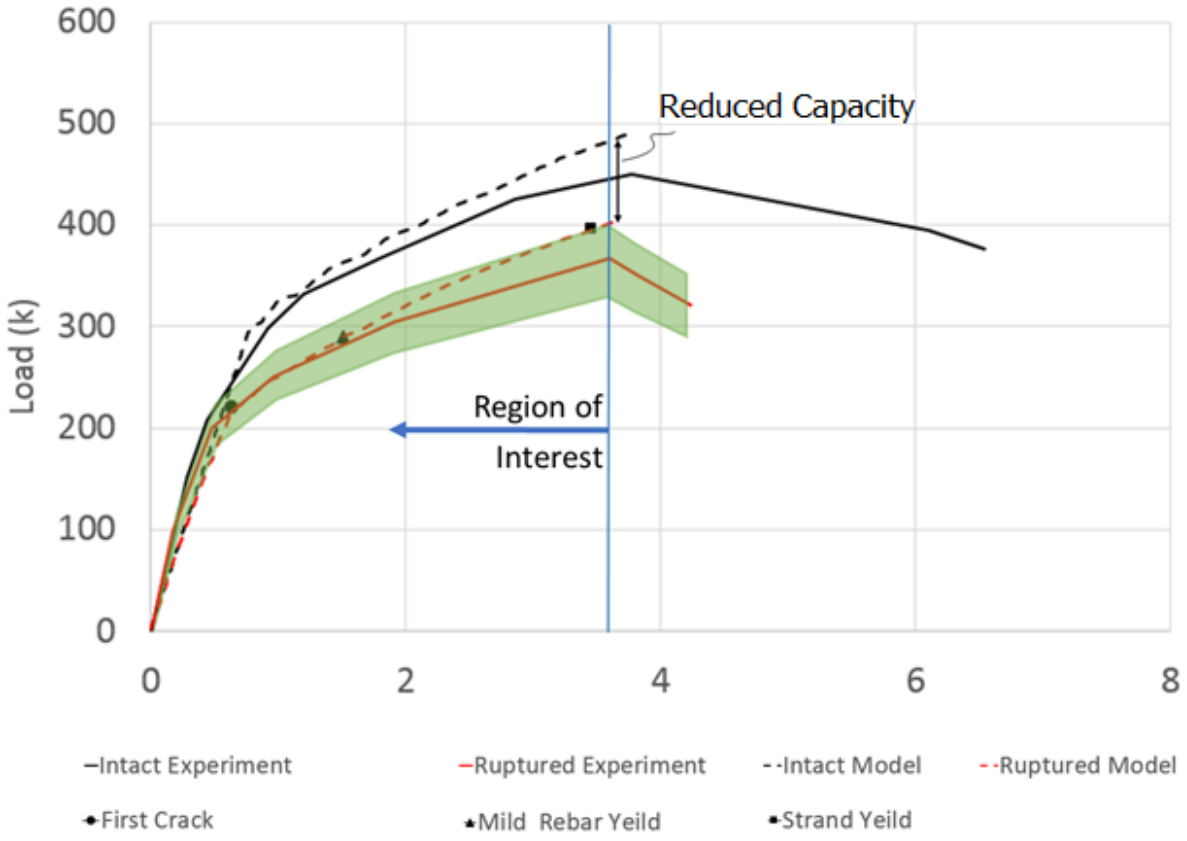


*Figure 47 - Load Deflection Curves for the Middle Girder in the Damaged Span*

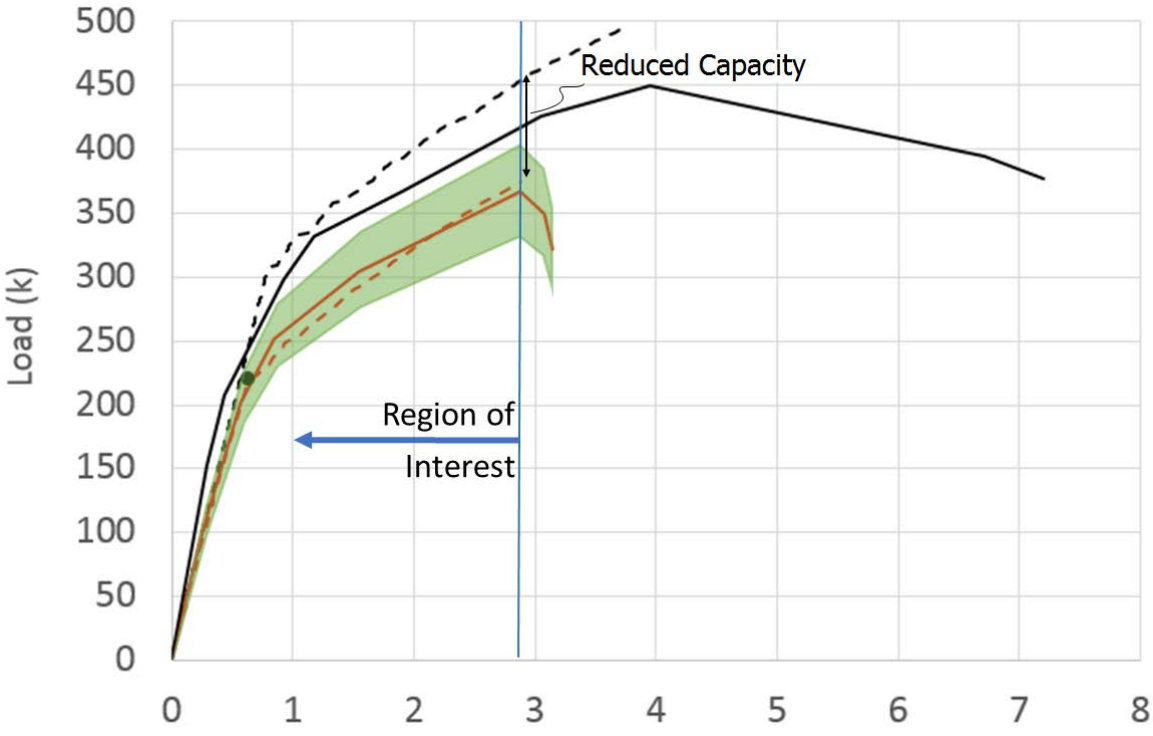


*Figure 48 - Load Deflection Curves for the Exterior Girder in the Damaged Span*

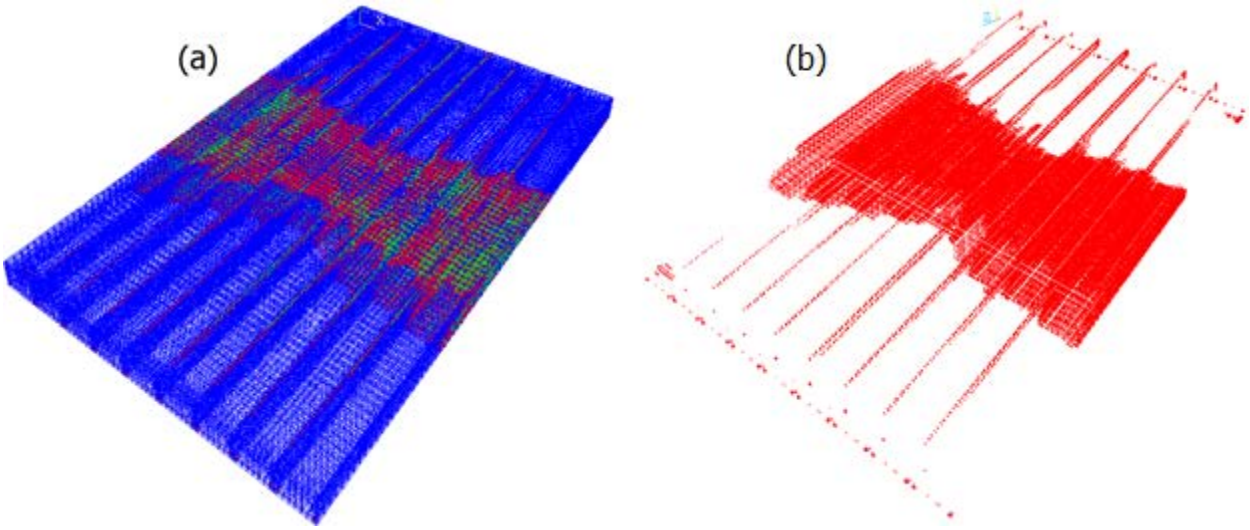


*Figure 49 - Phase III Failure Mechanisms (a) Flexural cracking (b) Shear Key Cracking*

As the results demonstrate, the addition of rupture damage to some strands has significant effects on the bridge superstructure in both the linear and non-linear sections. Similar to Phase II, the post-cracking results are stiffer than expected. Further refinement to the material properties and boundary conditions should improve that section of the model.

The integration of strand rupture reduced the capacity by about 20% when compared to the intact model results, and the damage instigated much more extensive flexural and shear key cracking throughout the structure. However, in contrast to the results of Phase II, the longitudinal reinforcement and the damaged strands exhibited signs of yielding at high levels of load. Figure 50 shows the change in system deflection due to the damage. Note that the loads are not exactly distributed on the bridge. Figure 50 (a) shows how the three cylinders are shifted about 6 inches off-center, towards beam 1. The response in section (a) of that figure was reported by the investigators. The simulated contour plot of the deflection in Figure 50 (b) correlates to the peak loads achieved by the model.

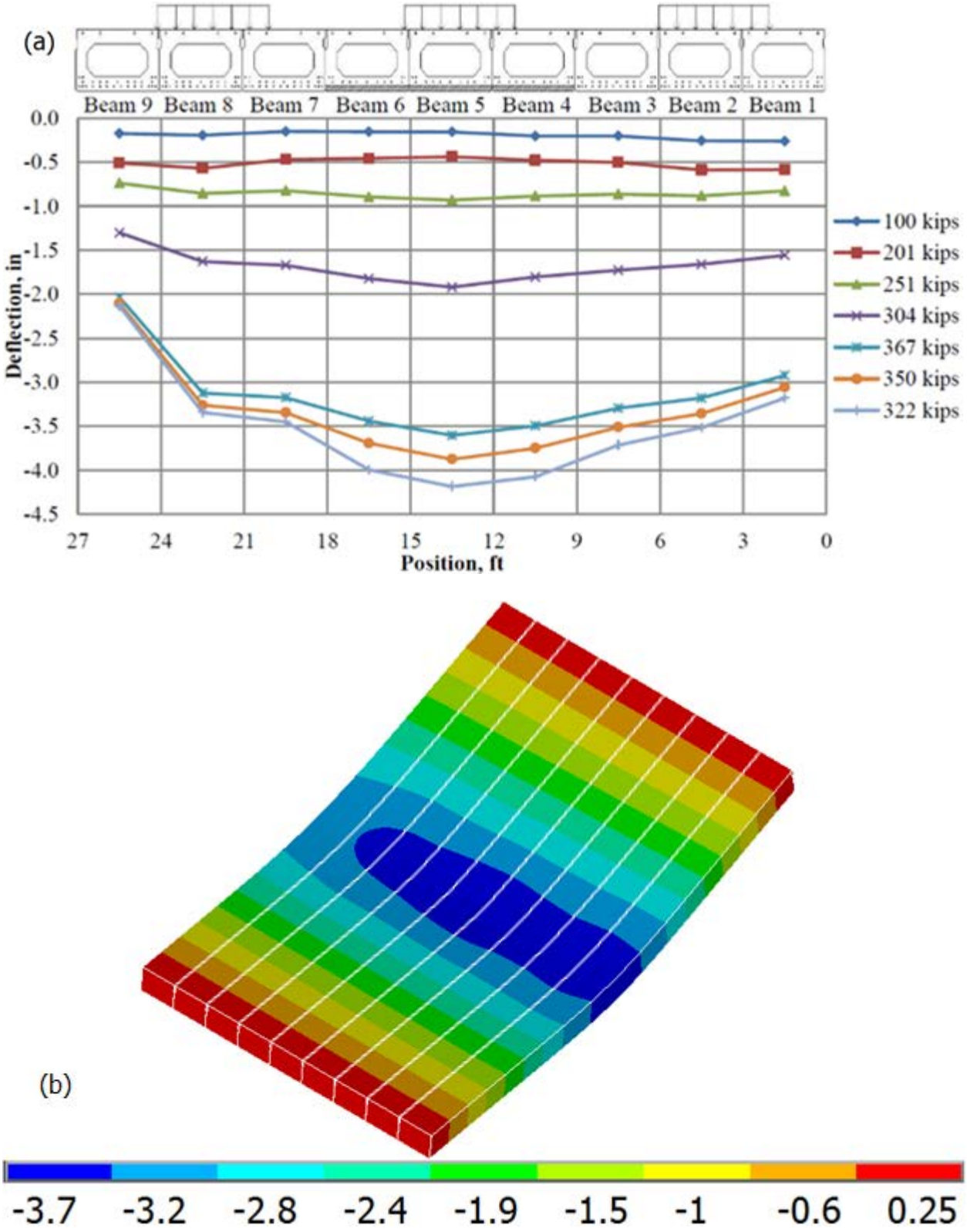


*Figure 50 - Phase III Cross-section Deflection Evolution (a), Deflection Contour at Peak Load (in)*

The distribution factor analysis was conducted for comparison against the Phase II distribution factors. Again, in the elastic stage, the factors were somewhat stable until flexural cracking occurs. At that stage, the load is channeled to the three damaged girders (4, 5, and 6). This redistribution is reinforced as steel begins to yield. By the end of the test, the two furthest girders from the point of load application (8 and 9) absorb the least amount of load while the other girders (1, 2, 3, and 7) have an average contribution to the system.

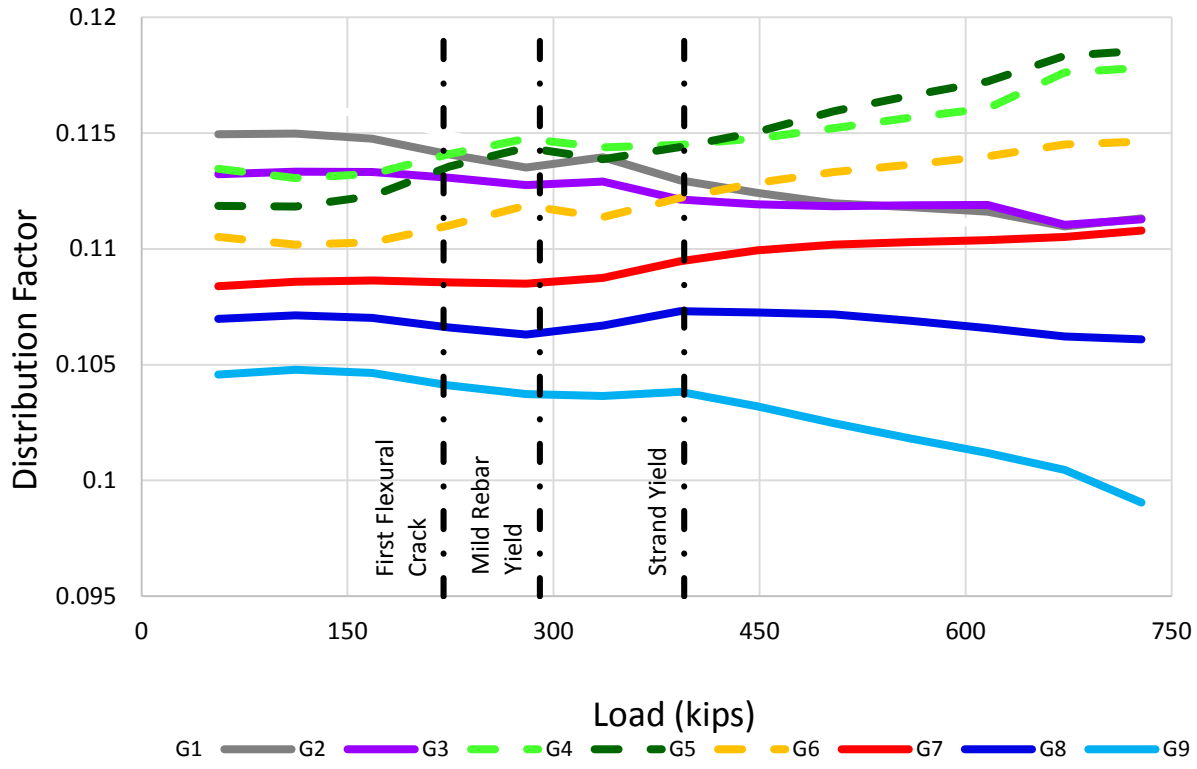


*Figure 51 - Damaged Bridge Distribution Factors*

# 5.0 CONCLUSIONS

This investigation's main objective was to characterize the system behavior of prestressed concrete girder bridge superstructures, and to assess the impact of damage on their performance. A previously developed framework based on a numerical platform was restructured and implemented to evolve the models incrementally from simple scenarios to the final product. The proposed methodology was followed to create models of related case studies using FEA. The models were designed to match the material, geometric, and boundary conditions described in the studies as closely as possible while keeping computational efficiency as a priority as well. Numerous modeling approaches were referenced and tested to find the most suitable techniques to recreate the individual components within the structure. Several iterative models were created to test all assumptions and maintain a balance between efficiency and accuracy. To validate the designs, simulated results were compared to available experimental data from case studies of bridges loaded to their ultimate capacities.

One of the most significant challenges faced along the progression of this research was the lack of information on various components of the modeled structure. Examples include insufficient information on the supports for the Phase I study and residual prestressing for Phases II and III. Much of the research efforts targeted the modeling optimization of the various structural components to determine the most appropriate assumptions to make on vaguely defined bridge elements. One of the reasons why this framework can be attractive to DOTs in particular is their almost unrestricted access to bridge structures. Since DOT engineers are usually heavily involved in structure construction or rehabilitation, they should have full access to structural plans. In the cases that plans may be missing or relatively old, field measurements can provide exact, present-state information on the structure's integrity. Updated and comprehensive information on

structures of interest considerably streamline the modeling process, and they allow for much more accurate results. With sufficient information and a relatively small manpower and time investment, an accurate structural model can be furnished to engineers to help them make decisions on inspection.

The findings of the study may be summarized as follows;

- The models recreated the reported deflection results as the structures were loaded to their ultimate capacities. The modeled performance was not perfect; some deviations existed between the two sets of data in both the linear and non-linear stages. These deviations could be minimized if further information was reported from the case studies, or if more research efforts are invested towards making better assumptions on material properties and boundary conditions, or developing more suitable modeling techniques.
- The models also replicated the qualitative response of the prestressed girders. Crack patterns, deflection contours, and failure stages were captured sequentially, and they compared well to reported experimental results. The validated response allows engineers to study the bridge's failure, observe its reaction at every increment of loading, and understand its devolution to failure.
- Load distribution within the system was analyzed as well to understand the load attraction trends exhibited by the bridge girders. The redistribution of load within the system at high loads was also a feature of interest as it helped explain how gravity loads move down the structure as components begin to fail. Studying this phenomenon in the damaged bridge model provided insight on how damaged elements take on higher loads as the superstructure is loaded.

- In addition to an increased understanding of the unique characteristics of this family of bridges, the developed framework demonstrated its ability to model the effects of damage on the overall behavior of prestressed concrete girder bridge superstructures. While the modeled damage case was strand rupture, the framework is generic and its methodology can be extended to other forms of damage encountered in practice such as strand corrosion and section loss. Most common damage scenarios, like prestress loss, strand corrosion, and cracking, are straightforward to model, but other ones including section loss require more effort to appropriately input the damage into the system.
- The discussed features and the developed relationships between damage and structural performance provide objective and reliable sources of information on the present condition of the superstructure. A large set of inspection and modeling results allow better estimating of the remaining service life under the effect of various damage and deterioration conditions. Engineers and inspectors can employ this approach to help in their decision-making processes, and that can in turn help them avoid unnecessarily conservative decisions and radical repair methods when less invasive solutions are sufficient.
- The Phase II/III case study had a significant amount of residual capacity when the modeled and experimental responses were compared to the AASHTO LRFD design methodology. This signifies an overly conservative approach with the design methods as they fail to take the load-sharing phenomenon among the girders into account. Future experiments on other similar structures can help determine the validity and applicability of this conclusion.

# 6.0 FUTURE WORK

Further work can always be invested in model refinement so that the simulated performance better represents the experimental results. Further improvement to the models discussed in this report can be achieved through multiple fronts including shear key, initial stress conditions, boundary conditions, and material properties refinement. For example, bond-slip behavior of transverse ties, dowel bars, and shear keys was not included in this research, but the investigators reported that steel reinforcement pulled out of the concrete in some locations.

Other improvements can include a more dense mesh design, and a more accurately represented cross-section. This can be more computationally expensive, but can provide much more detailed results. It would be beneficial to incorporate the use of super-computers into this research to disregard some of the simplifications applied for reduced computing time. This would allow engineers to create denser mesh patterns and achieve more accurate results while still extracting results within a reasonable timeframe.

Acquiring further information on the structure from the investigators can also significantly help reduce some of the discrepancies resulting from insufficient data. Finding exact information on residual prestressing force, boundary conditions and material properties, if available, can streamline the modeling process by reducing the number of variables in need of approximation.

To further investigate the capabilities of this framework to capture different damage mechanisms, other case studies could be referenced to help model other common forms of damage such as corrosion and section loss. Efforts have already been invested towards this issue by reaching out to inspectors and engineers in the state of Virginia to gather information on their experience while inspecting this family of bridge superstructures. Their response was limited but if further information is available, a sensitivity study with parametric variations in commonly

encountered types of damage can produce a product that has a significant influence on the assessments that are currently often based solely on an engineer's judgements. Moreover, as this framework was adopted from the investigation approach developed for composite steel girder bridges, the former can also be extended to other types of bridge superstructures as well.

Another possible application of this framework that also works towards assistance in the decision-making process consists of modeling potential repairs to a structure. Following the same method described for damage application, repair techniques such as external post-tensioning, permanent shoring, and FRP strengthening can be experimented with by engineers. The effects of various repair techniques can be similarly input onto the existing damaged or intact models. Modeling the effects of repair techniques on the structure provides another objective resource for engineers to make even more efficient and educated decisions on bridge maintenance.

# REFERENCES


Aalami, B. O. (2000). “Structural modeling of posttensioned members.” J. Struct. Eng., 126(2), 157–162.

AASHO. (1969) Standard Specifications for Highway Bridges. American Association of State Highway Officials, Washington, DC.

AASHTO. (2011) Manual for Bridge Evaluation 2nd edition. American Association of State Highway and Transportation Officials, Washington, DC.

ACI Committee 363 (2010). *ACI 363-10: Report on High-Strength Concrete*

Ahmad, S.H., and Shah, S.P. “Structural Properties of High Strength Concrete and Its Implications for Precast Prestressed Concrete.” PCI Journal. Vol. 30, No. 6, pp. 92-119. 1985.

ACI Committee 318 (2008). *ACI 318-08: Building Code Requirements for Structural Concrete and Commentary*

Aguilar, C. V., Jauregui, D.V., Newtson, C., Weldon, B., Cortez, T., “Load Rating a Prestressed Concrete Double-Tee Beam Bridge without Plans by Proof Testing” *Transportation Research Board, 94th Annual Meeting,* Washington D.C.

American concrete institute - (2010) 363R-10 Report on High-Strength Concrete

American Society of Civil Engineers. (ASCE) *“2013 Report Card for America’s Infrastructure.” http://www.infrastructurereportcard.org/*

*ASTM Standard A615, 1969, "*Standard Specification for Deformed and Plain Carbon-Steel Bars for Concrete Reinforcement*" ASTM International, West Conshohocken, PA, www.astm.org.*

ANSYS (2011). "User’s Manual Revision 15.0." *ANSYS, Inc., Canonsburg, PA.*

Araujo, Marcio C. 'Slab-on-Girder Prestressed Concrete Bridges: Linear and Nonlinear Finite Element Analysis and Experimental Load Tests ' Louisiana State University, 2009. Print.

Ayoub, A. (2011). ”Nonlinear Finite-Element Analysis of Posttensioned Concrete Bridge Girders.” J. Bridge Eng., 16(3), 479–489.

Byung Hwan Oh, Kwang Soo Kim, and Young Lew: Ultimate Load Behavior of Post-Tensioned Prestressed Concrete Girder Bridge through In-Place Failure Test (2002)

Carbonell Muñoz, M., Harris, D., Ahlborn, T., and Froster, D. (2014). ”Bond Performance between Ultrahigh-Performance Concrete and Normal-Strength Concrete.” *J. Mater. Civ. Eng.*, 26(8), 04014031.

Chang, T. Y., Taniguchi, H., and Chen, W. F. (1987). "Nonlinear finite element analysis of reinforced concrete panels."/. Struct. Engrg., ASCE, 113(1), 122-140.

Chung, W.; Sotelino, E., Three-dimensional finite element modeling of composite girder bridges, Engineering Structures, Volume 28, Issue 1, January 2006, Pages 63-71

J. E. Cook. 1989. *10,000 PSI Concrete*. Concrete International: Design and Construction, Oct, Vol. 11, No. 10, pp. 67-75.

Cook, Ronald A, Damon T. Allen, and Marcus H. Ansley. *Stiffness Evaluation of Neoprene Bearing Pads Under Long Term Loads*. Gainsville, Fla: Florida Dept. of Transportation, 2009. Print.

Coronelli, D. (2002). “Corrosion cracking and bond strength modeling for corroded bars in reinforced concrete.” ACI Structural Journal, 99 (3):267-276.

Dagher, H. J., and Kulendran, S. Finite element modeling of corrosion damage in concrete structures. ACI Structural Journal, 89(6):699-708, 1992.

Fanning, P., “Nonlinear models of reinforced and post-tensioned concrete beams”, Electronic Journal of Structural Engineering, vol. 2, pp. 111-119, 2001.

FHWA (2012). "Bridge Inspector’s Reference Manual." *U.S. Department of Transportation, Federal Highway Administration* Washington, D.C.

Gheitasi, Amir. 'Performance Evaluation Of Damage-Integrated Composite Steel Girder Highway Bridges' University of Virginia, 2014. Print.

Gheitasi, A., and Harris, D. K. (2014a). "A Performance-Based Framework For Bridge Preservation Based On Damage-Integrated System-Level Behavior." *Transportation Research Board, 93rd Annual Meeting,* Washington D.C.

Gheitasi, A., and Harris, D. K. (2014b). "Failure Characteristics and Ultimate Load-Carrying Capacity of Redundant Composite Steel Girder Bridges: Case Study." *Journal of Bridge Engineering, doi:10.1061/(ASCE)BE.1943-5592.0000667*, 0(0), 05014012.

Gheitasi, A., and Harris, D. K. (2014c). “Effect of Deck Deterioration on Overall System Behavior, Resilience and Remaining Life of Composite Steel Girder Bridges” Structures Congress, pp. 623-634, Boston, MA.

Gheitasi, A., and Harris, D. K. (2014d). “Performance assessment of steel–concrete composite bridges with subsurface deck deterioration.” Structures, doi:10.1016/j.istruc.2014.12.001.

Higgs, Arek Tilmann(2013), "Shear and Flexural Capacity of High Strength Prestressed Concrete Bridge Girders". *All Graduate Theses and Dissertations.* Paper 1757. http://digitalcommons.usu.edu/etd/1757

Hossain, T., Okeil, A., and Cai, C. (2014). *”Field Test and Finite-Element Modeling of a Three-Span Continuous-Girder Bridge.” J. Perform. Constr. Facil. 28, SPECIAL SECTION: Performance of Bridges under Critical Natural Hazards, 136–148.*

Huffman, J. (2012). “Destructive Testing of a Full-Scale 43 Year Old Adjacent Prestressed Concrete Box Beam Bridge: Middle and West Spans,” Masters Thesis, Ohio University, Russ College of Engineering and Technology.

Huffman, J. Steinberg, E., and Sargand, S., (2012), “Finite Element Modeling a Full Scale Adjacent Prestressed Concrete Box Beam Bridge Span,” 2012 PCI Annual Convention and National Bridge Conference, Nashville, TN, September 29 - October 2.

Hucklebridge, A., El-Esnawi, H., and Moses, F. 1995. Shear key performance in multibeam box girder bridges. J. Perform. Construct. Factors, 9(4), 271-285.

Kenneth K. Walsh, Brendan T. Kelly, and Eric P. Steinberg, “Damage Identification for Prestressed Adjacent Box-Beam Bridges,” Advances in Civil Engineering, vol. 2014, Article ID 540363, 16 pages, 2014. doi:10.1155/2014/540363

Laskar, A., Howser, R., Mo, Y.L., Hsu, T.T.C. “Modeling of prestressed concrete bridge girders”. Proceedings of the 12th International Conference on Engineering, Science, Construction, and Operations in Challenging Environments - Earth and Space 2010, p 2870-2887, 2010.

Mamlouk, Michael S., Zaniewski, John P., (2011) Materials for Civil and Construction Engineers, Third Edition. Addison Wesley Longman, Inc. Menlo Park, CA.

Martinez, S., Nilson, A.H., and Slate, F.O., 1982. Spirally reinforced High Strength Concrete Columns, Cornell University Department of Structural Engineering Research Report No. 82-10, 255 pp.

McDonald BM, Saraf V, Ross B. A spectacular collapse: The Koror-Babeldaob (Palau) balanced cantilever prestressed post-tensioned bridge. Indian Concrete J 2003; 77(3).

Metrisin, J. T. (2008). *Guidelines for obtaining Contact Convergence – 2008 International ANSYS Conference* [PowerPoint slides]. Retrieved from http://goo.gl/rMCEQW

Miller, A., Rosenboom, O., Rizkalla, S., (2007) “ Repair of prestressed concrete bridge girders with FRP” The 8th International Symposium on Fiber Reinforced Polymer Reinforcement for Concrete Structures, FRPRCS

Mtenga, P. V., Project Title: Elastomeric Bearing Pads Under Combined Loading, FDOT-FHWA Sponsored Research Project, Florida Department of Transportation, March 2007

National Bridge Inventory Data (NBI), Washington, 2013.

National Transportation Safety Board. (NTSB) (2008) Collapse of I-35W Highway Bridge Minneapolis, Minnesota. Accident Report.

National Transportation Safety Board. (NTSB) (2014) Collapse of I-5 Skagit River Bridge Following a Strike by an Oversize Combination Vehicle, Mount Vernon, Washington. Accident Report.

Nawy (2009) Prestressed Concrete: A Fundamental Approach 5th (Fifth) edition [Hardcover])

Nilson (1987), Arthur H. Design of Prestressed Concrete, Second Edition. New York: John Wiley and Sons.

Nguyen, T.T.D., Matsumoto, K., Iwasaki, A., Niwa, J.. “Performance of Pretensioning Prestressed Concrete Beams with Ruptured Strands Flexurally Strengthened by CFRP Sheets”, Proceedings of 3rd International Conference on Sustainable Construction Materials and Technologies, e-036, CD-ROM,, pp. 10, Aug. 2013.

NS 3473 (1992). Concrete Structures – Design Rules, Norges Standardiseringsfund, Oslo, Norway.

Osborn, G., Barr, P., Petty, D., Halling, M., and Brackus, T. (2012). ”Residual Prestress Forces and Shear Capacity of Salvaged Prestressed Concrete Bridge Girders.” J. Bridge Eng., 17(2), 302–309.

Phillips and Zienkiewicz (1976). "Finite element non-linear analysis of concrete structures." Proa, Institution of Civil Engineers, 61(2), 59-88

Plos, Mario; Gylltoft, Kent, (2006). “Evaluation of Shear Capacity of a Prestressed Concrete Box Girder Bridge using Non-Linear FEM” Structural Engineering International, Volume 16, Number 3, August 2006, pp. 213-221(9)

Radain, T.A., Samman, T.A., Wafa, F.F. (1993). “Mechanical Properties of High-Strength Concrete.” Proceedings of the Third International Symposium on Utilization of High-Strength Concrete, Lillehammer, Norway, Vol. 2, 1209-1216.

Rosenboom, O., Miller, A. and Rizkalla, S. (2012), "Repair of Impact-Damaged Prestressed Concrete Bridge Girders Using CFRP Materials" J. Bridge Eng.

Steinberg, E., Miller, R., Nims, D., Sargand, S., (2011), Structural Evaluation of LIC-310-0396 and FAY 35-17-6.82 Box Beams with Advanced Strand Deterioration, Ohio Department of Transportation Office of Research and Development, Federal Highway Administration, Ohio University, the University of Cincinnati, and the University of Toledo.

Stolarski, T. A., Y. Nakasone and S. Yoshimoto, Engineering Analysis with ANSYS Software, Elsevier, New York, 2006.

Thomas, J. and Ramaswamy, A. Nonlinear Analysis of Shear Dominant Prestressed Concrete Beams using ANSYS. Indian Institute of Science, Bangalore, India. http://www.ansys.com/events/proceedings/2006

Tavarez, F.A. (2001). "Simulation of behavior of composite grid reinforced concrete beams using explici/PAPERS/t finite element methods." Master's Thesis, University of Wisconsin-Madison, Madison, WI.

Trujillo, S. (2010). "Analytilcal Evaluation of Damaged Prestressed Concrete Box Beams Bridge Girders," Masters Thesis, Ohio University, Russ College of Engineering and Technology.

Van Greunen, J. and Scordelis, A. (1983). "Nonlinear Analysis of Prestressed Concrete Slabs." J. Struct. Eng., 109(7), 1742–1760.

Wolanski, A. J. (2004). "Flexural behavior of reinforced concrete beams using finite element analysis." Master's thesis, Marquette Univ., Milwaukee.

Zeljana Nikolic, Ante Mihanovic, (1997) "Non-linear finite element analysis of post-tensioned concrete structures", Engineering Computations, Vol. 14 Iss: 5, pp.509 – 528

Zhou, K., Martin-Perez, B., and Lounis, Z. (2005). "Finite element analysis of corrosion-induced cracking, spalling and delamination of RC bridge decks." 1st Canadian Conference on Effective Design of Structures, Hamilton, Ont., July 10-13,187-196.

# APPENDIX

## Phase I:

- The following is a sample version of the displacement-controlled solver adopted in some of the earlier models. This work was developed by Mr. Muhammad Sherif during his work on the finite element modeling of cellular beams.

```
/SOLU                ! Enter the solver
!* Set Solution Parameters*****************************************************************
ANTYPE,STATIC,NEW      ! Static Analysis
!* Define and monitor mid-span node*********************************************************
Node1=Node(8,0,217.5)
MONITOR,VAR1,Node1,UY                          ! Monitor UY(Nod1)
!********************************** Nonlinear Solution **********************************
SOLCONTROL,ON
AUTOTS,ON
!SSTIF,ON                                      ! Stiffening ON
PSTRES,ON                                      ! Prestress Effect ON
NLGEOM,ON                                      ! Include geometrical nonlinearity
!* Apply equal downward displacements (UY in in) on the nodes of the line across the top flange at mid-span
Total_Disp=2.5                                 ! Total applied displacement
D,LoadNodes,,-Total_Disp,,,,UY
TIME,Total_Disp                                ! TIME corresponds to Total Applied Displacement
NSUBST,1000                                    ! No of substeps = Total Displacement
NEQIT,100                                      ! No. of non-linear equlibrium iterations=15
!NCNV,1                                        ! Terminate analysis and program if unconverged NCNV=1
NCNV,2                                         ! Terminate analysis only if unconverged NCNV=2
CNVTOL,U,0.01,,2                               ! Use displacement convergence Tol=0.001
OUTRES,ALL,ALL                                 ! Output ALL results
*IF,SOL,EQ,'YES',THEN
SOLVE
*ENDIF
SAVE                                           ! Save Database
!* Postprocess the results*****************************************************************
/POST1
!* Write heading for the output file********************************************************
/OUTPUT,Results,txt,
*VWRITE
('          ')
*VWRITE
(' Disp(in)      Load(Kips)')
INRES,ALL                                      ! Set flag to read all results
FILE,'file','rst','.'                          ! Read from the result file
*GET,No_Sets,ACTIVE,0,SET,NSET                 ! Get number of results sets
CMSEL,S,LoadNodes,NODE                         ! Select component LoadNodes
*GET,NoNodes,NODE,0,COUNT                      ! Get # of Nodes
*DO,J,1,No_Sets                                ! Loop over results sets
SET,,,1,,,,J                                   ! Read Set J
CMSEL,S,LoadNodes,NODE                         ! Select component LoadNodes
*GET,SetTime,ACTIVE,0,SET,TIME
*GET,CurNode,NODE,0,NUM,MIN                    ! Get Min Node #
```

```
Sum_R=0                                  ! Initialize total reaction Sum_R
*DO,I,1,NoNodes
*GET,RFY,NODE,CurNode,RF,FY              ! Get the FY reaction at CURNOD
Sum_R=Sum_R+RFY
CurNode=NDNEXT(CurNode)                                  ! Get next node in the selected nodes
*ENDDO
/OUTPUT,Results,txt,,APPEND
*VWRITE,SetTime,-Sum_R
(F9.4,5X,F9.4)
/OUTPUT
*ENDDO
ALLSEL,ALL
FINISH
```

- The following script was extracted from the Phase I case study and contains details on some of the material properties that were not included in the document itself:

```
!Material Variables
Es=29000
Eps=28500
E=500000000
Emus=0.3
fys=240
fy=75
fyu=1000
Ec=3500
!use test info, beam prop
Emuc=0.18
fc=17.5
ft=1.5
Ecd=2000
!use test info, deck prop
Emucd=0.2
fcd=10.0
ftd=.9
Eg=3122
fg=3
!Reduced from 7
fgt=0.411
!Reduced from 0.575
MP,EX,1,Es
MP,PRXY,1,Emus
TB,BISO,1
TBDATA,,fy,2.9
MP,EX,3,Eps
MP,PRXY,3,Emus
!MP,DENS,3,0.7331E-6
TB,BISO,3,,2
TBData,,fys,1000
MP,EX,2,Ec
MP,PRXY,2,Emuc
MP,DENS,2,1.188E-4
```

```
R,1,,
!BEARING PLATES
R,2,.31,
!REBAR
R,3,.15,0.0057
!PRESTRESSED STRANDS
R,4,1,0.018,90,90
!CONCRETE
R,5,.62,,
!SHEAR BARS
R,6,1,0.026,90
!CONCRETE SMEARING
R,7
 !CONCRETE
R,8,.15,0.0048
R,9,.15,0.0038
R,10,.15,0.0029
R,11,.15,0.0019
R,12,.15,0.00094
R,13,1,0.013,90
R,14,1,0.009,90
!TYPES FOR EACH MATERIAL
!LOOK UP ELEMENTS IN CATALOG
ET,1,SOLID45
!BEARING
TB,CONCR,2
TBDATA,,.2,.8,ft,fc,
!see
element types
PLATES
ET,2,LINK8
STRANDS
!BAR OR
MP,EX,4,Ecd
MP,PRXY,4,Emucd
MP,DENS,4,1.188E-4
TB,CONCR,4
TBDATA,,.2,.6,ftd,fcd,
MP,EX,5,E
MP,PRXY,5,Emus
TB,BISO,5
TBDATA,,fyu,2.9
!REAL CONSTANS FOR STEEL
ET,4,SOLID65
!CONCRETE
```

- To find the residual force in the strands, the concept of stress accumulation was used. Equation 3.6 was used to find the residual prestressing force in the strands.

$$P = \frac{\frac{M_{sw}C_g + M_{xt}C_g}{I_g}}{\frac{1}{A_g} + \frac{e_p C_g}{I_g}} \qquad (eq.\ 3.6)$$

Where:

P = Effective prestressing force

e = Eccentricity of the strands

$C_g$ = Distance from the girder neutral axis to the bottom of the girder

$M_{sw}$ = Moment due to self-weight at crack location

$M_{xt}$ = Moment due to decompression load at crack

$A_g$ = Girder Cross-sectional area

$I_g$ = Girder moment of inertia

The effective residual prestressing force was then divided by the area of the strands to find the effective stress in the strands.

- AASHTO LRFD Nominal Moment Capacity Calculation

$$M_n = A_{ps}f_{ps}\left(d_p - \frac{a}{2}\right) + A_s f_s\left(d_s - \frac{a}{2}\right) - A'_s f'_s\left(d'_s - \frac{a}{2}\right) + 0.85 f'_c (b - b_w) h_f \left(\frac{a}{2} - \frac{h_f}{2}\right)$$

$$M_n = 1.95 * 270\left(28.9 - \frac{5.12}{2}\right) + 0.62 * 60\left(26 - \frac{5.12}{2}\right) - 1.24 * 60\left(11 - \frac{5.12}{2}\right)$$

$$+ 0.85 * 8.5(12 - 6) * 8 * \left(\frac{5.12}{2} - \frac{8}{2}\right) = 1134.39\ k.ft$$

- Prior to the completion of the Phase I model, several numerous modeling techniques and assumptions were tested along the model advancement process. The following section displays some of the failed works developed along the way.
    a) One of the issues encountered with the Phase I models consisted of premature shear cracking for the 1D and 2D scenarios near the supports. After much material property and boundary refinement, no model could be created which performed satisfactorily for all 4 loading scenarios. In effort to solve this problem, multiple hypotheses were attempted to converge on a viable solution. Figure 44 shows the poor performance of one the early Phase I models.

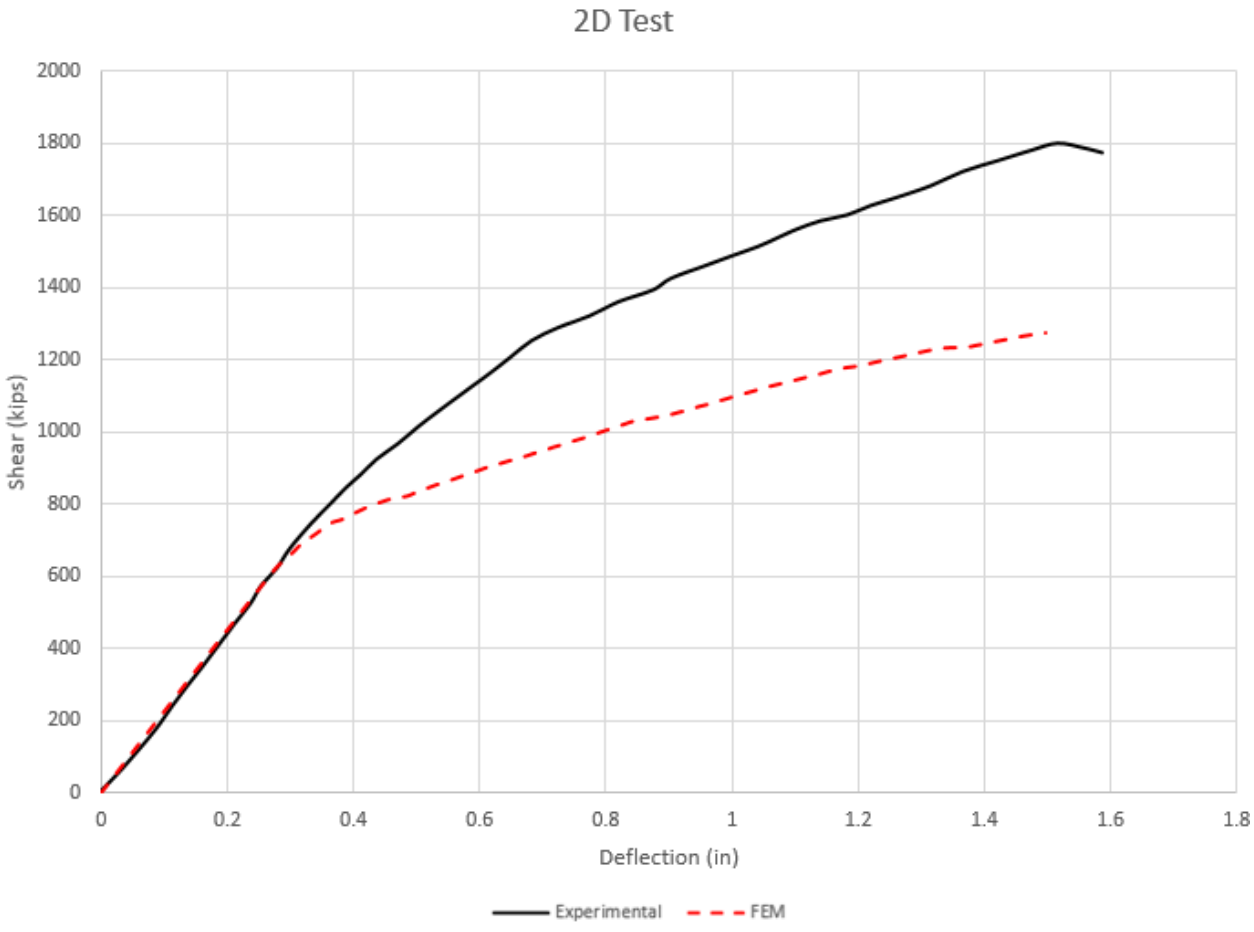


*Figure 52 - Early 2D model*

b) Hybrid beam hypothesis: as an attempt to overcome this issue, it was theorized that the tensile capacity of the concrete is not modeled appropriately at the location of crack initiation. Due to the proximity of the shear reinforcement near the supports, some concrete confinement effects could be present, thereby boosting the concrete's tensile capacity. Literature review reinforced this idea so some research efforts were invested towards this investigation. Figure 45 shows the volume divisions within the beam where the large middle section had a tensile capacity of $12\sqrt{f'_c}$ and the smaller sections near the ends had a tensile capacity of $15\sqrt{f'_c}$. The model's performance did improve, but the qualitative response would not match the reported results. After multiple iterations, this idea was abandoned and efforts were invested into the redesign of the bearing pad.

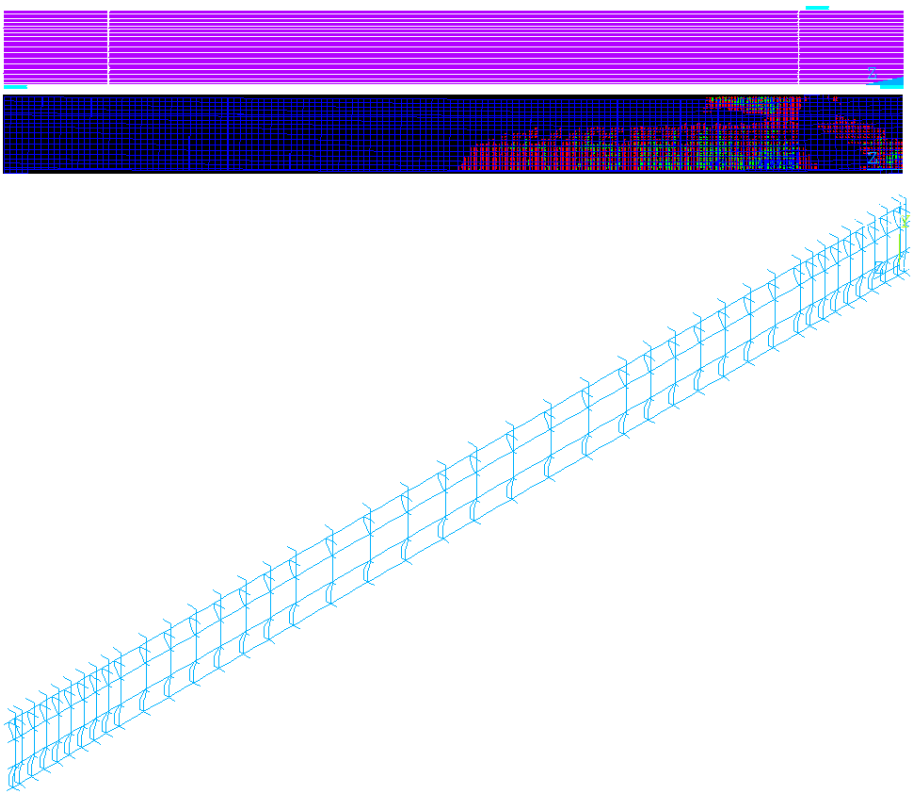

*Figure 53 - Hybrid Phase I beam*

## Phases II and III:

- The following set of calculations show the theoretical accumulated losses in the system over 43 years of service:

    a) Elastic Shortening: $\Delta f_{pES} = \frac{E_s}{E_c} * \ -\frac{P_i}{A}\left(1 + \frac{e^2}{r^2}\right) + \frac{M_D e}{I_c}$

    b) Creep: $\Delta f_{pCR} = \ \frac{t^{0.6}}{10+t^{0.6}} * \ C_u \frac{E_{ps} f_{cs}}{E_c}$

    c) Shrinkage: $\Delta f_{pSH} = \ 8.2 * 10^{-6} * K_{SH} E_{ps} * \left(1 - 0.06\frac{V}{S}\right)(100 - RH)$

    d) Steel Relaxation = $\Delta f_{pR} = \left[K_{re} - J\Delta\left(f_{pES} + \ f_{pCR} + f_{pSH}\right)\right] * C$

- In effort to converge on a proper estimate of the residual prestressing force in the strands, a Magnel (Allowable prestressing - eccentricity) diagram was created. The following section lists the equations used to find the "safe zone" in which any combination of eccentricity and prestressing would not exceed the beams' capacity (Nilson 1987).

    a) $\frac{1}{P_i} \geq \frac{-1 + \frac{e.c}{r^2}}{A_c\left(f_{ti} + \frac{M_O}{S}\right)}$

    b) $\frac{1}{P_i} \geq \frac{1 + \frac{e.c}{r^2}}{A_c\left(-f_{ci} + \frac{M_O}{S}\right)}$

    c) $\frac{1}{P_i} \leq \frac{R(1 + \frac{e.c}{r^2})}{A_c\left(-f_{ts} + \frac{M_t}{S}\right)}$

    d) $\frac{1}{P_i} \leq \frac{R(-1 + \frac{e.c}{r^2})}{A_c\left(f_{cs} + \frac{M_t}{S}\right)}$

Where:

$P_i$ is the initial prestressing force in the strands

e is the eccentricity of the strands

c is the distance from the beam's centroid to its extreme compressive/tensil fiber (both distances were the same in this scenario due to the symmetric cross section).

$r^2$ is the beam's radius of gyration

$A_c$ is the beam's cross sectional area

$f_{ci}$ is the allowable compressive stress in concrete at the critical section when prestress is initially applied

$f_{ti}$ is the allowable tensile stress in concrete at the critical section when prestress is initially applied

$f_{cs}$ is the allowable compressive stress in concrete at the critical section at service

$f_{ts}$ is the allowable tensile stress in concrete at the critical section at service

$M_o$ is the moment due to self-weight at the critical section

$M_t$ is the total final moment at the critical section

- AASHTO LRFD Nominal Moment Capacity Calculation

$$M_n = M_d - M_{LL}(DF)$$

*where* $M_n$ *is the nominal moment capacity;* $M_d$ *is the moment at midspan due to self weight;*

$M_{LL}$ *is the moment due to self weight, and* $DF$ *is the distribution factor*

$M_n$ *was calculated through strain compatibility*

1. *Strain in tendon at* $P_e$

$$P_e = 110\ kips;\ fs_e = \frac{110}{2.16} = 50.926\ ksi;$$

$$\varepsilon_1 = \frac{fs_e}{E_{ps}} = \frac{50.926}{27500} = 0.00185$$

2. *Strain due to decompression*

$$\varepsilon_2 = \frac{P_e}{A_c * E_c}\left(1 + \frac{e^2}{r^2}\right) = \frac{110}{488 * 5000} * \left(1 + \frac{7.77^2}{12.73^2}\right) = 0.000062$$

*3. Strain due to ultimate load*

$$Initial\ f_{ps}\ guess\ of\ 210\ ksi\ and\ assuming\ mild\ steel\ yielded$$

$$\varepsilon_{ps} = \frac{210}{27500} = 0.00764$$

$$T = C; a = \frac{A_{ps}\, f_{ps} - A_s * f_y}{0.85 * f'_c * b} = 1.38"$$

$$C = \frac{a}{\beta_1} = \frac{1.38}{0.65} = 2.12"$$

$$\varepsilon_3 = \frac{0.003\left(d_p - c\right)}{c} = \frac{0.003(18.27 - 2.12)}{2.12} = 0.02285$$

$$\varepsilon_1 + \varepsilon_2 + \varepsilon_3 = \varepsilon_{ps}$$

$$0.00185 + 0.000062 + 0.0228 \neq 0.00764 \qquad iterate$$

After multiple iterations, solution converged on:

$$f_{ps} = 250\ ksi, \varepsilon_{ps} = 0.01955\ , a = 1.74", c = 2.67"$$

$$M_n = 0.8 * 11.6 * \left(d_{ps} - d'\right) + 0.85 f'_c b \left(d_{ps} - \frac{a}{2}\right)$$

$$M_n = 0.8 * 11.6 * (18.27 - 2.3) + 0.85 * 10 * 36\left(18.27 - \frac{1.74}{2}\right) = 5472k.in = 456k.ft$$

$$M_{LL} = \frac{M_n - M_d}{DF}$$

$$M_d = (self\ weight) * \frac{L^2}{8} = \left(Ac + A_{Asphalt}\right) * unit\ weight * \frac{L^2}{8}$$

$$M_d = \frac{488 + 216}{144} * 0.15 * \frac{\left(\frac{574}{12}\right)^2}{8} = 210k.ft$$

$$M_{LL}interior = \frac{456 - 210}{0.1115} = 2206.3\ k.ft$$

$$P_{LL}interior = \frac{M_{LL} * 4}{L} = \frac{2206.3 * 4}{\frac{574}{12}} = 184.5\ kips$$

- Contact Element failed model

Figure 54 illustrates the results of the contact element route taken as an attempt to model the shear key bond between the beams. The contact elements failed prematurely, causing the loaded beams to acted independently of their counterparts thus producind the deflection pattern in Figure 54 (a). These extreme loads placed on the shear keys cause the transverse ties connectinng the beams to yield and give way to the deflecting beams as shown in Figure 54 (b).

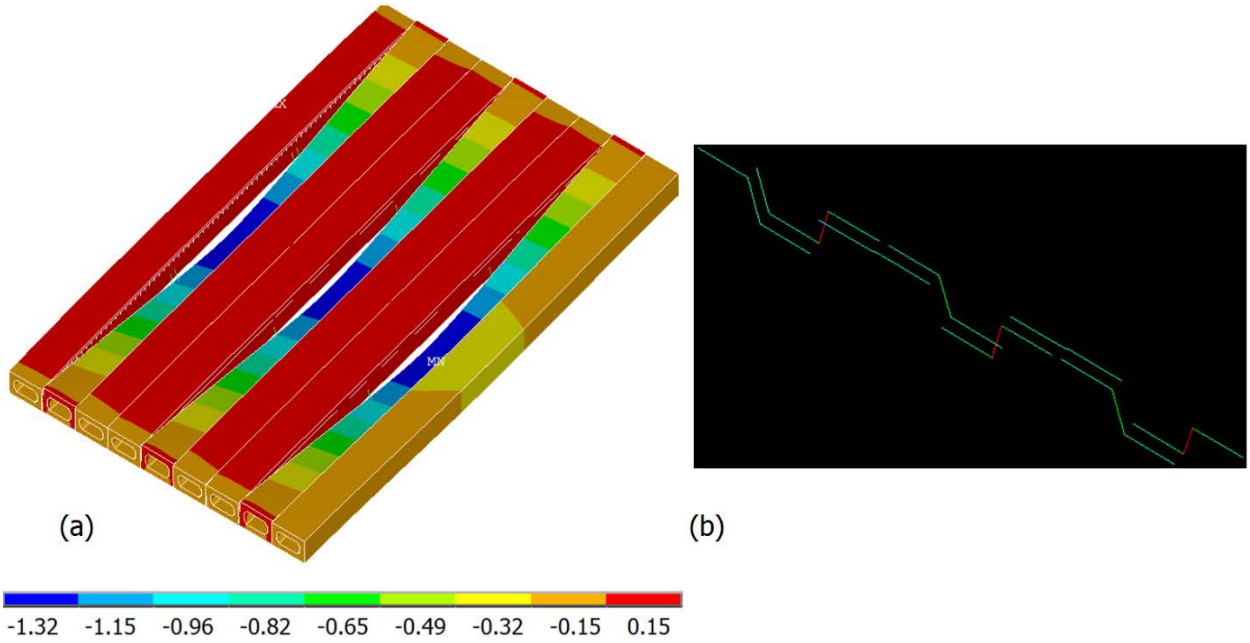


*Figure 54 - Phase II Contact Element Model (a) Deflection Contour (b) Yielded Transverse Ties*